Hyperspectral reflectance of vegetation affected by underground hydrocarbon gas seepage

Marleen F. Noomen

Promotoren:

Prof. Dr. A.K. Skidmore
Hoogleraar in de Vegetation and Agricultural Land Use Survey
International Institute for Geo-information Science and Earth Observation (ITC), Enschede en Wageningen Universiteit, Wageningen, Nederland

Prof. Dr. F.D. van der Meer
Hoogleraar in de Earth Subsurface Systems Analysis
International Institute for Geo-information Science and Earth Observation (ITC), Enschede en Universiteit Utrecht, Utrecht, Nederland

Prof. Dr. H.H.T. Prins
Hoogleraar in de Resource Ecology
Wageningen Universiteit, Wageningen, Nederland

Promotiecommissie:

Prof. Dr. M.E. Schaepman
Wageningen Universiteit, Nederland

Prof. Dr. S.M. de Jong
Universiteit Utrecht, Nederland

Prof. Dr. M.D. Steven
University of Nottingham, United Kingdom

Prof. Dr. M. Hale
Universiteit Utrecht, Nederland

Dit onderzoek is uitgevoerd binnen de onderzoeksschool Production Ecology and Resource Conservation (PE&RC) te Wageningen.

Hyperspectral reflectance of vegetation affected by underground hydrocarbon gas seepage

Marleen F. Noomen

PROEFSCHRIFT

ter verkrijging van de graad van doctor
op gezag van de rector magnificus
van Wageningen Universiteit,
Prof. Dr. M.J. Kropff,
in het openbaar te verdedigen
op vrijdag 22 juni 2007
des namiddags te drie uur
in het auditorium van het ITC
te Enschede

Title: Hyperspectral reflectance of vegetation affected by underground hydrocarbon gas seepage

ISBN: 978-90-8504-671-4
International Institute for Geo-information Science & Earth Observation, Enschede, the Netherlands (ITC)
ITC Dissertation Number: 145

Table of contents:

List of Figures:

List of Tables

Abstract

Anomalous concentrations of natural gas in the soil may be sourced from leaking underground gas pipelines or from natural microseepages. Due to the explosive nature of hydrocarbon gases, early detection of these gases is essential to avoid dangerous situations. It is known that natural gas in the soil affects vegetation health, which may be detected through analysis of reflectance spectra. This thesis characterizes the effects of underground gas leakage on plant and canopy development and reflectance. Based on the reflectance properties, a general gas leak detection method is proposed.

It was assumed that natural gas displaces the soil air and that oxygen shortage is the cause of changes in vegetation growth and reflectance; however it was not known whether the hydrocarbon gases have an additional effect on the vegetation. Therefore two experiments were performed to compare the effects of small gas leaks (without oxygen shortage) with large leaks (with oxygen shortage) on plant growth and reflectance. The small gas leaks were simulated by delivering natural gas, methane and ethane to pots with maize (*Zea mays*) and wheat (*Triticum aestivum*) plants. The large natural gas leak was simulated by delivering 2200 l of gas per day to 2 by 2 m maize and wheat canopy plots. Whereas in several studies a decrease in vegetation chlorophyll was one of the main indicators of large gas leaks, this study showed that leaf area is a better indicator of gas leakage. Moreover, it was shown that when the ethane concentration in the soil reaches 0.75%, plant growth is not only affected by oxygen shortage but also by the gas itself.

The leaf reflectance of the plants was analysed using continuum removal of the blue (400-550 nm), red (550-750 nm) and two water absorption features (1370-1570 nm and 1870-2170 nm). The analysis showed that ethane caused an initial increase of 10% in reflectance between 560 and 590 nm, followed by a decrease during the course of the experiment. All gases caused an increase in reflectance in the water absorption bands. The physiological reflectance index PRI, which has previously linked water stress to photosynthetic activity, suggested that the hydrocarbon gases (particularly ethane) decreased the photosynthetic activity of the plants. The combination of reduced band depths in the chlorophyll and water absorption regions and the increased PRI suggests that ethane gas in the soil hampered a normal water uptake by maize plants in an early stage of their growth.

Since gas leaks are often accompanied by elevated carbon dioxide concentrations due to bacterial methane oxidation, an additional experiment was performed to study the effects of CO_2 gas in concentrations ranging from 2% to 50% on vegetation reflectance. The red edge position in combination with a new index named the 'yellow edge position' showed that an increasing CO_2 concentration corresponded to decreasing leaf chlorophyll. Two water absorption features at 1400 and 1900 nm indicated that a concentration of 50% CO_2 decreased leaf water content. However, since other aspects such as the effects of oxygen shortage and ethane may either diminish or enhance the effects of CO_2 on plant reflectance, the effects should be separated to know whether CO_2 affects vegetation reflectance in a larger leak.

To define the effects of oxygen shortage on vegetation reflectance, measured oxygen concentrations were correlated with reflectance indices. Statistical covariance analysis indicated that at 29 days after oxygen shortage occurred, the reflectance indices had the highest correlation with oxygen concentrations in the soil, for both species. The effect was consistent within species, but the absolute values varied between the species. Normalization between species resulted in significant linear regression models for six reflectance indices. However, the performance of each index varied in time, resulting in the best predictions 29 days after gassing started, which was halfway through the growth cycle of the plants. When the same normalization procedure was applied to differences in time, the Vogelmann index (Vog1; $R740/R720$) could predict oxygen concentrations under the maize canopy at any timestep. Oxygen concentrations predicted from the Lichenthaler index (LIC3; $R440/R740$) based on the wheat canopy were less reliable (R^2 of 0.55) due to patchy growth on the control plots. When these indices were used to predict the oxygen concentration in the soil in order to detect the gas leak, the maximum distance to the gas source at which the oxygen concentration was reduced was just 0.5 m. However, when a filter is applied that searches for the round shape of the leak, the chance of detecting a gas leak is increased significantly. Leak detection should optimally take place when canopy cover is between 40 and 80%, or when the NDVI is between 0.6 and 0.9. LIC3 should be used at NDVI values below 0.75, while Vog1 will be a better predictor under canopies of higher NDVI.

In a large leak, ethane, CO_2 and oxygen shortage all occur together. The effect of oxygen shortage in the simulated gas leak however was so strong that the additional effect of ethane could not be measured. The actual CO_2 concentrations in the leak were calculated using a model that incorporates bacterial oxidising activity and continuous replenishment of the soil with methane and air. Soil CO_2 concentrations did not reach values that are harmful to plants. It is therefore concluded that in a large leak, low oxygen concentrations are the main cause for changes in reflectance.

Finally, the results of the simulated gas leaks were tested in the field in a natural hydrocarbon seepage area. Even though the hyperspectral imagery dated from several years earlier, the patterns observed in the field were also observed in the image using the indices proposed earlier. This supports the conclusion that the selected indices are not season dependent and can be used at any moment in time. Moreover, using indices that are related to biomass makes the method generally applicable. The disadvantage is that such indices lead to large number of false anomalies, however, including a filter in the analysis reduced the number of false anomalies remarkably and should therefore be an integral part of the detection process.

In conclusion, this thesis has shown that gas leaks cause changes in vegetation reflectance as early as 2 weeks after gas leakage starts. If the spectral resolution of the sensor is high in the visible and NIR and the spatial resolution as high as possible (preferably as high as 1 m), vegetation reflectance can be used as indicator of gas leakage.

Samenvatting

Abnormale concentraties aardgas in de bodem kunnen afkomstig zijn van ondergrondse lekkende gasleidingen of van natuurlijke gas sijpelingen. Omdat koolwaterstofgassen explosief zijn, is het van essentieel belang dat een gaslek zo vroeg mogelijk opgespoord wordt. Het is bekend dat aardgas in de bodem de gezondheid van de vegetatie aantast. De reflectie van deze vegetatie zou gebruikt kunnen worden om de gaslekken op te sporen. In dit proefschrift worden de gevolgen van ondergrondse gaslekkage op de ontwikkeling en de reflectie van vegetatie onderzocht.

Tot nu toe werd aangenomen dat aardgas de normale bodemlucht verplaatst en dat zuurstoftekort de oorzaak is van veranderingen in de gezondheid en reflectie van planten. Het is echter niet bekend of de koolwaterstofgassen zelf een effect hebben op de vegetatie. Daarom zijn twee experimenten uitgevoerd waarin de effecten van kleine gaslekken (zonder zuurstoftekort) op plantengroei en reflectie vergeleken werden met de effecten van grote gaslekken (met zuurstoftekort). De kleine lekken werden gesimuleerd door kleine hoeveelheden aardgas, methaan en ethaan potten met mais (*Zea mays*) en tarwe (*Triticum aestivum*) te laten stromen. Het grote lek werd gesimuleerd door per dag 2200 l aardgas door een begroeid oppervlak van 2 bij 2 m te laten stromen. Terwijl tot nu toe gedacht werd dat een vermindering van bladchlorofyl een indicator was van gaslekkage, toont dit onderzoek aan dat bladoppervlak een betere indicatie is. Daarnaast werd aangetoond dat als de concentratie ethaan in de bodem 0.75% is, plantengroei niet alleen door zuurstoftekort wordt beïnvloed, maar ook door het gas zelf.

De bladreflectie werd geanalyseerd door ‘continuum removal’ toe te passen op de reflectie in het blauwe licht (400-550 nm), het rode licht (550-750 nm) en in twee waterabsorptie gebieden (1370-1570 nm and 1870-2170 nm). Analyse van de reflectie in die gebieden toonde aan dat ethaan vroeg in het experiment een 10% hogere reflectie veroorzaakte in het gebied tussen 560 en 590 nm, maar dat dit verschil weer verminderde gedurende de rest van het experiment. Daarnaast veroorzaakten alle gassen een hogere reflectie in de waterabsorptie gebieden. Tenslotte suggereerde een verhoging van de fysiologische reflectie index (PRI) dat de koolwaterstofgassen (met name ethaan) de fotosynthese in de planten verminderden.

Naast aardgas worden in een gaslek ook verhoogde concentraties koolstofdioxide aangetroffen. Koolstofdioxide (CO_2) wordt geproduceerd door methaan-oxiderende bacteriën. Om te testen wat het effect is van verhoogde CO_2 concentraties in de bodem op plantreflectie werd een experiment uitgevoerd waarin concentraties CO_2 in de bodem varieerden van 2% tot 50%. De ‘red edge position’ (de reflectie tussen het rode en het nabij infrarode gebied) en een nieuwe index genaamd ‘yellow edge position’ toonden aan dat toenemende hoeveelheden CO_2 overeenkwamen met een afnemend bladchlorofyl gehalte. Bovendien liet de reflectie in de waterabsorptie gebieden rond 1400 en 1900 nm zien dat 50% CO_2 in de bodem het watergehalte in de plant verlaagde. Omdat in een lek naast een (potentieel) verhoogd CO_2 gehalte ook zuurstoftekort en ethaan de reflectie kunnen beïnvloeden, zullen de effecten afzonderlijk bestudeerd moeten worden om te begrijpen welk gas het grootste effect heeft.

Om het effect van zuurstoftekort op mais en tarwe bedekking te bestuderen, werd het zuurstofgehalte in de bodem gecorreleerd met 51 reflectie indices. Een covariantie analyse toonde aan dat de hoogste correlatie tussen de reflectie indices en zuurstof plaatsvond na 29 dagen. Het effect van de zuurstof op de indices was consistent voor de twee soorten, maar de absolute waarden verschilden. Nadat hiervoor genormaliseerd werd konden zes indices het zuurstofgehalte onder de vegetatiebedekking van beide soorten voorspellen, waarbij de hoogste correlatie halverwege de groeicyclus van de planten plaatsvond. Wanneer eenzelfde normalisatieprocedure toegepast werd op de verschillen in de tijd, kon de index Vog1 (R740/R720) de zuurstofconcentraties onder de mais bedekking voorspellen op elk tijdstip. Onder de tarwe bedekking was LIC3 (R440/R740) een goede voorspeller van de zuurstofconcentraties, hoewel de regressiecoëfficiënt daar lager was door de onregelmatige groeipatronen. Wanneer deze indices gebruikt werden om zuurstofconcentraties onder de hele bedekking te voorspellen en daarmee de locatie van het gaslek te bepalen, bleek dat het zuurstofgehalte slechts tot een afstand van 0.5 m tot de gasleiding sterk verlaagd was. Wanneer echter een filter gebruikt werd dat zoekt naar de ronde vorm van een lek is de kans dat het lek ook daadwerkelijk ontdekt wordt sterk verhoogd. Tenslotte bleek dat de detectie van gaslekken het best plaats kan vinden wanneer de vegetatiebedekking tussen 40% en 80% ligt, of in andere woorden, als de NDVI tussen de 0.6 en 0.9 ligt. Voor NDVI waarden onder 0.75 zou LIC3 dan gebruikt kunnen worden, terwijl voor hogere NDVI waarden VOG1 beter zal werken.

In een groot gaslek komen ethaan, CO_2 en zuurstoftekort tegelijkertijd voor. Het effect van zuurstoftekort op de reflectie is echter zo groot, dat het effect van ethaan niet gedetecteerd werd. Het effect van CO_2 werd indirect bepaald door aan de hand van de gemeten zuurstofgehalten de CO_2 concentraties te berekenen. Hierbij werd rekening gehouden met de oxiderende activiteiten van de methanotrofe bacteriën en de continue aanvulling van de bodem met methaan. Hieruit bleek dat de CO_2 concentraties in de bodem geen waarden bereikten die de reflectie beïnvloeden. Hieruit kon geconcludeerd worden dat lage zuurstofconcentraties de voornaamste reden van reflectieveranderingen zijn.

Tenslotte zijn de resultaten van de experimenten getest in een natuurlijke situatie. Terwijl de hyperspectrale beelden van dit gebied enkele jaren eerder gevlogen waren, konden de patronen in de begroeiing die in het veld werden waargenomen ook in de beelden worden gezien als de eerder voorgestelde indices gebruikt werden. Dit versterkt het vermoeden dat de indices seizoensonafhankelijk zijn en op elk moment gebruikt kunnen worden. Bovendien zijn indices die verschillen in biomassa aangeven plaats en soort onafhankelijk. Het nadeel is echter dat zulke indices meer gaslekken zullen vinden dan er in werkelijkheid zijn. Daarom zou het gebruik van een filter dat zoekt naar de ronde vormen van een gaslek een integraal onderdeel van de analyse moeten zijn.

Tenslotte heeft dit proefschrift aangetoond dat gaslekken al veranderingen in vegetatiereflectie kunnen veroorzaken binnen twee weken na het begin van de lekkage. Geconcludeerd kan worden dat, als de spectrale resolutie van een sensor hoog is in het zichtbare en nabij infrarode licht en de ruimtelijke resolutie zo hoog mogelijk (minstens 1 m), vegetatiereflectie als indicator kan dienen bij het opsporen van gaslekkage.

Acknowledgements

First of all, I would like to thank my promotors Andrew Skidmore, Freek van der Meer and Herbert Prins. I enjoyed working with you, and I have learnt a lot from each of you. Thank you for all the support. Christie and Esther, thank you for all your help with such impossible tasks as organising a meeting with all supervisors; and Loes, thanks for your support during the last stages of my Ph.D.

During the three months that I stayed in Nottingham, I enjoyed the support of Karon Smith, Jeremy Colls and Mike Steven. Not only are the results of the experiment a vital part of this thesis, I also thoroughly enjoyed the collaboration. I like to thank Matthew Beardsley for his assistance in the field in Nottingham, and Geurt Versteeg and Jan van Walsem for their help in the greenhouse and the laboratory in Wageningen.

My roommates contributed for a great deal to my working pleasure. Harald, our collaboration ranged from investigating oil samples in a hotel bathroom in California to decorating our room. Thanks for all the fun. Wiebke, I enjoyed having you as my 'kamergenootske' during the last stage of my Ph.D.

Many people made ITC-life memorable: Daniël for our daily discussions about the ups and downs of our Ph.D. life; Arko, Jelle, Nicky, Petra and the 'younger generation' ESA and NRS staff for all the fun during coffee/lunch/ and other breaks; Prasun, Pravesh and Ajay (K.) for organising great diner parties. Ajay (M.) and Joshi, I enjoyed the good times we spent in Enschede, but most of all thank you for giving me the best 'after-Ph.D.-holiday' I could imagine! Outside ITC I would like to thank all friends that in one way or the other have supported me during my Ph.D.

Finally, I am lucky to have such a great support team residing in Hoenderloo. Pap and Sas, your support in every aspect is invaluable. But the greatest support I have enjoyed from Ulan! With your never-ending jokes, you always managed to put my worries and doubts into perspective. Thank you for everything!

CHAPTER 1

INTRODUCTION

1.1 Why study hydrocarbon seepage?

The presence of high concentrations of hydrocarbon gases such as methane (CH_4) and ethane (C_2H_6) in the soil may have several reasons. When the pattern is very localized, a leaking underground gas pipeline may be the cause for the high gas concentrations, whereas large areas of increased hydrocarbon concentrations may be sourced from an underlying oil or gas reservoir. Hydrocarbon gases are explosive, so early detection of anomalous gas concentrations is essential to avoid dangerous situations. Moreover, leakage from gas transporting pipelines leads to a loss of revenue for gas companies. In the United States alone, the National Transportation Safety Board (NTSB) reported millions of dollars in losses and several casualties due to gas pipeline leakage (NTSB, 2001; 2003). Besides the safety and economic issues related to gas leakage, long-term gas seepage can contribute to global warming as methane has an 8 times stronger global warming potential than CO_2 (IPCC 2001). Fast and reliable detection methods therefore assist in decreasing the risk of gas explosions and facilitate the quantification of the methane budget. In this thesis the potentials of remote sensing techniques are studied in relation to the detection of anomalous concentrations of hydrocarbon gases in the soil. The following sections describe the mechanisms of gas leakage, its influence on the environment and the research questions of this thesis.

1.1.1 Gas pipeline leakage

Natural gas transporting pipelines can leak for long periods without being noticed, giving rise to potentially dangerous situations. One of the largest gas pipeline accidents in history took place in Ufa, Russia in 1989, where a spark from a bypassing train resulted in a gas explosion that killed 1400 people (Gurpinar *et al*., 2001). To ensure a safe gas transportation network, monitoring of pipelines should ideally take place continuously. Many gas pipelines are covered by 1 m of soil (Zirnig *et al*., 2002), which complicates the monitoring. Presently the most regularly used methods for monitoring gas pipelines are surveillance on foot and by helicopter, methods that are both time consuming and expensive (Zirnig *et al*., 2002; Van Persie *et al*., 2004). Other methods in use include measuring differences in pressure within the pipeline, acoustic methods that detect the hissing sound of escaping gas, and sniffer methods (Kennedy, 1993).

1.1.2 Natural hydrocarbon gas seepage

High soil gas concentrations have been long documented. The gas was often accompanied by oil and tar, which was used by local inhabitants as an adhesive or coating. Native Indians in California used the tar to make their canoes waterproof (Kuhn, 2000). For over 100 years hydrocarbon gas seepage has been associated with underground oil and gas reservoirs (Link, 1952). Midway during the 19th century the first wells were drilled near oil seeps, after which many oil and gas reservoirs have been discovered.

Hydrocarbon seepage results from oil or gas bearing reservoirs that are under pressure. Due to this pressure the hydrocarbons seep towards the surface. Higher molecular weight hydrocarbons (oil) often follow faults and cracks, whereas migration paths of low weight hydrocarbons (gases such as methane, ethane and propane) may be vertical, (long-distance) lateral (Schumacher, 2000) or along with groundwater movements (Horvitz, 1972; Abrams, 1996). The composition of the gas seeps varies with the reservoir, but in general the main constituent is methane, followed by ethane, propane and small quantities of other gases such as carbon dioxide and nitrogen (Olah and Molnar, 2003; Hoeks, 1972a).

Hydrocarbon seeps are not only a link to underground reservoirs; they also pollute the environment. Offshore oil seepage causes large oil slicks floating on the water surface (MacDonald *et al*., 1989; Hornafius *et al*., 1999), while onshore oil seepage flows into rivers and pollutes the soil (Hodgson, 1980). Gas seepage can contribute to smog (Luyendyk *et al*., 2003) and gas-air mixtures can be explosive. Hydrocarbon microseepage contributes to global warming (Van der Meer *et al*., 2000), as methane has an 8 times stronger global warming potential than CO_2 (IPCC 2001). Etiope and Klusman (2002) estimated that onshore and offshore hydrocarbon seepage emissions range from 30 to 70 Mt/y, which corresponds to 5 - 13% of the total methane budget as indicated by the Intergovernmental Panel on Climate Change (IPCC, 2001). To detect and quantify the escaping gas, several methods have been developed to map the location of hydrocarbon seeps, however due to the variability in seepage size, shape and activity, this has been a difficult task (Schumacher, 2000).

1.1.3 Effects of high gas concentrations on soil

Although pipeline leakage generally takes place on a shorter time-scale than natural hydrocarbon seepage, both seepage types result in anomalous gas concentrations in the soil. Hydrocarbon gases cause a wide range of changes in the soil environment, depending on soil type and duration of the gas seepage. When hydrocarbon gases such as methane and ethane collect in the soil, the

normal soil atmosphere is displaced, resulting in a decrease in soil oxygen (Schumacher, 1996). The oxygen concentration in the soil may decrease further due to methanotrophic bacteria that oxidize methane, thereby generating carbon dioxide and water (Hanson and Hanson, 1996). A study by Steven *et al*. (2006) showed that in addition to oxygen displacement by methane, bacterial oxygen depletion ranged from 1.8 to 4.7 % (as percentage of total soil air). These anaerobic soil conditions change the pH and cause a drop of the redox potential (Eh) (Schumacher, 1996; Adams and Ellis, 1960). The low redox potential reduces the pH of alkaline soils and increases the pH of acid soils (Neue, 1993). Adams and Ellis (1960) demonstrated that this neutralization of the pH in gassed soil led to increased availability of trace elements such as manganese and ferric iron. Schollenberger (1930) and Godwin *et al*. (1990) also detected increased manganese and ferric iron in gassed soil. Mineralogical changes due to changes in the pH and Eh include the formation of near-surface carbonates, pyrites, uranium, sulphides and bleaching of red beds (Schumacher, 1996; 2001).

1.1.4 Effects of hydrocarbon gas seepage on vegetation

The changes in the soil atmosphere can have adverse effects on vegetation health. Most plants need oxygen for respiration of the roots and for proper uptake of water and nutrients (Drew, 1983). Generally, soil oxygen shortage leads to reduced root and shoot growth and reduced dry weight (Drew, 1991), although rice (*Oryza sativa*) is a well-known exception to this (Justin and Armstrong, 1991; Jackson and Pearce, 1991). The reaction of plants on soil oxygen shortage depends on the duration of the oxygen shortage, the species, as well as on the cultivar (Huang *et al*., 1994; Huang *et al*., 1997b; Zaidi *et al*., 2003). Wheat cultivars showed a decrease in photosynthesis 8 days after initiation of low oxygen concentrations, while another three days later leaf chlorophyll content had decreased by 20 to 40% (Huang *et al*., 1997b).

Bacterial oxygen depletion is accompanied by an increase in carbon dioxide (CO_2) in the soil environment up to concentrations of 5% - 15% (Hoeks, 1972a). High soil CO_2 is known to kill trees and other vegetation by disrupting the root respiration and by acidification of the ground water (Macek *et al*., 2005; Bergfeld *et al*., 2006). Boru *et al*. (2003) showed that soybean (*Glycine max)* subjected to CO_2 concentrations ranging from 15 to 50% showed a reduction in leaf "greenness" as well as in shoot and root growth, whereas rice (*Oryza sativa*) was not affected by these concentrations. 10% CO_2 in combination with 5% O_2 in the soil significantly decreased shoot growth of two wheat (*Triticum aestivum*) cultivars, but photosynthesis and leaf chlorophyll content decreased for only one of the two cultivars (Huang *et al*., 1997b). CO_2 concentrations up to 2% did not affect citrus (*Citrus volkameriana*) or bean (*Phaseolus vulgaris*) dry weight (Bouma *et al*., 1997).

Changes in soil pH and redox potential (Eh) cause mobilization of possibly phytotoxic nutrients such as manganese and aluminium. Adams and Ellis (1960) suggest that the increased manganese found in gas-saturated soil could reach toxic levels for plant growth. Godwin *et al*. (1990) showed that up to a distance of 9 m from a leaking gas well, manganese increased 5 to 10-fold, approaching toxic levels. Dalziel and Donovan (1980) showed that leaves of pine and sagebrush growing over an oil field had an increased manganese-iron ratio.

It is not known if hydrocarbon gases themselves affect plant growth. It is assumed that methane is not toxic to plant roots (Arthur *et al*., 1985) or aboveground parts of plants (Gustafson, 1944). In the 1960's, several studies were done on the toxicity of natural gas after gas companies switched from delivering manufactured gas to natural gas. Whereas manufactured gas contained gases that are known to be toxic to plants such as ethylene and cyanogen compounds, natural gas is free of these (Bray, 1958; Braverman *et al*., 1962). The main cause of injury to vegetation was believed to be oxygen shortage (Pirone, 1960), with a possible additional effect of the dryness of the gas (Bray, 1958), methane (Braverman *et al*., 1962) or CO_2 (Hoeks, 1972a).

In general, gas seepage causes a yellowing of the leaves (*chlorosis*), early fall of leaves and eventually premature death (Hoeks, 1972b; Bray, 1958). Pysek and Pysek (1989) showed that artificial gas leakage caused restricted growth, failure of reproduction and a change in vegetation diversity and cover. Godwin *et al*. (1990) showed that the growth of wheat (*Triticum aestivum*) was restricted within a radius of 2.5 to 3 m of a gas well, whereas rape seed (*Brassica napus*) showed a reduction in height up to 7 m away. Up to a distance of 1.5 m away from the wells, the weight of the roots of both species and the weight of the wheat stems were lower. Other studies also show that plants growing in soil contaminated by natural gas have chlorotic leaves or reduced growth (Oliveira *et al*., 1997; Smith *et al*., 2004b).

1.2 Exploration methods

Over time, several methods have been developed for the detection of gas seepage. A distinction is made between methods that measure the hydrocarbon gases directly, and methods that detect changes in the environment caused by hydrocarbon gases (Tedesco, 1995). Sokolov (1933) showed that the subsoil located over a gas field contained increased concentrations of hydrocarbon gases, while over large reservoirs elevated gas concentrations are found in the atmosphere (Tedesco, 1995). Tedesco (1995), Jones *et al*. (2000), Jones and Drozd (1983), and Harbert *et al*. (2006) describe several methods that could detect and quantify these subsoil hydrocarbon gases. The most well known

methods include the soil-probe technique where soil gases are sampled using a probe, the headspace technique where gases absorbed to clay particles are measured, and airborne sniffer methods where the atmosphere is sampled for hydrocarbon gases (Jones *et al*., 2000; Tedesco, 1995). Changes in mineralogy as a result of hydrocarbon gas seepage have been the focus of methods using magnetism, electricity and radioactivity (Schumacher, 1996; Smith and Rowe, 1997; Ellwood and Burkart, 1996 and Aldana *et al*., 2003). Wagner *et al*. (2002) describe a microbial prospecting method that could separate methane-oxidizing bacteria from higher hydrocarbon oxidizing bacteria.

For exploration of large areas, airborne detection methods are promising as they are time-consuming and rapid (Jones *et al*., 2000). However, direct detection of hydrocarbons has shown to be complicated. Leifer *et al*. (2006) recently quantified methane from natural marine hydrocarbon seeps using the absorption features between 2200 and 2340 nm on an AVIRIS image. This method is however less reliable to detect onshore seeps as background variability may obscure the absorption features (Leifer *et al*., 2006). Experimental studies on oil and gas seepage revealed that oil absorbs light at several wavelengths in the shortwave infrared region (SWIR), particularly around 1730 nm and between 2300 to 2600 nm (Cloutis, 1989; Hörig *et al*., 2001; Kühn *et al*., 2004). Ellis *et al*. (2001) mapped oil seeps in California using field reflectance of oil seeps. A complicating factor of oil mapping is that the absorption features are subtle and the spectral signature of oil resembles the spectral signature of other organic materials and asphalt (Hörig *et al*., 2001).

1.2.1 Vegetation remote sensing

Since vegetation health is affected by hydrocarbon seepage, remote sensing may be used to detect these vegetation changes. The reflectance of healthy vegetation in the visible light is characterised by absorption features caused by plant pigments such as chlorophyll and carotenoids, while the near infrared (NIR) and shortwave infrared (SWIR) are characterised by four major water absorption features (Figure 1.1). The major absorption features are listed in Table 1.1.

Another typical feature of healthy vegetation is the high reflectance in the NIR between 800 and 1100 nm, which is dependent on the internal leaf structure and leaf area (Gausman, 1974; Knipling, 1970). A decline in plant health is often noticed as an increase in reflectance in the absorption features and a decrease in NIR reflectance. This results in a shift of the slope between the red and NIR – called the ‘red edge position’ – towards shorter wavelengths.

Figure 1.1 (left) Typical vegetation reflectance curve, with indication of major absorption features.
Table 1.1 (right) Major absorption features in vegetation reflectance.

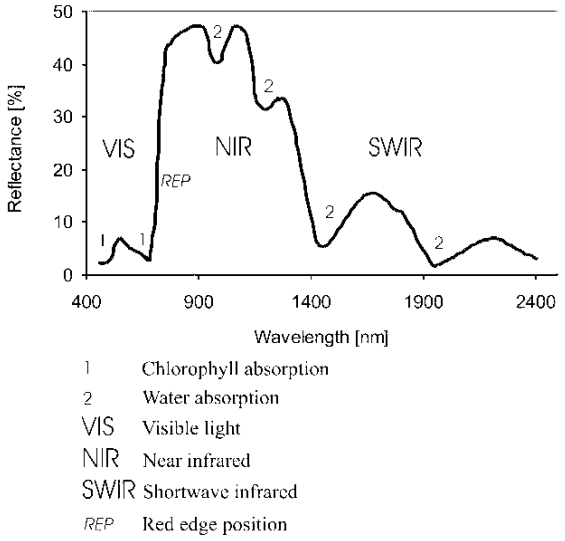

Wavelength [nm]	Caused by
430	Chlorophyll *a*
460	Chlorophyll *b*
640	Chlorophyll *b*
660	Chlorophyll *a*
970	Water
1200	Water
1400	Water
1940	Water

Although several authors have attempted to determine the effects of hydrocarbon seepage on vegetation reflectance, the results are inconclusive (Table 1.2). Almeida-Filho *et al*. (1999) showed that the combination of bleached soil and lower vegetation cover in the microseepage area was detectable on Landsat TM images as an increase in the red and decrease in the near infrared reflectance. Richers *et al*. (1986) found a tonal anomaly on Landsat images of sagebrush (*Artemisia tridentata*) growing in the Patrick Draw hydrocarbon seepage area. However, two years later Scott *et al*. (1988) concluded that the tonal anomaly was more likely a result of other environmental causes than of hydrocarbon seepage. Several studies showed that the 'red edge' of vegetation canopies shifted towards shorter wavelengths when exposed to natural hydrocarbon seepage (Reid *et al*., 1988; Bammel and Birnie, 1994) or to simulated gas leakage (Oliveira *et al*., 1997; Smith *et al*., 2004b). Yang *et al*. (1999; 2000) however found a shift of the red edge towards longer wavelengths in a wheat field growing in a microseepage area.

Table 1.2 Literature overview. NHS = Natural hydrocarbon seepage; NG = natural gas. - and + represent a decrease respectively increase in reflectance in VIS (visible) and NIR (near infrared), and a shift towards blue respectively red of the red edge position (REP)

Literature	Gas	Species	Vegetation	VIS	NIR	REP
Richers *et al.*, 1986	NHS	Sagebrush, grassland	Stunted	Tonal anomaly		
Scott *et al.*, 1988	NHS	Sagebrush, grassland		Conclusions by Richers incorrect		
Reid *et al.*, 1988	NHS	Deciduous trees			-	-
Pysek and Pysek, 1989	NG; 250-300 l/h [experimental]	53 different species	Restricted growth, decrease in vegetation cover		-	
Godwin *et al.*, 1990	NG leakage from oil wells	Wheat, rape seed	Reduction in plant height			
Bammel and Birnie, 1994	NHS	Big sagebrush		Red & green shift towards blue		-
Oliveira *et al.*, 1997	NG [experimental]	Grass, eucalyptus		-	-	-
Almeida-Filho *et al.*, 1999	NHS	'Savannah-like vegetation'		+	-	
Yang *et al.*, 1999, 2000	NHS	Wheat				+
Smith *et al.*, 2004a	NG, argon, 13 l/h, between 50 and 70% [experimental]	Barley, bean				-
Smith *et al.*, 2004b	NG; 100 l/h; up to 54 % [experimental]	Grass, wheat, bean	Decrease in leaf chlorophyll			Change of shape

1.3 Aim of this thesis

Monitoring gas pipelines and gas seepage detection involves large areas, which are often vegetated. Since vegetation health is affected by gas in the soil, it could potentially be used as an indicator of anomalous soil gas concentrations. With the development of hyperspectral (high spectral resolution) remote sensing techniques, vegetation can now be studied in more detail, both spatially and spectrally. Promising relationships have been found between hyperspectral remote sensing and vegetation parameters (e.g. Thenkabail *et al.*, 2000; Curran, 1989; Carter and Miller, 1994; Kumar *et al.*, 2001), but so far these have not led

to a full understanding of the effects of hydrocarbon seepage on vegetation health. The overview in Table 1.2 suggests that high gas concentrations in the soil lead to a decrease in plant growth and a shift of the red edge position towards the blue and/or a decrease in NIR (Pysek and Pysek, 1989; Oliveira *et al*., 1997; Smith *et al*., 2004b). However, the effects of lower gas concentrations are less conclusive (a shift of the red edge position towards the *red* (Yang *et al*., 1999); the different conclusions of Richers *et al*. (1986) and Scott *et al*. (1988)). To fully understand the effects of hydrocarbon gas seepage on vegetation reflectance, in this thesis the effects of anomalous hydrocarbon gas concentrations on vegetation growth and reflectance are studied from leaf level to canopy patterns, using hyperspectral remote sensing.

The following research questions form the basis of the thesis:

- How does hydrocarbon seepage affect vegetation growth and reflectance?
- Are the measured effects caused by the hydrocarbon gases themselves or by oxygen shortage?
- Can anomalous soil gas concentrations be detected using vegetation remote sensing?

The aim of the thesis is to characterize the effects of hydrocarbon gas seepage on vegetation growth and reflectance in order to design a general method for hydrocarbon gas detection - whether natural or from pipelines. To include all aspects of hydrocarbon gas seepage, the study was split in a) the effects of small quantities of hydrocarbons (methane, ethane and natural gas) on vegetation reflectance, and b) the effects of high soil gas concentrations accompanied by oxygen shortage. In addition, it was studied whether carbon dioxide concentrations that develop as a result of bacterial methane consumption affect vegetation reflectance.

1.4 Structure of the thesis

The structure of this thesis is as follows (see Table 1.3 for an overview of what is described in each chapter):

Two experiments form the basis of this thesis. Both experiments deal with the effects of gas in the soil on vegetation growth and reflectance. In Chapter 2 these experiments are described in detail; the subsequent chapters refer to this chapter for the methods. The aim of Chapter 2 is to understand the effects of low and high natural gas concentrations on maize and wheat growth and

morphology. Methane, ethane and natural gas are delivered in small concentrations to study the effects of the gases on plant morphology, while large concentrations of natural gas are delivered to maize and wheat canopies to study the combined effects of high gas concentrations and low oxygen concentrations on plant growth and canopy patterns.

Whereas in Chapter 2 the effects of methane, ethane and natural gas were studied on plant morphology, in Chapter 3 the effects of these gases on leaf reflectance are studied. Continuum removal is applied to analyse the reflectance in two chlorophyll and two water absorption features.

Since gas leaks are often accompanied by elevated carbon dioxide concentrations, in Chapter 4 it is determined whether soil carbon dioxide affects plant reflectance. Four indices are calculated on the first derivative reflectance to study the effect of 5 different carbon dioxide concentrations on maize leaf reflectance. A new index based is proposed to study chlorophyll differences.

In Chapter 5 the effect of high gas concentrations on maize and wheat canopy reflectance is studied. 51 vegetation indices are correlated with soil oxygen concentrations. After normalizing for time or species, several reflectance indices can be used to estimate soil oxygen concentrations. The chance of detecting a gas leak is increased when the shape of the leak is incorporated.

Chapter 6 analyses whether the effects of ethane and carbon dioxide as found in Chapters 3 and 4 can be measured when gas concentrations are high and oxygen concentrations low. The carbon dioxide concentrations are estimated by calculating the methanotrophic oxygen depletion in the gas leak.

Whereas Chapters 2 to 6 are based on experiments, Chapter 7 describes vegetation patters and reflectance in a natural seepage area in California. The results from the previous chapters are used to detect seeps using hyperspectral imagery.

In Chapter 8 (Synthesis) the results of all chapters are compared and combined, and the possibilities of using remote sensing for the detection of hydrocarbon gas leaks are discussed.

Table 1.3 Structure of thesis

Where	Gas [concentration]	O_2 shortage	Species	Measured	Chapter
Greenhouse (simulated)	Natural gas [2.50 %] Methane [2.49 %] Ethane [0.73 %]	No	Maize, wheat	Plant morphology, leaf reflectance	2, 3
	CO_2 [2, 5, 10, 20, 50%]	Partly	Maize	Plant morphology, leaf reflectance	4
Field (simulated)	Natural gas [9.13 %]	Yes	Maize, wheat	Plant & canopy morphology, leaf & canopy reflectance	2, 5, 6
Field (natural)	Hydrocarbon seepage [unknown]	Yes	Grassland vegetation	Canopy patterns, canopy reflectance	7

CHAPTER 2

THE EFFECTS OF UNDERGROUND NATURAL GAS LEAKAGE ON PLANT GROWTH

2.1 Introduction

Hydrocarbon gases in the soil may be sourced from natural hydrocarbon seeps or from leaking gas pipelines. Gas pipeline leaks are caused by aging of the pipelines or through human activities. If the leak is large or undiscovered for a long time, substantial volumes of gas are lost with an associated loss of revenue. Natural hydrocarbon seepage emissions contribute approximately 5 - 13% of the total methane budget (Etiope and Klusman, 2002). In general, the locations of long-term natural hydrocarbon seeps are known if they are located in populated areas so that care can be taken to avoid explosions. However earthquakes may cause a shift of their location (Jones and Burtell, 1996). When the hydrocarbon gases reach the atmosphere, they can form an explosive mixture with air, resulting in dangerous situations. Early detection of anomalous soil gas concentrations could therefore help to prevent dangerous situations.

Remote sensing has been suggested as a new method for gas detection (Zirnig *et al*., 2002; Van Persie *et al*., 2004). The changes in vegetation growth due to gas leakage may be detected using remote sensing and as such could serve as indicator of gas leakage. For reliable gas leakage detection using vegetation reflectance, it is essential to know how the gas in the soil affects the vegetation and how this is related to the reflectance. The influence of leaking gas on vegetation was investigated by Pysek and Pysek (1989), who tested the influence of natural gas on 35 plant species. Nearly all species showed a moderate to strong reduction in growth. Many of the species did not flower or reproduce, while some did not grow at all. A similar trend was identified by Godwin *et al*. (1990), who tested the influence of gas migrating from two oil wells on the growth of wheat (*Triticum aestivum*) and rape seed (*Brassica napus*). The wheat showed a reduction in height within a radius of 2.5 to 3 m of the wells, whereas the rape seed showed a reduction in height up to 7 m away. Up to a distance of 1.5 m away from the wells, the weight of the roots of both species and the weight of the wheat stems were lower. The changes in growth were believed to be a result of low oxygen levels in combination with excess availability of nutrients such as manganese. Other studies show that plants growing in soil contaminated by natural gas have chlorotic leaves (Oliveira *et al*., 1997), reduced growth (Hoeks, 1972b; Smith *et al*., 2004b) and changes in

the spectral reflectance (Bammel and Birnie, 1994; Oliveira *et al*., 1997; Reid *et al*., 1988; Smith *et al*., 2004b; Yang *et al*., 1999).

There is general consensus that stress symptoms in the plants arise from changes in the soil environment. The natural gas displaces the soil air, which results in oxygen shortage in the soil environment (Braverman *et al*., 1962; Hoeks, 1972a). The oxygen concentration in the soil may decrease further owing to methanotrophic bacteria, which oxidize the methane present in natural gas, generating high concentrations of carbon dioxide and water (Hanson and Hanson, 1996). A study by Steven *et al*. (2006) showed that in addition to oxygen displacement by methane, bacterial oxygen depletion ranged from 1.8 to 4.7 % (as percentage of total soil air), depending on temperature and crop type.

Although in large gas leaks oxygen shortage may be the cause of growth and reflectance changes, in small leaks there may be no oxygen shortage. Since all work so far was done on large leaks - e.g. 250 l/h (Pysek and Pysek, 1989), 100 l/h (Smith *et al*., 2004b), - and natural hydrocarbon seeps, it is not known if natural gas itself affects plant growth. It is assumed that methane is not toxic to plant roots (Arthur *et al*., 1985) or aboveground parts of plants (Gustafson, 1944). Natural gas however comprises not only methane (CH_4; 70 to 95%) but also ethane (C_2H_6; 0 to 20%), higher hydrocarbons such as propane and butane (< 1%) and small concentrations of other components such as nitrogen, carbon dioxide and oxygen (Olah and Molnar, 2003; Hoeks, 1972a). If natural gas (or one of its components) affects plant growth, small leaks that do not cause oxygen shortage could then be detected in addition to larger leaks that cause oxygen shortage.

The objective of this chapter is to understand how natural gas and two of its components methane and ethane affect plant growth. Two experiments were undertaken to compare the effects of a small natural gas leak without oxygen shortage with a large leak. In both experiments, plant morphology and chlorophyll content were measured for maize and wheat plants. The results of this study are discussed in respect to their importance for the detection of gas leakage using vegetation reflectance.

2.2 Materials and methods

2.2.1 Greenhouse experiment

The first experiment was performed in a greenhouse in Wageningen, the Netherlands from January 8, 2004, to March 22, 2004. The species used in the experiment were maize (*Zea mays* cv *Nescio*) and spring wheat (*Triticum*

aestivum cv *Pasteur*). Natural gas, methane and ethane were delivered to pots such that oxygen shortage in the soil was avoided. Each gas was mixed with air before use by a gas company (Hoek Loos B.V., Schiedam, the Netherlands) and put in cylinders, after which each gas-air mixture was delivered to separate sealed pots. Natural gas, methane and ethane gas-air mixtures are explosive so all the gas was mixed up to 50% of the Lower Explosive Level (Table 2.1). The oxygen concentration in the gas-air mixes ranged from 20.4% to 20.8%. In this manner the plants would not experience oxygen shortage in the soil and the gas concentration could be kept constant in the pots. The natural gas consisted of 81% methane, 3% ethane, less than 1% of higher hydrocarbons and 15% of other gases, of which nitrogen comprised the major part. The control consisted of pure air (containing 21% O_2, 79% N_2 and less than 0.05% CO_2 and H_2O; Hoek Loos B.V., Schiedam, the Netherlands) and was delivered similarly to the hydrocarbon mixtures. Each gas was delivered through plastic pipes of 1 mm diameter to eight pots with maize and eight pots with wheat (resulting in a total of 64 pots). Each pot (diameter 25 cm, volume 10 l) was lined at the base with 1 kg of gravel for easier dispersal of the gas and then filled up with 8 l of sandy loam (consisting of 80% sand, 10% silt and 10% clay) that was fertilized with 8 g of NPK fertilizer (1:0.8:0.7). Porosity of the soil was 49% and the pH was 6.0 (measured following the method of Henderschot *et al*. (1993). The pots were placed in the greenhouse at a distance of 35 cm from each other in a randomized block design (Cochran and Cox, 1992; Figure 2.1). Each block contained one replicate per gas, ensuring that each replication was located at a different location in the greenhouse thereby minimizing 'nuisance' effects of temperature and light differences, while within each block the gas treatments were positioned randomly. On January 2nd 8 seeds were sown in each pot, and at January 8th the seedlings emerged. When each plant had developed two leaves, the four smallest plants were removed and the pots were covered with black and white plastic containing holes for four plants to grow through (Figure 2.2). To seal the pots airtight, the holes around the plants were closed with tape and petroleum jelly after which gas delivery started (t = 1; 14 days after sowing). Since the soil porosity was 49%, approximately 5 l of gas mixture was needed to fill all pores. To ensure that the soil was flushed thoroughly, 10 l of gas mixture was delivered per pot each day at 10.00 hrs (which corresponded to 12 minutes of gassing). The number of days that gas delivery took place varied between 35 and 43 (Table 2.1). During the gas delivery, a small hole in the pot was opened to release pressure in the pot. Directly after the gas was switched off, the hole was closed again. The temperature in the greenhouse was kept between 15 and 22°C. To ensure that the plants received a constant minimum amount of light independent of daily incoming light, UV lamps were switched on from 7.00 to 19.00 hrs. Average incoming photosynthetically active radiation (PAR) received from the UV lamps as measured at different locations in the greenhouse was on average 153 ± 7 µmol/m^2/s (measured with the Beam Fraction sensor of the SunScan Canopy Analysis System, Delta-T Devices Ltd,

Cambridge, UK). Since this is a relatively low value (as a comparison, Stewart *et al*. (2003) measured values up to 1500 µmol/m^2/s), most of the primary production was dependent on incoming light from outside. The pots were watered twice a week starting with 120 ml and increasing up to 600 ml.

Figure 2.1 (left) Gas delivery to pots placed in randomized blocks in the greenhouse.

Figure 2.2 (right) Pot with 4 maize plants

2.2.2 Field experiment

In the field experiment, a large natural gas leak was simulated at the Sutton Bonington campus of the University of Nottingham, UK (52.8°N, 1.2°W). Natural gas was delivered to 2.5 m square canopy plots of maize (*Zea mays* cv *Nescio*) and wheat (*Triticum aestivum* cv *Pasteur*). Two maize plots (Mg1 and Mg2) and two wheat plots (Wg1 and Wg2) received gas, while two other plots were gas-free (Mc1 and Wc1; Figure 2.3). The seeds were sown on the 10th of June 2003 at a density of 16 maize plants per m^2 and 64 wheat plants per m^2. As in the greenhouse experiment, 14 days after sowing the gas was switched on (t = 1). The soil consisted of a 30 cm top layer of clay loam overlying a 70+ cm clay and marl horizon (Reeve, 1975). Mains gas is dehydrated during processing (Kennedy, 1993), so in order to avoid dehydration of the soil, the plots were watered regularly. The average temperature ranged from 15 °C (night) to 22.4 °C (day).

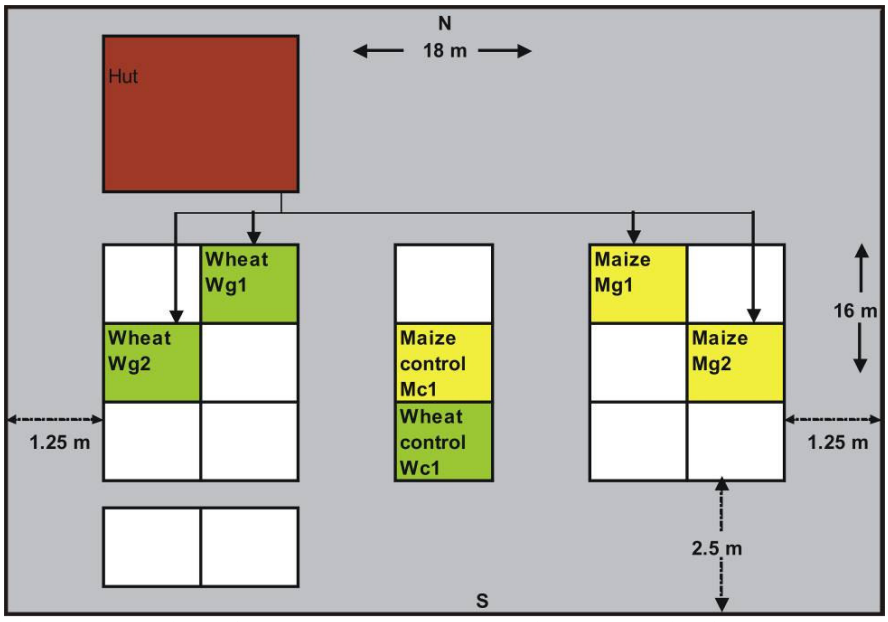

Figure 2.3 Locations of the two gassed wheat plots, the two gassed maize plots and the control plots. The unnamed (white) plots were used for other experimental work.

Mains natural gas was delivered through 25 mm pipe into the soil 1 m below the centre of each plot for 45 days. The gas flow, which was fixed at approximately 100 l/h, was distributed through small holes at 3 cm intervals around the lower 20 cm of the pipes. To enable soil gas and oxygen concentration measurements, four plastic tubes of 4 cm diameter were inserted in the soil up to 50 cm deep, on 50, 100, 150 and 200 cm from the edge of each plot. A GMI Gasurveyor methane monitor was attached to the outflow side of each tube to measure the volume % of soil methane and oxygen in the soil. Gas measurements were performed daily between 8:00 and 9:00 am.

2.2.3 Growth analysis

In the greenhouse, the height and number of leaves of all plants were measured once a week. Leaf chlorophyll was measured at t = 32 on the fourth upper leaf of each plant and analysed according to the method described by Wellburn (1994). The absorption of the chlorophyll content was read on an Ultrospec II spectrophotometer (Biochrom Ltd., Cambridge, UK).

In the field experiment, the height and number of leaves of twelve plants per plot were measured weekly, using a stratified random sampling design (Webster and Oliver, 1990). Fractional canopy cover (%) was estimated on 1 m^2 in the centre and at the edge of the plots. Canopy cover is dependent on canopy

structural attributes such as leaf area, leaf angle distribution and clumping (Bacour *et al*., 2006). In both experiments, an indication of maize leaf area was obtained by measuring leaf width and length of the same plants that were used for the chlorophyll measurements, multiplied by a correction factor of 0.75 (Daughtry, 1990). Only in the field experiment this could be translated to the more commonly used leaf area index, or LAI, which is the leaf area per unit area of soil surface (Daughtry, 1990). Since each plant occupied a space of 25 by 25 cm, an indication of the LAI was obtained by dividing the leaf area by 625 cm^2. Chlorophyll content was measured at t = 35 on eight leaves taken from each plot, following the method described by Bruinsma (1963). Also at t = 35, leaf moisture content was measured on eight leaves from each plot centre. The leaves were clipped, weighed, cooled in ice and transported to the laboratory within 2 hours after clipping. After the leaves had dried in an oven at 70°C for four days, the leaves were weighed again, and the moisture content was calculated as

$$100 * \frac{FreshWeight - DryWeight}{FreshWeight} \tag{2.1}$$

At the last day of the experiment (t = 45) the number of maize plants that had developed aboveground adventitious roots and the number of ears per plant were counted. Finally, since Godwin *et al*. (1990) found increased manganese levels in the soil, a visual inspection of the leaves was performed to determine if the plants suffered from manganese toxicity. Typical manganese toxicity is visible as brown speckles on the leaves and crinkled leaves with chlorotic spots (Wu, 1994).

2.2.4 Statistical analysis

In the greenhouse each pot was considered a separate treatment. Therefore, data of all plants in one pot were averaged and the pot average was used subsequently for statistical analyses. In the field, the plots were the different treatments. The Kruskal-Wallis test was used to determine whether the measured variables differed among the different treatments. The Kruskal-Wallis test is the non-parametric alternative to the one-way ANOVA test and is used when the samples do not follow a normal distribution. It tests the null hypothesis that the different treatments belong to the same group. When the null hypothesis was rejected, the post hoc test described by Conover (1999) was used to find out which groups caused the significant differences.

Table 2.1 Characteristics of greenhouse and field experiment

Variables	**Greenhouse**				**Field**
Gas	Control	Natural gas	Methane	Ethane	Natural gas
Number of gas delivery days	43	41	35	39	45
Percentage gas in mixture [%]	0	2.5	2.49	0.73	100
Pure gas per p(l)ot [l/day]	0	0.246	0.283	0.075	2250
Measurement days (t) of:					
Plant height	7, 12, 22, 28, 32, 42, 49, 60				11, 16, 22, 29, 35, 42
Nr of leaves	7, 12, 22, 28, 32, 42, 49, 60				11, 16, 22, 29, 35, 42
Reflectance	11, 19, 26, 32, 40, 47, 63				11, 16, 22, 29, 35, 42
Chlorophyll	32				35
Species	*Zea mays Nescio; Triticum aestivum Pasteur*				*Zea mays Nescio; Triticum aestivum Pasteur*
Date of sowing	02-Jan-04				10-Jun-03
Number of days between sowing and first gassing date:	14				14

2.3 Results

2.3.1 Gas concentration

The number of gas delivery days was 39 ± 4 days in the greenhouse and 45 days in the field (Table 2.1). In the greenhouse the average gas flow per pot varied between 75 ml and 283 ml per day, while in the field the gas flow per plot varied between 768 and 3276 l per day (Table 2.2). The gas distribution within the plots was similar for each plot with a high gas concentration in the centre of the plot, which decreased towards the edges. The oxygen concentration in the control plots was on average 20%, which is a normal concentration for well aerated soils (Brady, 1984). In the gassed plots oxygen concentrations decreased towards the centre to an average of 11%, while average methane concentrations in the centre varied between 4% and 13%. The weekly average gas and oxygen concentrations were used for further analyses. The correlation between the average methane and oxygen concentration in the soil was weakly linear (R^2 of 0.44; Figure 2.4).

Table 2.2 Average gas flow per day under the four plots.

Plot	Average gas flow [l/h]	CH_4 concentration [%] ± st. dev		O_2 concentration [%] ± st. dev	
		25 cm	*75 cm*	*25 cm*	*75 cm*
Maize plot 1	102	10.01 ± 7.78	1.39 ± 1.82	12.62 ± 4.28	17.08 ± 1.19
Maize plot 2	32	3.80 ± 4.79	1.07 ± 1.37	13.02 ± 3.40	18.99 ± 0.55
Wheat plot 1	153	12.64 ± 7.79	0.65 ± 0.70	9.73 ± 4.98	18.13 ± 1.26
Wheat plot 2	88	10.06 ± 8.37	1.09 ± 1.59	11.80 ± 4.92	19.20 ± 0.52
Average	*93.75*	*9.13 ± 7.18*	*1.05 ± 1.37*	*11.79 ± 4.39*	*18.35 ± 0.88*

2.3.2 Plant growth - greenhouse

During the first week after the gas had been switched on, the height of the plants growing in gas was not affected. At $t = 12$ (nearly two weeks after the gas had been switched on), the first differences between the different treatments became noticeable in the height of the maize plants (Figure 2.5). From $t = 12$ till $t = 49$, the plants growing in ethane were 12% to 19% smaller than the control plants on each measurement day ($p \leq 0.05$). The plants growing in natural gas and methane were 4% to 8% smaller, but only the difference between natural gas and control at $t = 22$ was statistically significant. On the last gas delivery day ($t = 43$), plants growing in natural gas, methane and ethane were respectively 8%, 8% and 15% shorter than the control plants. The height of the treated wheat plants was not reduced.

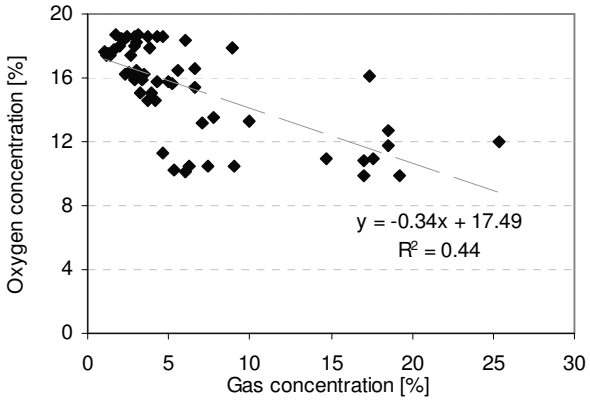

Figure 2.4 Oxygen as a function of methane concentration. The regression equation and R^2 are shown.

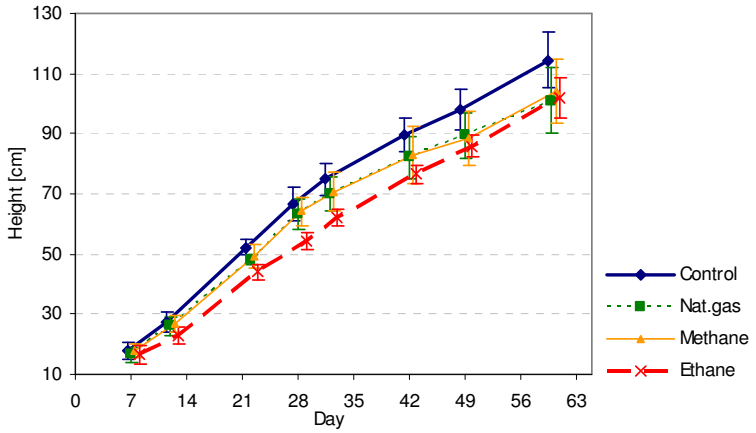

Figure 2.5 Height of maize plants in the greenhouse. Between $t = 12$ and $t = 49$ the difference between the ethane and control treatments was significant on each measurement day ($p \leq 0.05$), while at $t = 22$, the natural gas treatment was significantly lower than the control. Methane did not cause significant differences in height.

Although the ethane-treated plants had the highest number of leaves for both species (maize: 6.3 leaves compared to 6 leaves on the control plants; wheat: 4.3 leaves compared to 4.1 on the control plants), the differences between the treatments were not significant (Table 2.3). However the leaf area of the ethane-treated plants was significantly lower than the leaf area of the control plants (94 cm^2 compared to 147 cm^2, $p \leq 0.05$). The differences in chlorophyll content were not significant for both species.

Table 2.3 Plant height (cm), number of leaves and chlorophyll content (mg/g) at $t = 32$. Similar letters behind the values indicate that these treatments belong to the same group ($p \leq 0.05$; Conover post-hoc test). * The number of leaves of the wheat plants was not measured after $t = 12$. Data shown here are from $t = 12$.

Treatment	Plant height [cm]	Number of leaves	Total chlorophyll [mg/g]	Leaf area [cm^2]
		Maize		
Control	74.8 ± 5.3^{a}	6.0 ± 0.2^{a}	3.3 ± 0.2^{a}	691.9 ± 101.9^{a}
Natural gas	69.9 ± 5.6^{a}	5.9 ± 0.3^{a}	3.2 ± 0.3^{a}	620.6 ± 190.5^{a}
Methane	70.8 ± 6.3^{a}	6.0 ± 0.3^{a}	3.2 ± 0.3^{a}	613.2 ± 65.9^{a}
Ethane	62.2 ± 2.6^{b}	6.3 ± 0.6^{a}	3.3 ± 0.2^{a}	434.0 ± 130.9^{b}
		Wheat		
Control	47.6 ± 0.9^{a}	$4.1 \pm 0.6^{a*}$	3.3 ± 0.2^{a}	
Natural gas	47.1 ± 1.7^{a}	$4.1 \pm 0.7^{a*}$	3.3 ± 0.3^{a}	
Methane	47.7 ± 1.7^{a}	$4.1 \pm 0.5^{a*}$	3.4 ± 0.2^{a}	
Ethane	46.6 ± 1.7^{a}	$4.3 \pm 0.6^{a*}$	3.3 ± 0.1^{a}	

2.3.3 Plant growth - field

Plant height, number of leaves, leaf area and leaf chlorophyll of both species reduced considerably in the centre of the gassed plots. The decrease was first visible between t = 11 and t = 16 (Figure 2.6). At t = 35 maize plant height had decreased with over 50% in the centre 50 by 50 cm, while chlorophyll content and leaf area had decreased with over 60% (Table 2.4). Outside the centre 50 by 50 cm, maize plant height was approximately 10% lower than the control plant height, however, leaf chlorophyll and canopy cover were higher than on the control plots. The number of plants with aboveground adventitious roots and the number of ears per plant at the last day of the experiment (t = 42) were higher on the gassed plots than on the control plots (Table 2.5). The wheat number of leaves and chlorophyll had decreased with over 60%, whereas plant height had barely decreased in the centre of the gas-plots and had increased at the edges of the gas-plots (not statistically significant). Leaf moisture content was similar for the gassed and control plants (Table 2.4). There were no signs of manganese toxicity.

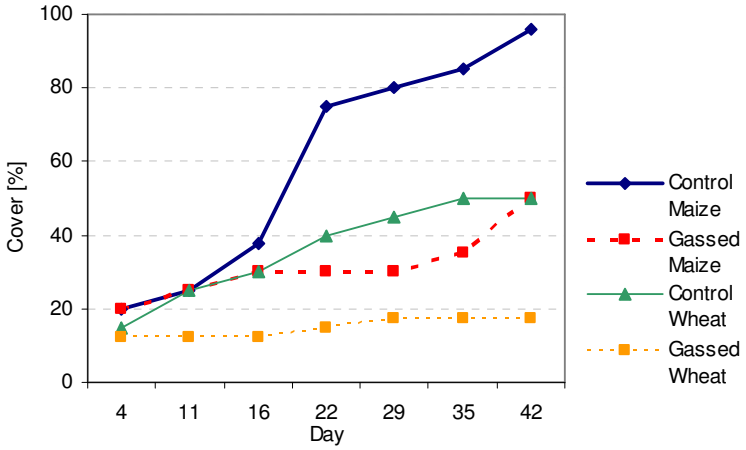

Figure 2.6 Canopy cover between t = 4 and t = 42 on the control and gassed plots.

Table 2.4 Average canopy characteristics (field) at $t = 35$. Leaf area is shown in cm^2; an indication of the leaf area index LAI is stated in brackets. Similar letters behind the values indicate that these treatments belong to the same group ($p \leq 0.05$; Conover post-hoc test). As canopy cover was estimated on two locations per plot, there were not enough variables for a statistical comparison.

Location	Plant height [cm]	Number of leaves	Total chlorophyll [mg/g]	Canopy cover [%]	Leaf area [cm^2] (LAI)	Leaf moisture [%]
			Maize			
Control	129.6 ± 5.4^{a}	10.3 ± 0.9^{a}	2.54 ± 0.01^{a}	85.0 ± 0.0	2573.7 ± 327.8^{a} (4.1)	80.5 ± 0.3^{a}
Edge	114.6 ± 20.2^{b}	10.0 ± 1.3^{a}	3.36 ± 0.02^{b}	90.0 ± 0.0	1919.5 ± 598.5^{a} (3.8)	-
Centre	57.5 ± 17.7^{c}	7.0 ± 1.4^{b}	1.01 ± 0.00^{c}	32.5 ± 3.5	609.2 ± 255.5^{b} (1)	80.3 ± 1.3^{a}
			Wheat			
Control	44.1 ± 6.6^{a}	9.1 ± 2.4^{a}	4.49 ± 1.02^{a}	50.0 ± 0.0	-	76.1 ± 0.5^{a}
Edge	44.6 ± 5.8^{a}	6.1 ± 2.3^{a}	3.78 ± 0.56^{a}	50.0 ± 0.0	-	-
Centre	42.5 ± 3.5^{a}	3.5 ± 0.7^{b}	1.21 ± 0.12^{b}	15.0 ± 0.0	-	75.8 ± 1.2^{a}

Table 2.5 Number of ears per plant; number of plants with adventitious roots at $t = 45$

	Number of plants [with percentage of total]	
	Control [N = 178]	Gassed [N = 191]
0 ear	2 [01.1%]	24 [12.6%]
1 ear	171 [96.1%]	136 [71.2%]
2 ears	5 [02.8%]	31 [16.2%]
Adventitious roots	22 [12.4%]	78 [40.8%]

2.4 Discussion

2.4.1 Greenhouse

Since the effects of gas leakage on vegetation growth were mostly studied in large leaks, it was not known how vegetation reacts to small gas leaks that do not cause oxygen shortage in the soil. The results of this study show that ethane gas in concentrations less than 1% affected maize growth. Ethane caused a lower plant height and lower leaf area compared with the control. Natural gas and methane both caused a slightly lower (less than 8%) height and leaf area. Since the natural gas used in this experiment consisted of 81 % methane, the effects of both gases were expected to be comparable. This was indeed the case: the plant characteristics in the natural gas and methane treatments were nearly similar and mostly took an intermediate position between the control and ethane treatments.

The hydrocarbon gases caused a delay in the reaction of maize height of approximately 10 days for ethane and 20 days for natural gas and methane.

Although ethane caused a delay in growth early in the experiment, after approximately t = 28 the difference between the control and ethane height reduced. In contrast, the difference in height between the control and the natural gas or methane treatments increased after this date. Between t = 28 and t = 60 (three weeks after gassing finished), the plants growing in ethane changed from 81% to 89% of the control height, whereas the plants growing in natural gas decreased in height from 95% to 89% of the control height. This suggests that ethane caused a reduced growth early in the experiment, whereas natural gas caused a decrease in height approximately ten days later. It is not clear why, compared with methane and natural gas, ethane caused a lower plant height and leaf area. Several strains of bacteria are known to degrade ethane, propane and butane (Wagner *et al*., 2002), chlorinated ethane components (Janssen *et al*., 1987) and small quantities of ethane and propane (Hoeks, 1972a). Belay and Daniels (1987) demonstrated that methanogenic bacteria were able to produce ethylene from halogenated hydrocarbons such as bromoethane, dibromo- and dichloroethane. In addition Adamse *et al*. (1972) showed that several strains of bacteria and fungi generated ethylene during growth on methane. Ethylene is a plant hormone that promotes plant maturing and in larger quantities is inhibitory to plant growth (Leopold and Kriedemann, 1975). In seedlings, ethylene causes inhibited stem elongation and stem thickening (Abeles, 1992). Since Adamse *et al*. (1972) tested merely two fungi, other fungi might exist that are able to generate ethylene from pure ethane, which would then explain the decrease in plant height.

The hydrocarbon gases had no noticeable influence on wheat plant development. Wheat plants have a different photosynthesis method ('C3') than maize plants ('C4'), which enables them to survive at lower light intensities and temperatures than C4 plants (Ehlinger and Monson, 1993). Although maize is tolerant of a wide range of temperatures (Grubben and Soetjipto Partohardjono, 1996), the greenhouse temperature was closer to the wheat optimum (10 to 24°) than to the maize optimum (between 20 and 30°). The relatively low temperatures may have made the maize plants more susceptible than the wheat plants to changes in the root zone.

2.4.2 Field

Whereas the wheat plants had a similar height in both the greenhouse and the field at t = 35, the maize plants in the field were approximately 50 cm taller than the greenhouse plants. Exceptional high temperatures in summer 2003 caused this increased growth rate in the maize plants, which grow best in (sub) tropical conditions (Grubben and Soetjipto Partohardjono, 1996). Between t = 16 and t = 22 the average daily temperature was 26.2 °C (over 7 °C higher than a week earlier), which is reflected in a very fast increase in maize canopy cover (Figure 2.6).

The high gas flow in the field caused a significant drop in oxygen levels in the centre of the gas-plots. Plants need oxygen in their root-zone for respiration and in general a shortage of soil oxygen leads to reduced plant growth (Drew, 1991). In this study, both maize and wheat canopy cover, plant height and leaf chlorophyll had decreased in the centre 50 cm of the gas-plots. The small extent of this area of reduced growth is reflected in the gas concentrations. Although the gas flow was as high as 150 l/h, only the centre 50 cm of the gas-plots had high gas concentrations. At 75 cm distance from the source, the average gas concentration had decreased to about 1%, with oxygen concentrations ranging between 17 and 19%. The reason for the small area with high gas concentrations is most likely the fact that the gas pipeline ended in a very dense clay soil. Due to the low porosity of the clay, the gas did not spread far from the exit point of the pipe.

The first changes in the cover and plant height were visible at $t = 11$. This is relatively soon compared to similar studies on the effects of gas on plant growth. Pysek and Pysek (1989) observed a decrease in plant height and vegetation cover 15 to 30 days after the start of their experiment in which they gassed several species with natural gas, while two studies by Smith *et al.* (2004a; 2004b) showed that the first visible stress symptoms in grass and dwarf bean (*Phaseolus vulgaris*) gassed with natural gas occurred respectively 44 days and 2 to 3 weeks after the gassing had started. As shown by these studies the first evidence of stress symptoms is dependent on species and at which point during the growth cycle the leakage starts. In our experiment, gassing started early in the growth cycle when the plants are most sensitive to oxygen shortage (Mason *et al.*, 1987; Zaidi *et al.*, 2003).

The relatively high leaf chlorophyll content and canopy cover in the edges of the maize gas-plots was unexpected, particularly because plant height had decreased in this area. The increased number of adventitious roots and the higher number of ears per maize plant both suggest that the plants surrounding the gas leak were further in their development than the control plants. Surface plots of the maize plant height at the last measurement day ($t = 45$) clearly show a gap in the centre of the plot (Figure 2.7).

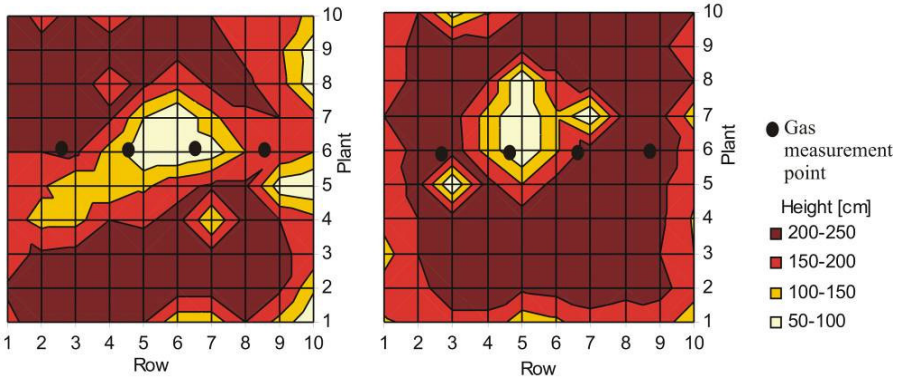

Figure 2.7 Plant height in the gassed maize canopy at t = 45. The plants growing in the centre 50 by 50 cm are significantly smaller than the surrounding plants. For easier interpretation, the plant height was interpolated.

Due to the decreased plant height in the centre, more light could enter the canopy, thereby creating favourable growth conditions for the plants surrounding the gap. These plants could orient their leaves horizontally compared to the plants in the control plots (Figure 2.8a), which explains the higher cover at the edges of the gas-plots. The wheat plants growing around the gassed area were not further developed than the control plants. Although there was a gap in the canopy in the centre of the gas-plots (Figure 2.8b), this did not seriously improve the light conditions in the surrounding canopy, where the low cover already enabled the light to enter the canopy.

Another reason for the advanced development of the plants may have been a build-up of ethylene in the soil or in the plants. As discussed in the greenhouse section, fungi or bacteria that consume methane or ethane may produce ethylene. Plants that experience oxygen shortage in the root zone generally have increased internal ethylene concentrations, which are known to induce the growth of adventitious roots in maize (Drew *et al.*, 1979). Ethylene also promotes maturing of plants, which would explain the higher number of ears. However, the maize leaves showed a relatively high leaf chlorophyll content, whereas ethylene is in general associated with decreasing leaf chlorophyll (Abeles *et al.*, 1992). Therefore it is assumed that the better light conditions were the reason for the advanced growth surrounding the gassed area.

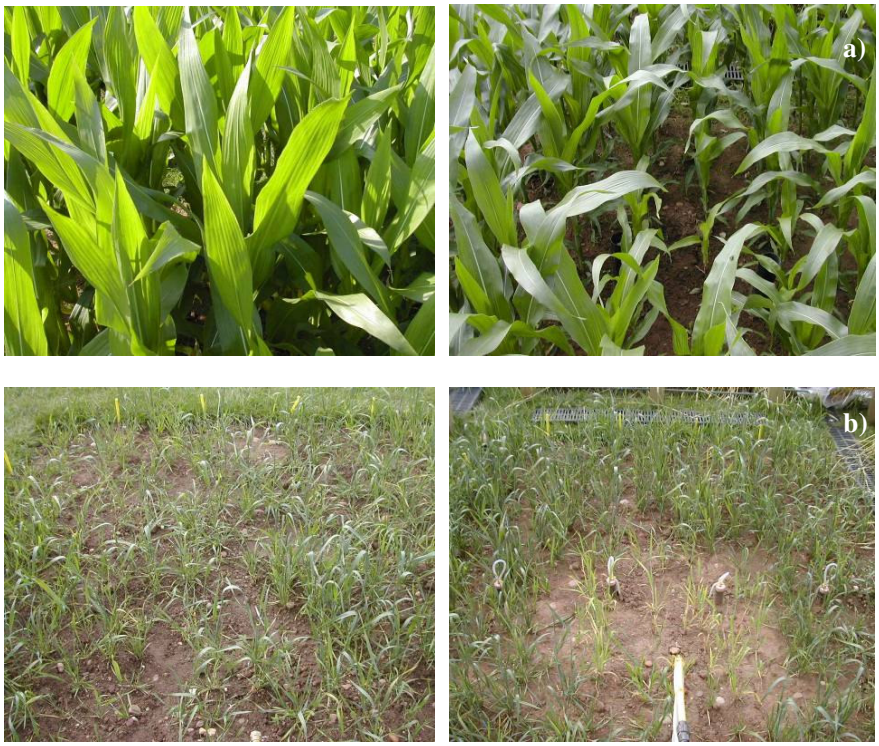

Figure 2.8 Control and the gassed canopy at t = 35 on the maize (a) and wheat (b) plots. The canopy cover is lower in the centre of the gassed plots and maize plant height has significantly reduced. The maize plants surrounding the gassed centre have more horizontally oriented leaves than the plants on the control plots.

2.4.3 Detection of gas leaks using vegetation growth

The purpose of the experiments was to understand which changes occur in plant growth as a result of natural gas leakage in order to define how these changes can serve as indicators of gas leakage. The results showed that ethane caused a decrease in leaf area and height of the maize plants, but did not affect chlorophyll. Methane did not affect plant growth. The ethane concentration in the natural gas treatments was too low to have an effect. For a concentration of 0.75% of ethane in the soil (as in this study), the natural gas concentration should be between approximately 4 and 20%, depending on the concentration of ethane in natural gas. In this experiment, gas concentrations higher than 10% resulted in a strong decrease in plant height, leaf area, canopy cover and leaf chlorophyll content, most likely due to oxygen shortage in the root zone. Since plant height and leaf area decreased in both experiments, these characteristics should be the main focus of gas leak detection.

2.5 Conclusions

This chapter shows that a decrease in leaf area is the clearest indication that plants are affected by gas leakage. Large leaks with gas concentrations over 10% cause a significant reduction in leaf area and chlorophyll, which is in accordance with earlier studies (Pysek & Pysek, 1988; Smith *et al*., 2004b). However, the effects of small leaks on plant growth had not been studied before. Whereas most authors assumed that natural gas itself does not affect plant growth, this study shows that in small leaks without oxygen shortage ethane causes a reduction in maize height and leaf area. This means that small natural gas leaks that do not cause oxygen shortage can be detected if the ethane concentration is at least 0.75%, which in theory occurs at natural gas concentrations of 4 to 20%. Methane itself did not affect plant growth, which supports the results of Arthur *et al*. (1985). To detect both small and large leaks using maize reflectance, the focus should therefore be on leaf area and less on leaf chlorophyll. However, although the leaf area of the maize plants decreased in ethane concentrations of 0.75 %, the wheat plants were not affected. The next chapter will investigate whether the difference between the reactions of maize and wheat to hydrocarbon gases also occurs in the leaf reflectance.

CHAPTER 3 *

CONTINUUM REMOVED BAND DEPTH ANALYSIS FOR DETECTING THE EFFECTS OF NATURAL GAS, METHANE AND ETHANE ON LEAF REFLECTANCE

3.1 Introduction

Vegetation growing in soil contaminated with natural gas is known to show changes in spectral reflectance, particularly in the 'red edge' region (the slope between red and near infrared reflectance). The red edge commonly shifts towards shorter wavelengths in stressed vegetation (Boochs *et al*., 1990; Horler *et al*., 1983). In most studies, the red edge of vegetation canopies shifted towards shorter wavelengths when exposed to natural hydrocarbon seepage (Reid *et al*., 1988; Bammel and Birnie, 1994) or to simulated gas leakage (Oliveira *et al*., 1997; Smith *et al*., 2004b). Smith *et al*. (2004a) demonstrated that soil oxygen displacement by natural gas, argon and waterlogging caused an increase in reflectance in the visible region and a change in the shape and position of the red edge. These results suggested that the changes in reflectance due to gas leakage are caused by oxygen shortage and not by the natural gas itself (Smith *et al*., 2004a). Detecting gas leakage using vegetation reflectance would then be similar to detecting the effects of soil oxygen shortage, making the use of additional data such as gas pipeline maps necessary for reliable gas detection (Smith *et al*., 2004a). However, Chapter 2 showed that ethane causes a reduction in maize height and leaf area, suggesting that at least one component of natural gas affects plant growth. This chapter investigates whether the changes in plant growth are accompanied by changes in leaf reflectance. The gases were confined to the root zone of the plants so that any effect by the gases is likely to be noticed first in the root function. Since a major function of roots is supplying plants with water and nutrients (Lynch, 1995), it is expected that malfunctioning of the roots will result in reflectance changes commonly related to plant stress, such as increased reflectance in the chlorophyll and water absorption regions (Carter, 1993; Lichtenhaler *et al*., 1996). Chlorophyll has strong absorption in the visible region, while leaf water absorbs mainly in the near and shortwave infrared (Curran, 1989; Tucker, 1980). Absorption feature analysis using continuum removal has been shown to enhance the differences in

* This chapter is based on: Noomen, M.F., Skidmore, A.K., van der Meer, F.D. and Prins, H.H.T., 2006. Continuum removed band depth analysis for detecting the effects of natural gas, methane and ethane on maize reflectance. Remote Sensing of Environment 105: 262-270.

shape between the absorption features of interest (Kokaly and Clark, 1999). In this study, continuum removal was applied to two chlorophyll absorption features and two water absorption features to study whether natural gas, methane and ethane in the soil increase the reflectance in these absorption features. In addition, the red edge position (REP) and the physiological reflectance index (PRI; Gamon *et al*., 1992) were calculated to test whether photosynthesis was affected by any of the gases.

3.2 Methods

The experiment was carried out in a greenhouse in Wageningen, the Netherlands from January 8, 2004, to March 22, 2004. For a full description of the set-up of the experiment, refer to Chapter 2.2.1.

3.2.1 Reflectance measurements.

Leaf reflectance was measured weekly starting from t = 11 (Table 3.1). The measurements were made with a GER3700 spectroradiometer (Geophysical and Environmental Research Corporation, Buffalo, New York), which has 704 channels ranging from 1.5 nm bandwidth in the visible and near infrared to 9.5 nm in the SWIR. The sensor, a fibre optic with a 10° field of view, was held 6 cm above the leaf that was measured, which corresponded to approximately 1 cm in the field of view. A Lowel Pro-light (a 14.5V, 50W halogen lamp; Lowel-Light Mfg. Inc, New York) mounted on a tripod was used to illuminate the plants from 10 cm above the plants. To avoid shadows, the light was positioned a few degrees off-nadir. From each of the 4 maize plants in one pot, 5 spectral measurements were taken of random leaves. Afterwards the mean of all spectra from one pot was calculated to average out differences in reflectance as a result of different leaf angles or BRDF (Nicodemus, 1977; Sandmeier and Deering, 1999). The radiance output of the GER spectrometer was converted into reflectance using the reflectance of a white Spectralon reference panel as reference (Labsphere, North Sutton, UK) that was measured after each pot measurement.

3.2.2 Data analysis

The reflectance was analysed using continuum removal for four major absorption features. Continuum removal normalizes spectra by applying a convex hull over that part of the spectrum that will be analysed (Kokaly and Clark, 1999). Dividing the reflectance at a certain wavelength in the absorption feature by the value of the hull at that wavelength gives a relative value for the absorption between 0 and 1 (Clark and Roush, 1984). The edges of the

absorption features were chosen such that the deepest absorption was located approximately in the centre of the continuum removed region. Continuum removal has been used to correlate absorption feature depths with biochemical concentrations in dried and fresh plant material (Kokaly and Clark, 1999; Curran *et al*., 2001; Mutanga *et al*., 2004).

After continuum removal was applied, the band depth (BD) at each wavelength in the absorption feature was calculated by subtracting the continuum removed reflectance (CRR) from 1 (Kokaly and Clark, 1999):

$$BD(\lambda) = 1 - CRR(\lambda) \quad (3.1)$$

The band depth was normalized by dividing the band depth at a certain wavelength by the maximum band depth for that absorption feature (Kokaly and Clark, 1999):

$$NBD(\lambda) = \frac{BD(\lambda)}{BDmax} \quad (3.2)$$

where NBD(λ) is the normalized band depth at wavelength λ and BDmax the maximum band depth in the absorption feature.

Both band depth and normalized band depth were used to compare the difference between the control, natural gas, methane and ethane treatments. Note that in most studies only the maximum band depth was calculated, but in this study the band depth at each wavelength within the absorption feature was calculated to obtain an overview of the overall shape of the absorption feature. The wavelengths between which the continuum removal was applied were chosen such that the whole feature of interest was included (Figure 3.1, Table 3.1).

In the visible region, the main feature of interest was the chlorophyll content. Chlorophyll absorption occurs at 430, 460, 640 and 660 nm, thus continuum removal was applied between 400 and 550 nm - the latter being the green reflectance peak - and between 550 and 750 nm. The 550-750 nm region has been used before in a continuum removal study on canopy reflectance by Mutanga *et al*. (2005). Water absorption occurs mainly around 1450 and 1940 nm (Curran, 1989), so continuum removal was applied between 1370 and 1570 nm and between 1870 and 2170 nm.

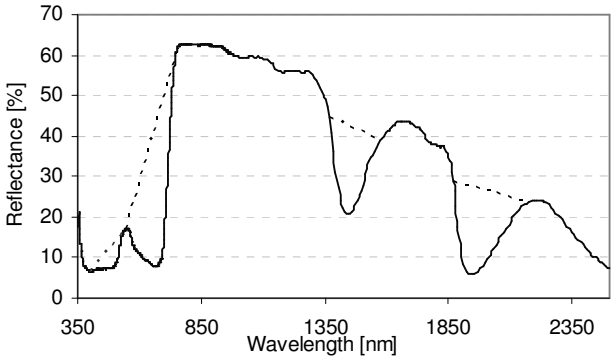

Figure 3.1 Reflectance spectrum showing the continuum removed regions (see Table 3.1 for exact location of starting and ending wavelengths of each region).

Table 3.1 Edge wavelengths between which continuum removal was applied and the days that spectral measurements were made.

Region	Wavelength [nm]	Days that spectra were measured:
Blue	400 - 550	$t = 11$; $t = 19$; $t = 26$; $t = 32$;
Red	550 - 750	$t = 40$; $t = 47$; $t = 63$
Water absorption	1370 - 1570	
Water absorption	1870 - 2170	

The differences in BD and NBD were compared statistically. The reflectance values were tested for normality using the Shapiro Wilk's W test. Since all values that were tested in this experiment were normally distributed, a one-way ANOVA test was used to test for significant differences (p-level ≤ 0.05). In the case of significant differences in the chlorophyll and water absorption regions, the Bonferroni post hoc test was applied to test which groups are significantly different. The Bonferroni test performs multiple comparisons based on the Student's t-test and adjusts the significance level for the fact that multiple comparisons are made (Miller, 1985).

Finally, a sensitivity analysis was performed on the absorption feature that yielded the highest number of significant differences compared to the control after continuum removal. The aim of the sensitivity analysis was to find out if the significant differences are related to the location of the convex hull. Continuum removal was performed 6 times using different edge wavelengths for each analysis. Subsequently the band depths were analysed statistically and compared to the bands of the original absorption feature.

The red edge position (REP) is a commonly used indicator of changes in chlorophyll. Although chlorophyll content was similar for all treatments at t =

32 (Chapter 2), the red edge position (REP) was calculated to test whether this was true for all timesteps. The REP was calculated using the method proposed by Guyot & Baret (1988; see Appendix I for the formula). Maracci *et al*. (1991) found that the photosynthetic efficiency of maize plants could decrease while chlorophyll content remained the same. Therefore the physiological reflectance index (PRI) was calculated to obtain an indication of the photosynthetic activity. The PRI $\frac{R(570)-R(531)}{R(570)+R(531)}$ (where R is reflectance at 570 nm and 531 nm) correlates with changes in xanthophyll cycle pigments, which in turn vary due to changes in photosynthetic light use efficiency (Gamon *et al*., 1992). An increasing PRI correlates with a decreasing photosynthetic efficiency (Strachan *et al*., 2002). Differences in REP and PRI were tested for significance using a one-way ANOVA.

3.3 Results

3.3.1 Comparison of band depths

Maize
On average, the control plants had the deepest band depths in all absorption regions while ethane-treated plants had the shallowest band depths. The band depths of the plants treated with natural gas and methane were intermediate. Figure 3.2 shows the difference between the control and the hydrocarbon treatments for each wavelength. Those wavelengths where the control band depths were more than 2% larger than any of the treated band depths were selected for further analysis (Table 3.2). Statistical comparison of the selected band depths showed that ethane caused a significant decrease in band depth for most of the wavelengths, except for the blue region (Table 3.2). Natural gas and methane showed a significant decrease at a few wavelengths in the 1420-1480 nm region (Table 3.2).

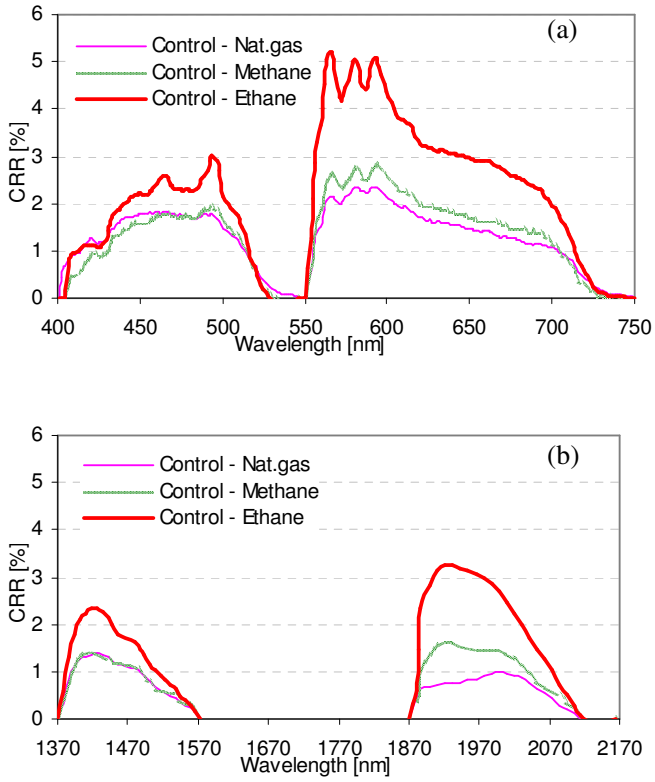

Figure 3.2 Average differences in band depth between control and hydrocarbon treatments in chlorophyll absorption features (a) and water absorption features (b). A positive difference means that the control reflectance had deeper band depths (or greater light absorption) than the hydrocarbon treatments. Ethane caused the largest difference with the control.

Table 3.2 Wavelengths at which the average band depths (BD) and normalized band depths (NBD) of any of the gas treatments were more than 2% different from the control and where the difference was statistically significant ($p \leq 0.05$).

Absorption region [nm]	Difference BD > 2%	Significance BD ($p \leq 0.05$)	Difference NBD > 2%	Significance NBD ($p \leq 0.05$)
400-550	455-510	None	None	None
550-750	560-700	Eth: 560-700	Eth: 560-600	Eth: 560-592
1370-1570	1420-1480	All gases: 1420-1448 Nat & Eth: 1456-1480	None	None
1870-2170	1920-2050	Eth: 1909-2052	None	None

Over the course of the experiment, the difference between ethane and control was greatest at the first measurement date (t = 11; Figure 3.3). After t = 11, the patterns are similar for the three gas treatments (ethane, methane and natural gas, though natural gas is not shown).

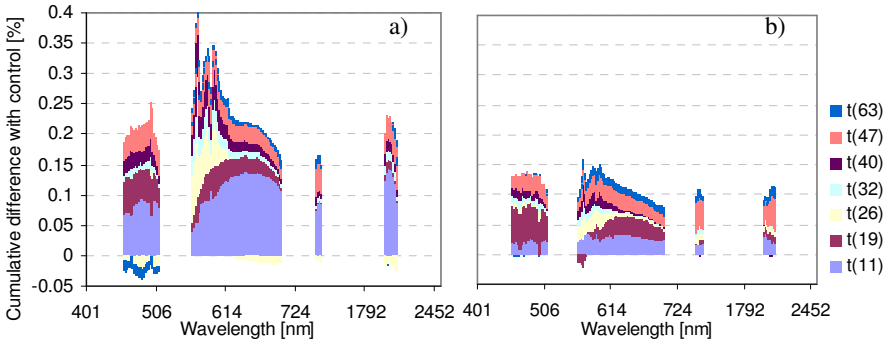

Figure 3.3 Stacked differences in band depth between ethane and control (a) and methane and control (b) for 7 timesteps. A positive difference means that the control band depth was larger than the gas band depth at that wavelength.

Wheat
There were no differences in the wheat band depths.

3.3.2 Comparison of normalized band depths

Maize
Normalization of the band depths enhances differences in the shape of the absorption features. After normalization, only the treatment band depths between 560 and 600 nm had on average 2% decreased compared to the control

band depths. The NBD of the ethane treatment between 560 and 592 nm was significantly ($p \leq 0.05$) lower than the control reflectance (Table 3.2).

Over time, the pattern of the normalized band depths of the ethane treatment shows an apparent shift in reflectance towards longer wavelengths in the visible region. The normalized band depths of the plants growing in ethane were deeper than the control band depths in the region of 500-550 nm, whereas at 550-670 nm the band depths of the control plants were deeper than the ethane bands (Figure 3.4). Between 670 and 750 nm (the red edge region) the band depths of the ethane plants were again deeper than those of the control plants. Translated into reflectance, this means that the ethane reflectance has shifted towards longer wavelengths compared to the control reflectance in the visible region (Figure 3.5). The maximum shift occurred between 570 and 670 nm, where ethane caused a shift of 1 to 5 nm towards longer wavelengths.

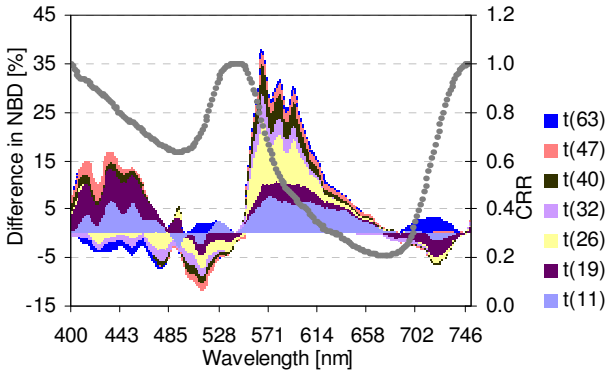

Figure 3.4 Difference between normalized band depths of control and ethane (left y-axis) of each timestep plotted against a reflectance curve. Exactly at the reflectance minima at 490 and 680 nm, the difference changes from positive to negative. At the reflectance peak at 550, the difference changes from negative to positive.

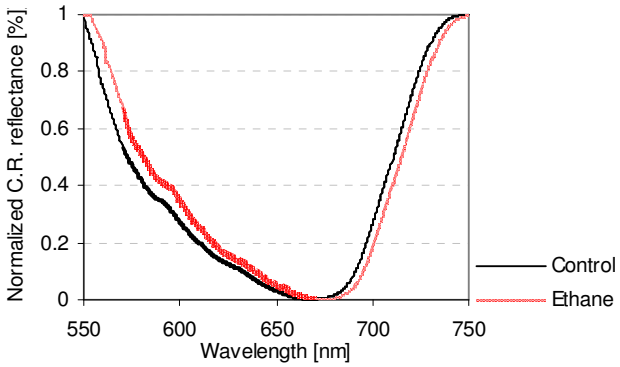

Figure 3.5 Normalized band depth analysis showed that ethane caused an apparent reflectance shift towards longer wavelengths in the blue and red absorption features. The maximum shift occurred in the red absorption feature (shown here), particularly between 570 and 670 nm (indicated by increased thickness of the line), where ethane caused a shift of 1 to 5 nm towards longer wavelengths.

Wheat

There were no differences between the normalized band depths of the wheat leaves.

3.3.3 Selection of wavelengths that best discriminate the treatments

The reflectance at those wavelengths that showed the largest difference between control and gas treatment for the maize plants was analysed for its patterns over time to find the wavelength that best discriminates between the four treatments over time. The continuum removed reflectance (= 1 – band depth) at all wavelengths was plotted in time and analysed visually. The region in which ethane caused a statistically significant different reflectance in both band depth and normalized band depth (between 560 and 590 nm) was also the best for discriminating between the gases. On all (except the last) dates, the continuum removed reflectance of the control was lowest, the ethane reflectance highest, while natural gas and methane were intermediate (Figure 3.6). The wheat reflectance in the region between 560 and 590 nm was the same for all treatments, except at $t = 26$ where ethane had a slightly higher reflectance. This difference was not statistically significant at $p \leq 0.05$.

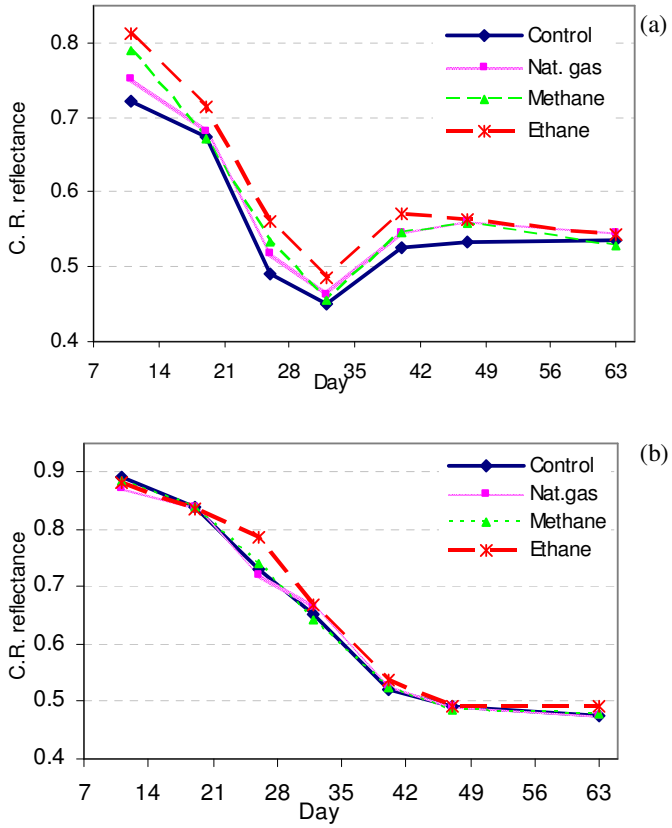

Figure 3.6 Continuum removed (C.R.) reflectance at 580 nm over time for maize (a) and wheat (b). Except for the last date, the control reflectance is always lower than natural gas and methane, which in turn always have a lower reflectance than ethane.

3.3.4 Sensitivity analysis

If the changes in band depth caused by ethane are genuine and not related to the location of the convex hull, the statistical significance of the difference between the control and ethane treatments should not be affected when the 'edge points' of the hull are changed. This was tested by narrowing the red absorption feature by 5 nm on each side, i.e. from 550-750 to 555-745 nm, followed by a one-way ANOVA. This was repeated six times until the absorption feature had its edge points at 580 and 720 nm. The results show that within each absorption feature, the significant differences in band depth between the ethane treatment and the control occurred at the same wavelengths (Table 3.3).

Table 3.3 Wavelengths at which the difference in band depth between the control and the ethane treatment was statistically significant ($p \leq 0.05$), analysed for 7 absorption features with varying width. Narrowing the absorption feature by 5 to 30 nm on each side shows that within each absorption feature, the difference between ethane and control is significant at the same wavelengths.

Feature width [nm]	Wavelengths at which difference control – ethane is significant [nm]
550-750	552-705
555-745	556-703
560-740	561-703
565-735	566-705
570-730	572-705
575-725	578-706
580-720	582-707

3.3.5 Red edge position and physiological reflectance index

The red edge position was similar for all treatments at all timesteps (Figure 3.7). Although the REPs of the wheat leaves showed slightly larger differences between the treatments, they were not statistically significant ($p \leq 0.05$).

Figure 3.8 shows that during much of the experiment, the PRI of the maize plants growing in ethane was higher than the PRI of the control plants. The maximum difference between the control PRI and the PRI of the hydrocarbon treatments occurred at t = 26 and was 0.02 (natural gas), 0.04 (methane) and 0.07 (ethane). The average difference between the ethane and control treatments over time was statistically significant ($p \leq 0.05$). The PRI of the wheat plants is similar for all treatments. As seen in the 580 nm reflectance, the plants growing in ethane have a slightly increased PRI at t = 26. The difference in time was not statistically significant.

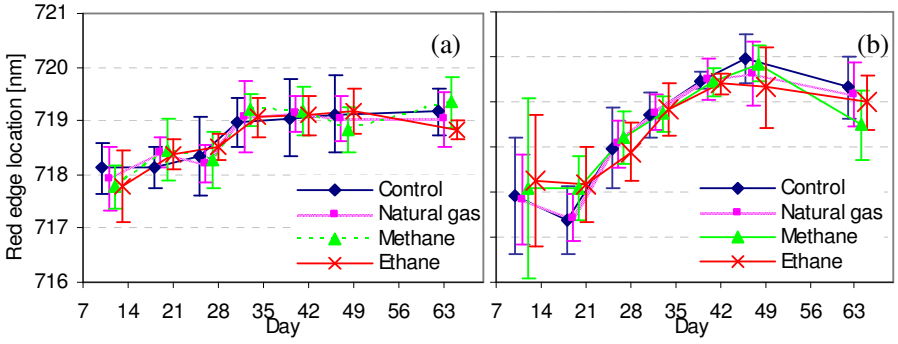

Figure 3.7 Red edge positions over time for maize (a) and wheat (b)

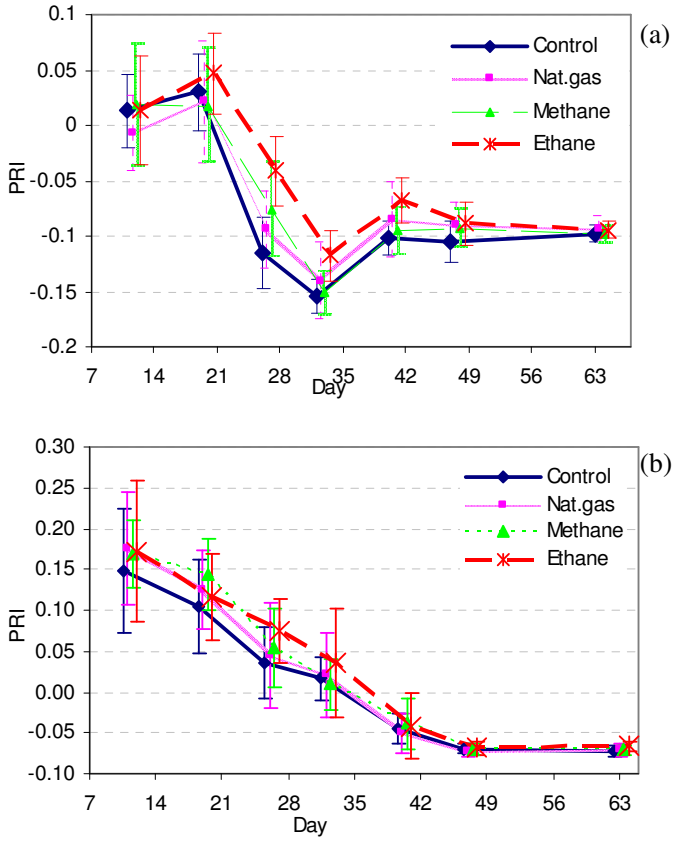

Figure 3.8 The physiological reflectance index PRI over time for maize (a) and wheat (b). The bars indicate the standard deviation.

3.4 Discussion

Only ethane caused a significant decrease in absorption in the red region (550-750 nm). In particular the 560-600 nm region of the red absorption feature was affected with a decreased band depth of up to 14% compared to the control (Figure 3.2). This is the slope between the green reflectance peak and the red absorption trough: the plants growing in ethane should therefore be more orange in colour than the control plants, but this was not visible by eye. An increased yellow leaf reflectance has been related to a lack of chlorophyll (Benedict and Swidler, 1961; Gates *et al*., 1965). Demetriades-Shah *et al*. (1990), Gitelson and Merzlyak (1998) and Adams *et al*. (1999) tested the relationship between chlorophyll content and ratios based on the reflectance in the yellow region, all

showing that a lower chlorophyll content caused higher reflectance values (or lower band depths).

When the pattern over time is considered, the difference between the ethane and the control reflectance was largest at the first measurement date (t = 11). After t = 11, the difference decreased (Figure 3.3). The large difference at t = 11 combined with the rapid decrease in difference between the control and ethane band depths thereafter suggests that the plants growing in ethane had a lack of chlorophyll early in experiment but recovered quickly, even during continued gas administration. Ethane gas delivery stopped at t = 37. In subsequent weeks, the difference between the control and ethane reflectance became minimal in the chlorophyll region (Figure 3.3). Chapter 2 showed that ethane caused a decrease in leaf area and plant height after two weeks of gassing. Since this chapter shows that the largest difference in chlorophyll occurred at t = 11, this confirms that ethane caused a delay in plant growth in the first two weeks of gassing. In section 2.4.1 it was suggested that a build-up of ethylene could be the cause of the decrease in leaf area and plant height. In the same way, ethylene may have caused a decrease in leaf chlorophyll.

The most remarkable effect of normalizing band depths was the apparent shift of the ethane reflectance towards longer wavelengths over the whole region between 400 and 750 nm. The shift is 'apparent' as it was caused by normalizing the band depths; in the normal (continuum removed) reflectance there is no such shift. To illustrate that the shift is purely caused by normalizing the absorption features, Figure 3.9 shows the band depths and normalized band depths of the control and the ethane treatments. The largest shift in the normalized reflectance occurred in the yellow region on the slope between the green reflectance peak and the red absorption trough (Figure 3.4). Between t = 11 and t = 32, the reflectance in the yellow region of both the control and ethane plants shifted towards shorter wavelengths which coincides with the highest growth rate of the plants during the experiment. This shift of the green-red slope reflectance towards shorter wavelengths can be explained by an increase in chlorophyll content due to the growth of the plants, which broadens the red absorption feature (Banninger, 1991). Since the difference between the control and ethane reflectance decreased over time, it is assumed that this is due to a faster increase in chlorophyll content in the plants treated with ethane than in the control plants. At t = 32 chlorophyll in the ethane treated plants is similar to the control (Table 2.3). This supports our earlier assumption that ethane stressed the maize plants at the start of the experiment, after which they began to recover. At t = 63, the difference between the normalized band depths of the control and ethane treatments was reduced to an average of less than 1% in the chlorophyll absorption troughs, confirming the full recovery of the plants gassed with ethane (Figure 3.4).

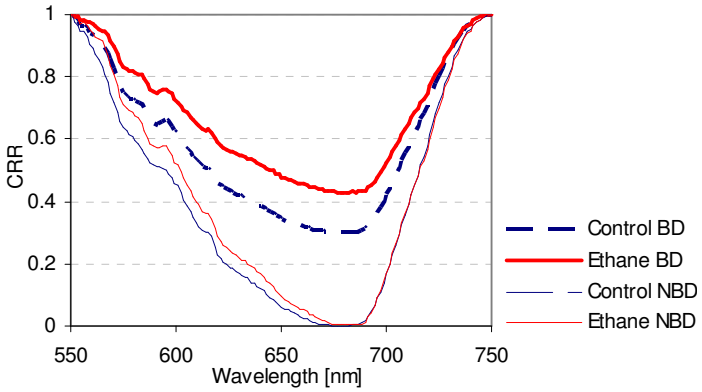

Figure 3.9 Control and ethane band depths (BD) and normalized band depths (NBD) at *t* = 11

In the water absorption features, all hydrocarbon gases caused reduced band depths (or higher reflectance), compared to the control. However, ethane caused a decrease in absorption for all wavelengths in the water absorption features, while natural gas and methane showed a decrease only in the 1420-1480 nm region. An increase in reflectance in the 1450 and 1950 nm regions is generally the result of a decrease in plant water status (Hunt and Rock, 1989; Carter, 1991; Cibula *et al*., 1992; Danson *et al*., 1992; and Sims and Gamon, 2003). This suggests that the hydrocarbon gases caused a reduction in water uptake, resulting in lower water content and higher reflectance in the water absorption regions. Even though delivering the gases directly to the soil could have caused slight dehydration of the soil resulting in a reduced water uptake, it is noted that the control received an air mixture in the same manner.

Although the results suggest that plants growing in ethane had lower leaf chlorophyll early in the growing season, the differences were too small to cause a shift of the red edge position towards shorter wavelengths. Maracci *et al*. (1991) found that dehydration of *Zea mays* barely affected the chlorophyll content in the leaves but that photosynthetic efficiency was reduced. The PRI is one of the few indices that measure the photosynthetic efficiency, and Thenot *et al*. (2002) and Evain *et al*. (2004) showed that the PRI could be used as a reliable water stress index. In this study, the PRI of the plants treated with ethane was higher than the PRI of the control plants. Natural gas and methane caused only a slightly higher PRI than the control, thus it is assumed that the water uptake reduction caused by methane and natural gas was minor, affecting the photosynthetic activity slightly but not affecting the chlorophyll content. Ethane caused a much larger decrease in water uptake particularly at the start of the experiment, affecting the photosynthetic activity (and chlorophyll content)

negatively. After t = 32, the PRI of the treatments increased, which coincided with the start of a slower plant growth rate, while after t = 40, the PRI of all treatments converged, indicating that the treated plants were recovering.

As was shown in Chapter 2, wheat growth was not affected by any of the gases. Band depth analysis showed that the plants did not show any difference in leaf reflectance either. Only the PRI of the ethane treated plants is slightly increased at t = 26. The difference is not significant, however it does occur at the same date that also the ethane-treated maize plants have the greatest increase in PRI. Although in Chapter 2 it was concluded that ethane did not affect wheat plants, the results from this chapter suggest that ethane did affect the plants, but very weakly. Unfortunately the low number of replicates cannot distinguish whether the measured differences are an artefact or not. The reason for the difference between the reactions of maize and wheat is unclear. In section 2.4.1 it was suggested that the wheat plants were less sensitive to the gases because the greenhouse temperature was closer to the wheat optimum (10 to 24°) than to the maize optimum (between 20 and 30°), which may have made the maize plants relatively susceptible to changes in the root zone.

3.5 Conclusion

The objective of this chapter was to test whether natural gas, methane and ethane in the soil cause an increase in continuum removed reflectance in the chlorophyll and water absorption regions. Although methane and natural gas caused a minor decrease in band depth in the chlorophyll absorption regions, only ethane caused a significant decrease in band depth in the 550-750 nm absorption feature, in particular in the yellow region (560-600 nm). Normalization of the band depths resulted in an apparent shift in reflectance towards longer wavelengths in the blue and red absorption features of the ethane treatment. The differences between the ethane and control treatments were most pronounced at the start of the experiment until t = 32 days, after which the plants growing in ethane appeared to recover.

The water absorption bands of the gassed plants were less deep than those of the control plants, although the decrease in water absorption caused by natural gas and methane was minor compared to the decrease caused by ethane. Since water stress has been shown to be related to a decrease in photosynthetic activity, the PRI was calculated to test if this had occurred. The PRI confirmed that gases (particularly ethane) seemed to decrease the photosynthetic activity. The red edge position was not affected.

The general assumption was that natural gas does not affect vegetation reflectance, but this chapter shows that ethane – which comprises up to 10% of natural gas – does affect the reflectance in the chlorophyll and water absorption regions of the maize plants. Although the physiological process is not yet understood, the combination of reduced band depths in the chlorophyll and water absorption regions and the increased PRI suggested that ethane gas in the soil hampered normal water uptake by maize plants in the early stage of their growth. Methane and natural gas caused a minor decrease in water uptake and photosynthetic activity, but are not believed to have caused a decrease in chlorophyll content.

Although further research is necessary to upscale the results from this experiment to the field, this chapter has shown promising results for the detection of natural gas leakage using vegetation reflectance. For the detection of small natural gas leaks, the increased reflectance in the 560-590 nm region caused by ethane - visible in both the BD and NBD analysis - together with the increased PRI are promising indicators of gas leakage. Since the ethane concentration in this study was approximately 0.75% and ethane comprises 3% - 20% of natural gas, the concentration of natural gas must be between 4 to 20% in the soil environment to make detection possible. Since gas concentrations in this range may be accompanied by methanotrophic bacterial activities, oxygen and carbon dioxide concentrations in the soil could change. The following chapter investigates whether anomalous carbon dioxide concentrations affect leaf reflectance.

CHAPTER 4 *

EFFECTS OF HIGH SOIL CO_2 CONCENTRATIONS ON MAIZE LEAF REFLECTANCE

4.1 Introduction

Carbon dioxide (CO_2) in the soil atmosphere occurs at most gas leaks and hydrocarbon seeps – either as component of the seepage gas or generated by methanotrophic bacteria that oxidize methane gas (Hoeks, 1972a; Steven *et al*., 2006). Bacterial oxygen depletion is accompanied by an increase in CO_2 in the soil environment up to concentrations of 5% - 15% (Hoeks, 1972a). Other sources of CO_2 are the decay of organic materials and landfills (Arthur *et al*., 1985; Hanson and Hanson, 1996; Schumacher, 1996). Geological sources of soil CO_2 include CO_2 seeps (Macek *et al*., 2005; Tóth *et al*., 1994) and volcanic CO_2 sources (Bergfeld *et al*., 2006). To mitigate the effects of CO_2 on global warming, CO_2 may be stored underground in depleted oil or gas reservoirs, adding one more potential source of CO_2 leakage (Holloway 2005; Li *et al.* 2006). Especially CO_2 seepage and volcanic CO_2 may be dangerous to humans and animals. As CO_2 gas is heavier than air, concentrations may build up close to the ground, resulting in atmospheric oxygen shortage, which may lead to suffocation (Hepple and Benson, 2001; Tóth *et al*., 1994). High soil CO_2 is known to have killed trees and other vegetation by disrupting the root respiration and by acidification of the ground water (Macek *et al*., 2005; Bergfeld *et al*., 2006). As Chapter 2 and 3 have shown, ethane gas causes a decrease in maize growth and leaf area and an increase in the yellow reflectance. As CO_2 may have an additional effect on plant growth or reflectance, the effects of five different concentrations of CO_2 on plant growth and reflectance are examined in this chapter. Direct detection of anomalous CO_2 concentrations is difficult and time consuming, as CO_2 fluxes as well as the natural background concentrations are variable (Tóth *et al*., 1994; Oldenburg *et al*., 2003). Therefore, De Jong (1998) attempted to detect CO_2 seepage indirectly using vegetation reflectance. Imaging spectrometry was shown to be a promising tool to monitor tree stress resulting from high soil CO_2 fluxes. The red edge position (REP), which is commonly used as an indicator of vegetation stress (Boochs *et al*., 1990; Horler *et al*., 1983), shifted towards shorter wavelengths over the area with killed trees (De Jong, 1998). Although vegetation reflectance made the detection of CO_2 seepage possible, the area

* This chapter is based on: Noomen, M.F. and Skidmore, A.K., *in review*. The effects of high soil CO_2 concentrations on leaf reflectance. International Journal of Remote Sensing.

studied by De Jong was a large region where CO_2 fluxes were high and the effects readily visible by the human eye. In this chapter, it was tested whether the REP can distinguish CO_2 concentrations varying from 2% to 50%. Increasing chlorophyll content causes a widening and deepening of the red absorption feature (Buschmann and Nagel, 1993, Dawson and Curran, 1998). A deepening of the absorption feature can be seen as an increase in height of the first derivative peak at around 720 nm and a shift of this peak towards longer wavelengths. However, since the REP is the transition between chlorophyll absorption and NIR, the height and location of the peak is not only related to an increase in chlorophyll, but also to a heightened NIR reflectance (Adams *et al.,* 1999; Maas and Dunlap, 1989; Bowman, 1989). A widening of the absorption feature can also be seen in the 550-670 nm region, which is less affected by cell structure and water content (Baret *et al.,* 1987, Gates *et al.,* 1965, Adams *et al.,* 1999). The previous chapter has shown that subtle differences in chlorophyll content were better visible in the yellow region than in the red edge. In this chapter the correlation between leaf chlorophyll and reflectance in both the red edge and the yellow region is studied using different methods. The aim of this study was twofold: I. to determine which method resulted in the highest correlation with leaf chlorophyll; and II. to use this method to study the effects of CO_2 on leaf chlorophyll. In addition, the first derivative peaks at 700 nm (REP), 1400 nm and 1900 nm (water absorption regions) were analysed to obtain an indication of leaf moisture content.

4.2 Methods

The experiment was undertaken in a greenhouse in Wageningen, the Netherlands from the 8th of January 2004 till the 22nd of March 2004. The species used in the experiment was maize (*Zea mays* cv *Nescio*). The gas that was delivered to sealed pots was mixed with normal air and put in 10-litre cylinders under a pressure of 150 Bar.

Table 4.1 Number of days that CO_2 gas was delivered to the maize plants, the average amount of CO_2-air mixture per pot (l) and the concentration (%) and amount (ml) of pure CO_2 per pot.

Concentration	Number of delivery days	Average amount per pot per day (l)	CO_2 in mixture (%)	Pure CO_2 per pot per day (ml)
2% CO_2	44	9.38	1.99	186
5% CO_2	48	8.52	5.01	426
10% CO_2	49	8.93	10.10	901
20% CO_2	40	10.42	20.18	2101
50% CO_2	20	20.83	50.53	10526

Carbon dioxide was mixed with air to 2%, 5%, 10%, 20% and 50% of CO_2 in air, corresponding to O_2 concentrations of approximately 19.6%, 19%, 18%, 16% and 10% (see Table 4.1 for the exact CO_2 concentrations in air). Delivering these gas mixtures to the soil ensured that the concentration of CO_2 in air would be constant. Each gas mixture was delivered to eight maize pots (resulting in a total of 40 pots), which were placed at a distance of 35 cm from each other in a randomized block design (Cochran and Cox, 1992). For additional information about the set-up of the experiment please refer to Chapter 2.2.1.

4.2.1 Growth analysis

At t = 32 (halfway the experiment) and t = 63 (after recovery) the height, dry weight and chlorophyll content of the plants were measured. Aboveground dry weight was measured after the plants had dried in an oven at 70°C for four days. Chlorophyll content was measured on the fourth upper leaf of each plant. The analysis was carried out according to the method described by Wellburn (1994). The absorption of the chlorophyll content was read on an Ultrospec II spectrophotometer (Biochrom Ltd., Cambridge, UK). A one-way ANOVA was used to test whether the differences between the treatments were statistically different. When differences occurred, the Bonferroni post-hoc test (which adjusts the significance level for the fact that multiple comparisons are made; Miller, 1985) was applied to determine which groups are differing from each other.

4.2.2 Reflectance measurements

Leaf reflectance was measured at t = 19, 26, 32, 47 and 63. For additional information about the reflectance measurements, please refer to Chapter 3.2.1.

4.2.3 Data analysis

When vegetation reflectance measurements are taken over time, illumination and background signals from soil and atmospheric may vary due to meteorological and seasonal changes. Reflectance band ratios and the first derivative of the reflectance minimize background noise (Broge and Leblanc, 2000; Demetriades-Shah *et al*., 1990; Kumar *et al*., 2001). In this chapter the first derivative is analysed to detect the effects of CO_2 on plant growth. Prior to analysis, the first derivative data were smoothed using the Savitsky-Golay second-order polynomial smoothing function over a 5-band window (Savitsky and Golay, 1964). The red edge position (REP) - which is the inflection point on the slope between the red absorption and near infrared reflectance - is often used to correlate chlorophyll content with reflectance (Collins, 1978; Boochs *et*

al., 1990; Horler *et al*., 1983; Curran *et al*., 1995). Decreasing chlorophyll causes the red edge position to shift towards shorter wavelengths (Collins, 1978). The red edge position appears as a peak in the first derivative of the reflectance spectra (Figure 4.1a). Several methods have been proposed for the calculation of the position of this peak, such as determining the wavelength at which the maximum in the first derivative occurs (Boochs *et al*., 1990; Horler *et al*., 1983), Lagrangian interpolation between 3 points on the first derivative maximum (Dawson and Curran, 1998), linear interpolation between four points in the spectra (Guyot and Baret, 1988) and higher order polynomial and Gaussian fitting (Bonham-Carter, 1988; Pu *et al*., 2003). Cho and Skidmore (2006) recently developed a simple and promising linear extrapolation method to determine the red edge position. Two straight lines were fitted through two wavelengths in the far-red (680 to 700 nm) and two wavelengths in the NIR (725 to 760 nm) of the first derivative (eq. 4.2 and 4.3), after which the intersection of the lines was calculated to determine the REP (eq. 4.4). This method showed high correlations with maize leaf nitrogen (which is closely correlated to chlorophyll (Lamb *et al*., 2002)) and appeared to be superior in predicting leaf nitrogen content compared to the other methods.

$$\text{Far red line} = m_1\lambda + c_1 \tag{4.2}$$

$$\text{NIR line} = m_2\lambda + c_2 \tag{4.3}$$

$$\text{REP} = \frac{-(c1 - c2)}{(m1 - m2)} \tag{4.4}$$

where m and c are the slope and intercept of the lines and λ is the wavelength at the intercept (Cho and Skidmore, 2006).

A random sample of 32 maize leaves (of which the chlorophyll content was known) was used to compare the linear extrapolation method by Cho and Skidmore (2006) with the first derivative peak maximum method and the interpolation methods by Dawson and Curran (1998) and Guyot and Baret (1988). The method with the highest correlation was subsequently used to determine the effects of soil CO_2 on maize leaf reflectance.

In addition to the REP, a new index was calculated by applying the method by Cho and Skidmore (2006) to the 550 – 670 nm absorption feature. Instead of using wavelengths in the red region, the lines were based on the 550-560 nm region and the 572-585 nm region (Figure 4.1b). This resulted in an index hereafter named ‘yellow edge position’ or ‘YEP’. It was expected that an increase in chlorophyll would cause a shift of the YEP towards shorter wavelengths. The YEP was correlated to leaf chlorophyll using the same test sample as was used for the REP, after which the method was applied to the

dataset. To gain an indication of the width of the absorption feature, the distance between the REP and YEP was calculated for each timestep. Since Chapter 3 has shown that the yellow reflectance is sensitive to subtle chlorophyll changes, the continuum removed reflectance in the yellow region was calculated as a comparison (see Chapter 3 for a description of the methods). In addition, the maximum height of the REP peak and the depth of the water absorption features at 1400 and 1900 nm were analysed to obtain an indication of leaf water status (Figure 4.1a). A one-way ANOVA followed by a Bonferroni post-hoc test (Miller, 1985) were used to determine if the differences between the treatments were statistically significant.

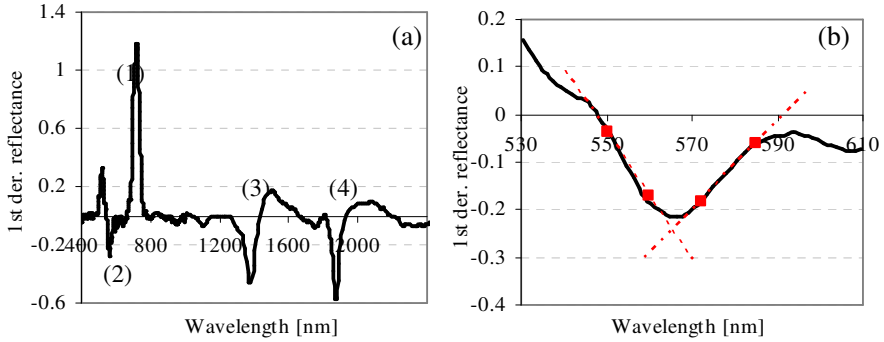

Figure 4.1a The features of interest in this study include the red edge position and the red edge maximum peak height (1), the yellow edge position (2) and the feature depths at 1400 nm (3) and 1900 nm (4) in the water absorption regions. Figure 4.1b shows the yellow edge region and the lines fitted through 550 and 560 nm, and 572 and 585 nm. The intersection point is the yellow edge position.

4.3 Results

4.3.1 Plant morphology

CO_2 delivery lasted for approximately 40 days (Table 4.1), except for 50% CO_2 which finished in 20 days. The plants in the 50% CO_2 treatment had therefore been able to recover for 12 days when the first plant morphology measurements were made (t = 32). At t = 63 all treatments had been able to recover for two weeks or more. At t = 32, plant height and leaf chlorophyll decreased with increasing CO_2 concentrations (Table 4.2). The 50% CO_2 treatment showed a decrease of 17% in plant height, 30% in dry weight and 10% in leaf chlorophyll. The differences between the 2% CO_2 treatment and the 5%, 10% or 20% treatments were not significantly different.

Although at $t = 63$ the height, dry weight and chlorophyll of all treatments have increased (Table 4.2), the 50% CO_2 treatment showed the largest relative increase. Leaf chlorophyll content of the 50% CO_2 treatment even exceeded the chlorophyll content of the 2% CO_2 treatment (3.57 mg/g compared to 3.41 mg/g). The 5% and 10% CO_2 treatments caused the lowest increase in all plant characteristics.

Table 4.2 Plant height (cm), dry weight (g) and leaf chlorophyll content (mg/g) during CO_2 delivery ($t = 32$) and during recovery ($t = 63$). Similar letters indicate that the treatments belong to the same group (ANOVA, $p \leq 0.05$).

	T = 32			T = 63		
Treatment	Height [cm]	Dry weight [g]	Chlorophyll [mg/g]	Height [cm]	Dry weight [g]	Chlorophyll [mg/g]
2% CO_2	79.67*a*	2.03*ab*	3.24*a*	118.07*a*	28.22*a*	3.41*ab*
5% CO_2	77.14*a*	2.30*a*	3.23*ab*	109.65*a*	26.75*ab*	3.32*ab*
10% CO_2	78.26*a*	2.21*a*	3.18*ab*	111.07*a*	25.34*ac*	3.15*b*
20% CO_2	71.97*ab*	1.72*ab*	3.06*ab*	105.72*a*	22.43*c*	3.23*ab*
50% CO_2	66.16*b*	1.44*b*	2.94*b*	113.25*a*	23.71*bc*	3.57*a*
Mean	*74.55*	*1.94*	*3.13*	*111.71*	*25.36*	*3.34*

4.3.2 REP and YEP correlation with leaf chlorophyll

Prior to analysing the dataset, a sample of 32 random leaves of 70-days old maize plants was used to correlate four indices with leaf chlorophyll. Leaf chlorophyll ranged from 2.8 to 3.8 mg/g. The lowest correlation with leaf chlorophyll was found for the continuum removed reflectance (R^2 under 0.2), followed by the first derivative peak and the method by Dawson and Curran (1998; R^2 under 0.5), whereas the methods by Guyot and Baret (1988) and Cho and Skidmore (2006) resulted in the highest correlations (Figure 4.2). The latter is used in the following sections to study the effects of CO_2 on leaf chlorophyll.

Although the YEP resulted in a low correlation with leaf chlorophyll, the distance between the REP and YEP (both calculated using the method proposed by Cho and Skidmore, 2006) resulted in the highest correlation (R^2 of 0.76; Figure 4.3). In the following sections the YEP and REP-YEP distance were used in addition to the REP to examine whether they can be used as indicators of high soil CO_2.

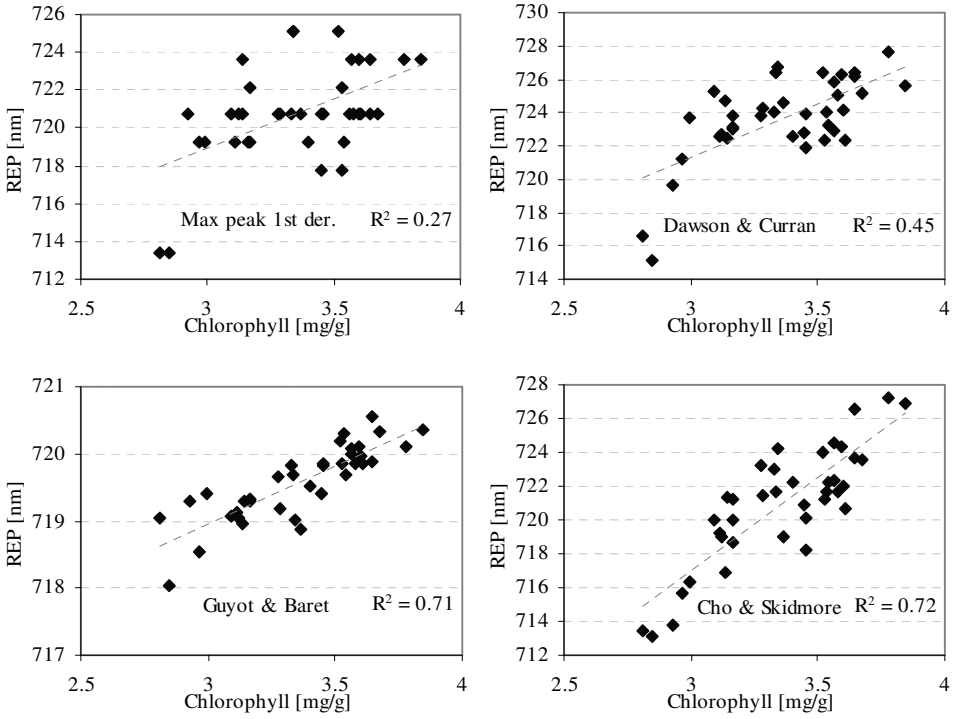

Figure 4.2 Correlation between chlorophyll content and red edge positions calculated from the first derivative maximum and the methods by Dawson and Curran (1998), Guyot and Baret (1988) and Cho and Skidmore (2006).

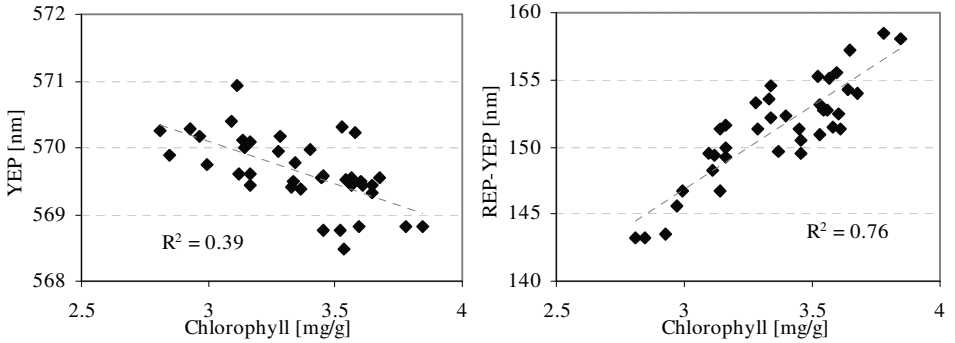

Figure 4.3 Correlation between the yellow edge position and the REP-YEP distance with chlorophyll content.

4.3.3 REP, YEP and REP-YEP distance as affected by soil CO_2

The REP of the 50% treatment caused a shift of 2 – 3 nm towards shorter wavelengths compared to the other treatments. The 2%-20% treatments were not different from each other (Figure 4.4a). The YEP of the 50% CO_2 treatment is located 3 - 5 nm towards longer wavelengths compared to the 2% CO_2 treatment, except at the last date. The YEPs of the 5%-20% treatments were located between the 2% and 50% treatments during most of the experiment (Figure 4.4b).

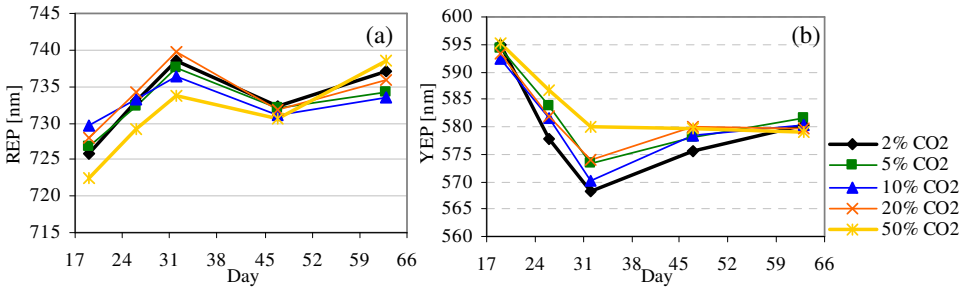

Figure 4.4a Red edge position (calculated using the method proposed by Cho and Skidmore (2006) of the five treatments over time. Figure 4.4b Yellow edge position (YEP) of the five treatments over time.

Subtracting the YEP from the REP gives an indication of the width of the red absorption feature. 50% CO_2 caused a narrowing of the absorption feature compared to the 2% CO_2 treatment of approximately 6 – 8 nm until t = 46 (Figure 4.5). The sharp increase in the REP after t = 46 is also visible in the REP-YEP distance.

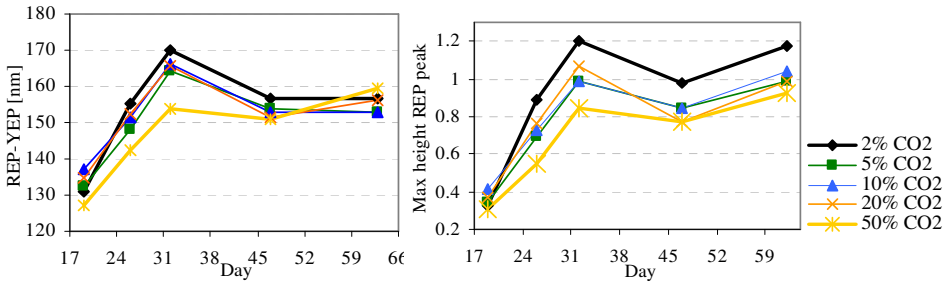

Figure 4.5 a) Distance between REP and YEP. b) REP peak height over time

The height of the REP peak indicates the length of the slope between the red absorption feature and the NIR plateau: the higher the NIR plateau compared to the red absorption feature, the higher the peak. After t = 27, the maximum peak height of 2% CO_2 was consistently higher than the peak height of the other treatments (Figure 4.5). The continuum removed reflectance in the yellow region showed an increase for the 50% CO_2 treatment; however the other treatments could not be distinguished from each other (Figure 4.6).

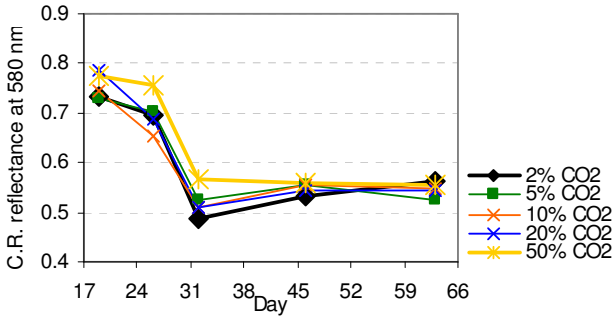

Figure 4.6 Continuum removed reflectance at 580 nm

4.3.4 Water absorption feature depths

The first derivative feature depths in the water absorption regions have been correlated to leaf water content (Danson *et al.*, 1992). The water absorption features were negatively correlated with the red edge maximum height (average R^2 of 0.97 and 0.61 (n = 40) for the 1400 and 1900 nm features respectively). Increasing CO_2 concentrations resulted in decreasing feature depths (Figure 4.7).

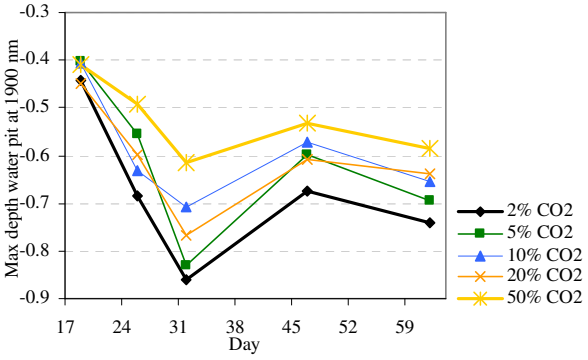

Figure 4.7 Maximum depth of the water absorption feature at 1900 nm

4.3.5 Significance of the results

To test if the differences between the indices were statistically significant ($p \leq 0.05$), a one-way ANOVA was performed for each timestep. Only at $t = 26$ and $t = 32$ could all indices distinguish the 50% treatment from the 2% treatment (Table 4.3).

Table 4.3 Statistically significant differences ($p \leq 0.05$) between the treatments of the REP, YEP, the REP-YEP distance, the maximum features heights at the REP and 1900 nm and the continuum removed reflectance (CRR) at 580 nm for 5 timesteps. Only significant results are shown. '<' or '>' show whether the REP, YEP or REP-YEP is located at shorter/higher wavelengths, or that the REP peak and 1900 nm peak are lower/higher.

Index (n = 40)	T = 19	T = 26	T = 32	T = 46	T = 63
REP	50% <10%, 20%	50%< all	50% < 2%, 5%, 20%	-	50% > 5%, 10%
YEP	-	50% > 2%	50% > 2%	-	50% < 2%, 5%
REP-YEP	50% < 5%, 10%, 20%	50% < all	50% < all	-	50% > all
Peak REP	-	50% < 2%	50% < 2%	-	-
Pit 1900 nm	-	50% < 2%	50% < 2%	-	-
Yellow CRR	-	50% > 2%	50% > 2%		

In addition, the REP-YEP distance could distinguish the 50% treatment from all other treatments. Apart from the REP, the results at $t = 26$ are similar to those of $t = 32$. After CO_2 delivery stopped, only the indices related to chlorophyll differences were statistically significant.

4.4 Discussion

4.4.1 Plant health

An aim of this study was to characterize the effects of CO_2 on leaf chlorophyll. The plant chlorophyll and morphology data at $t = 32$ suggest that an increase in soil CO_2 correlates to a decrease in leaf chlorophyll content, plant height and plant dry weight. Normal soil air contains around 0.5 to 2% CO_2 (Russell, 1973) so the 2% CO_2 treatment could be regarded as the control. This is supported by Bouma *et al*. (1997), who demonstrated that CO_2 concentrations up to 2% did not affect citrus (*Citrus volkameriana*) or bean (*Phaseolus vulgaris*) dry weight. Although literature on the effects of soil CO_2 on plant growth is sparse, it is

assumed that tolerance to high CO_2 concentrations is dependent on species, cultivar (Huang *et al*., 1997b) and duration of exposure (Boru *et al*., 2003). In this study leaf chlorophyll, plant height and dry weight decreased with increasing CO_2 (of which only the decrease caused by the 50% CO_2 treatment was statistically significant). These results are supported by Boru *et al*. (2003), who showed that soybean (*Glycine max*) subjected to CO_2 concentrations ranging from 15 to 50% showed a reduction in leaf "greenness" as well as in shoot and root growth. Huang *et al*. (1997b) demonstrated that 10% CO_2 in combination with 5% O_2 in the soil significantly decreased shoot growth of two wheat (*Triticum aestivum*) cultivars, but photosynthesis and leaf chlorophyll content decreased for only one of the two cultivars.

High CO_2 concentrations are generally related to low O_2 concentrations (Hoeks, 1972a; White, 1997). Although not much is known about recovery of plants from high soil CO_2 concentrations, plants are known to recover after a temporary low soil oxygen concentration, for example in waterlogged soils (Drew, 1990). Lizaso *et al*. (2001) showed that waterlogged maize plants exhibited a faster increase in biomass compared with the control plants after flooding ended, while Huang *et al*. (1994) showed that wheat plants subjected to hypoxia for 14 days had reduced root and shoot dry weights, but 7 days recovery increased the dry weight to 65 -100% of the control weight depending on cultivar. In the present study, chlorophyll, plant height and weight of the 50% CO_2 treatment increased faster compared to the other treatments. 20% CO_2 caused a faster increase in chlorophyll content only. This increase suggests that after a temporary exposure to up to 50% CO_2 in the root zone, maize plants can recover within one growing season.

4.4.2 Behaviour of the REP, YEP and REP-YEP distance

Since leaf chlorophyll content was affected by high CO_2 concentrations, the focus was on the chlorophyll absorption region between 550 and 750 nm. The first derivative maximum is often used for correlations with chlorophyll, however the main drawback of this method is a that a double peak occurs in the first derivative (Boochs *et al*., 1990; Horler *et al*., 1983; Zarco-Tejada *et al*., 2000), leading to a 'jump' in the REP from 700 to 725 nm. Although the derivative maxima in the sample dataset did not demonstrate double peaks, several peaks were flattened at the top (Figure 4.8). This resulted in three or more successive wavelengths having (nearly) the same reflectance value, leading to inaccurate REP estimates. The methods by Cho and Skidmore (2006) and Guyot and Baret (1988) resulted in higher correlations with chlorophyll. Although these methods had nearly the same correlation coefficient, the absolute values of Cho and Skidmore's method had a much wider range (713-727 nm) than the values of Guyot and Baret (718-720.5 nm).

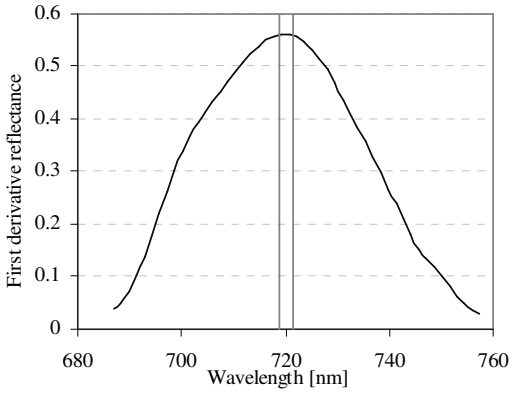

Figure 4.8 A typical first derivative peak at 720 nm of a test sample leaf. The peak is flattened at the top, resulting in inaccurate REP estimates.

Although the yellow edge position as well as the continuum removed reflectance in the yellow region were expected to have a stronger correlation with chlorophyll content than the REP, this was not the case in the test sample dataset (Figure 4.3). Adams *et al*. (1999) showed that the yellowness index, which is based on the reflectance between 580 and 660 nm, saturated at a chlorophyll content over 25 μg/cm^2. Average leaf chlorophyll in the test samples corresponded to approximately 33 μg/cm^2, which would explain the low correlations. Yet the REP-YEP distance had a stronger correlation with chlorophyll than the REP alone in the test samples (Figure 4.3) and the REP-YEP distance of the greenhouse data could better distinguish the treatments than the REP or YEP alone (Table 4.3). This suggests that even though the yellow reflectance alone is not functional at medium to high chlorophyll contents, in combination with the REP it increased the correlation with chlorophyll during the entire experiment.

In general the REP-YEP distance decreased with increasing CO_2, however only the difference between the 50% CO_2 and the lower concentrations was statistically significant. After t = 26 the REP-YEP distance of the 2% treatment is consistently 2 nm wider than the 5%, 10% and 20% treatments. The latter are nearly similar during the entire experiment, suggesting that CO_2 concentrations between 5% and 20% CO_2 have a similar effect on leaf chlorophyll. Although the 50% CO_2 delivery ended at t = 20, recovery started only four weeks later (t = 46), visible as an increase in REP-YEP distance and a shift of the REP towards longer wavelengths. 20% CO_2 delivery ended at t = 40 and signs of recovery were noticeable three weeks later (t = 63). The increase in chlorophyll in the recovered plants did not coincide with an increase in leaf water content (Figure 4.7). It is possible that an increasing chlorophyll content was the first

sign of recovery and that a longer recovery period would result in an increase in leaf water content.

4.4.3 Behaviour of the REP peak and the 1400 nm and 1900 nm peaks

The water absorption features and the REP peak were strongly correlated with each other and all indicated that 50% CO_2 caused a decrease in leaf water content during the whole experiment. A reduced water uptake has been related to a decreased respiration rate of roots caused by a reduced O_2 concentration in the soil (Drew, 1990). In addition, Macek *et al*. (2005) found that root respiration rates of plants decreased only in CO_2 concentrations over 20% and that the response was species specific. Since the 50% CO_2 concentration corresponded to O_2 concentrations that are lower than usual, it is likely that the 50% CO_2 treatment reduced the root respiration rate. Contrary to the 50% CO_2 treatment, the 20% CO_2 treatment caused a relatively shallow water absorption feature and high REP peak until t = 32. Huang *et al*. (1997b) showed that CO_2 enrichment during oxygen shortage in the soil reduced stress in wheat shoot growth, photosynthesis and leaf chlorophyll content. Several possible reasons were given for the observed effects, such as an increased N or P uptake and supply (Cramer and Lips, 1995; Arteca *et al*., 1979), or CO_2 absorption by roots and transport to the shoots where it could enhance photosynthesis (Enoch and Olesen, 1993). The latter may have occurred in the 20% CO_2 treatment early in the experiment, stimulating photosynthesis and early growth. The REP, YEP and REP-YEP distance confirm that the 20% CO_2 treatment had a relatively high chlorophyll content until t = 32. The same (but less clear) trend can be seen in the chlorophyll and water content of the 10% CO_2 treatment.

4.4.4 Monitoring soil CO_2 using first derivative reflectance

For monitoring the decline of plant health caused by high CO_2 concentrations, the REP-YEP distance is most functional. It had the highest correlation with chlorophyll content and it was the only index that could distinguish the 50% CO_2 treatment from all other treatments at three timesteps. In this study the first moment that 50% CO_2 could be distinguished from the other treatments was 19 days after initial delivery. When elevated CO_2 concentrations develop during later stages in the growing season, it is expected that the plant's response is slower due to lower metabolic activity of the roots (Smith, 2004b). When annual plants are monitored, the best time for monitoring is halfway the growing season of the plants. Early in the growth cycle leaf reflectance measurements are difficult due to the small leaf surface and may cause noisy first derivative spectra, which affect the accuracy of the YEP and REP. Late in

the growth cycle the plants show signs of senescence, which may obscure the effects of CO_2.

Since monitoring of vegetation ideally takes place on larger scales than leaf level, the patterns of the vegetation and canopy structure will be incorporated in the reflectance signal. Since the maize plants showed a consistent decrease in size with increasing CO_2 concentrations, plant cover and LAI of canopy affected by CO_2 seepage is expected to be lower. This is supported by observations from a natural CO_2 seep in Parádfürdő, Hungary, where grassland vegetation cover decreased towards the seep centre (Figure 4.9; see footnote[1]). These patterns will enhance the derivative differences in the chlorophyll region.

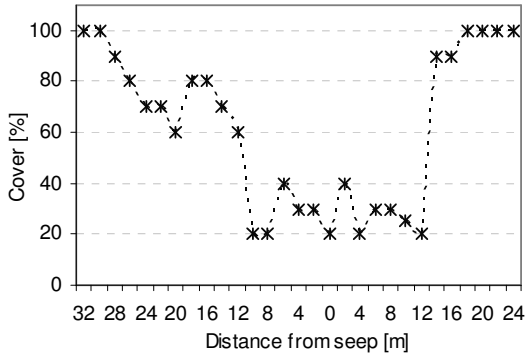

Figure 4.9 Grassland canopy cover in a natural CO_2 seep

4.5 Conclusion

Increasing CO_2 concentration decreased plant height, leaf chlorophyll content and dry weight of maize plants, however only 50% CO_2 had a statistically significant effect. The decrease in chlorophyll was best explained by the distance between the yellow edge position and the red edge position; both calculated using the method proposed by Cho and Skidmore (2006). The REP peak height and the water absorption pit depths at 1400 and 1900 nm showed that 50% CO_2 decreased leaf water content. 10% CO_2 and 20% CO_2 however had an increased chlorophyll and water content at the start of the experiment, suggesting that a moderate CO_2 concentration in the soil may be beneficial to maize growth. For the detection of CO_2 seepage using leaf reflectance, the results of this chapter suggest that the REP-YEP distance is a useful index, particularly halfway through the growing season.

[1] Observations date from 5 August 2002. Measurements were performed every 2 m along a transect over the seep. Vegetation cover was estimated on 1 m^2 patches.

In hydrocarbon gas leaks, bacterial methane oxidation can result in CO_2 concentrations between 10% (Steven *et al.*, 2006) to 15% (Hoeks, 1972a). Higher concentrations are unlikely to occur, as above these values either the oxygen or the methane supply will be limiting for methane oxidation (Steven *et al.*, 2006). Since the results in this chapter suggest that only the effects of 50% CO_2 on leaf reflectance can be detected with certainty, the effect of bacterial CO_2 production in gas leaks will be difficult to measure if only the leaf reflectance is taken into account. Moreover, the additional effects of oxygen shortage and ethane on vegetation reflectance may either diminish or enhance the effects of CO_2. In the next chapters an attempt is made to distinguish the effects of oxygen shortage, ethane and carbon dioxide on canopy reflectance.

CHAPTER 5 *

PREDICTING SOIL OXYGEN CONCENTRATIONS USING INDICES BASED ON HYPERSPECTRAL REFLECTANCE OF MAIZE AND WHEAT CANOPIES

5.1 Introduction

Chapters 3 and 4 dealt with the effects of natural gas, ethane, methane and CO_2 on plant growth and leaf reflectance. It was shown that a concentration of 0.73% of ethane caused a decrease in maize plant height, leaf area and an increased reflectance in the yellow region (560 – 600 nm). High concentrations of CO_2 also caused a decrease in maize plant height in addition to reduced leaf chlorophyll and changes in the reflectance in the chlorophyll and water absorption regions. The gas fluxes in the described experiment were kept low in order to avoid oxygen shortage. In reality however, leakage rates may be much higher and oxygen shortage will occur. Chapter 2 has shown that a gas flow of 2250 l/day led to a decrease in soil oxygen concentrations (Tables 2.1 and 2.2). This resulted in a decrease in both maize and wheat canopy cover, plant height and leaf chlorophyll in the centre 50 cm of the gas-plots (Table 2.4). Pysek and Pysek (1989) found that natural gas leakage of 250 l/h decreased canopy cover, reduced species diversity, increased reflectance at red wavelengths and decreased reflectance in the near infrared. Smith *et al*. (2004b) found a decrease in bean and wheat growth as a result of simulated gas leakage (100 l/h), and a change in reflectance properties in the 700-740 nm region (the 'red edge'). In another study, Smith *et al*. (2004a) demonstrated that soil oxygen displacement by natural gas, argon and waterlogging caused an increase in reflectance in the visible and a change in the shape and position of the red edge. These results suggested that the changes in reflectance due to gas leakage are caused by oxygen shortage and not by the natural gas itself (Smith *et al*., 2004a). In this chapter the effects of high soil gas concentrations on maize and wheat reflectance are studied. Based on the results of previous chapter and literature, it was expected that the following aspects play a role:

1. Large amounts of gas cause oxygen shortage (Chapter 2), possibly affecting the reflectance in the chlorophyll and water absorption regions;
2. Ethane may cause increased reflectance in the yellow region (Chapter 3);

* This chapter is based on: Noomen, M.F., Smith, K.L., Colls, J.J., Steven, M.D., Skidmore, A.K. and van der Meer, F.D., accepted. Predicting soil oxygen concentrations using indices based on hyperspectral reflectance of maize and wheat canopies. International Journal of Remote Sensing.

3. Oxygen depletion may take place, resulting in anomalous CO_2 concentrations that change the reflectance in the chlorophyll and water absorption regions (Chapter 4).

This chapter deals with the effects of oxygen shortage on canopy reflectance, while the effects of ethane and CO_2 on canopy reflectance are described in Chapter 6. The focus of the chapter is twofold: I. finding reflectance indices that are correlated with leaf area; and II. correlating soil oxygen concentrations with these indices in addition to 51 indices that are known to react on changes in vegetation vigour. The aim was to find indices that can predict oxygen concentrations based on both maize and wheat canopy reflectance and at several moments in time, increasing the probability of finding a general reflectance index that can serve as a non-destructive method for gas detection.

5.2 Methods

5.2.1 Canopy spectral measurements

The plots were divided into 16 virtual blocks of 50 by 50 cm (Figure 5.1a). Twelve blocks were used for the canopy spectral measurements, while four were used for destructive analysis (respectively R and D in Figure 5.1b). The outer 25 cm of the plots was not used for measurements to avoid edge effects. Spectral measurements were taken weekly using an ASD Fieldspec Pro spectroradiometer, which has a sampling interval between 1.4 nm and 12 nm but produces 1 nm interval readings over the full wavelength range (350-2500 nm). The sensor, a 1.5 m long fibre optic cable with 25° field of view, was held approximately 1 m above the plant surface to view a block of 50 by 50 cm. Spectral measurements were made between 10.30 and 13.00 hrs in sunny weather. Every 10 minutes, reference measurements were taken of a halon white panel for the internal calibration of the instrument. Each spectrum is an average of 25 samples, while five spectra of each block were averaged to compensate for differences in reflectance owing to varying leaf angles (or BRDF) (Nicodemus, 1977; Sandmeier and Deering, 1999).

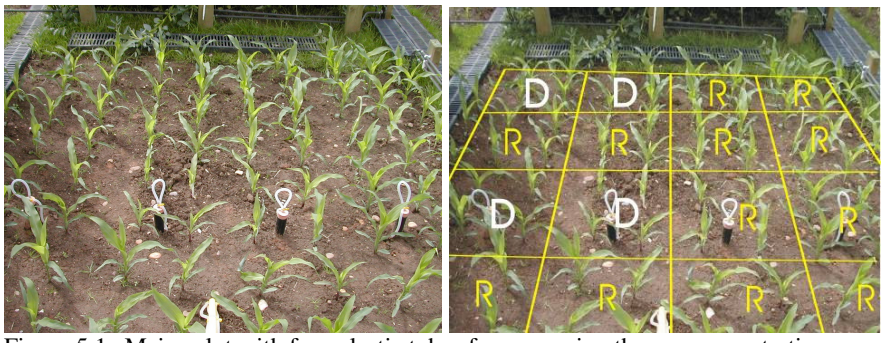

Figure 5.1a Maize plot with four plastic tubes for measuring the gas concentration.
Figure 5.1b Division of the plot in virtual blocks of 50 by 50 cm. R = blocks used for reflectance measurements, D = blocks used for destructive measurements.

5.2.2 Correlation of reflectance indices with LAI

In remote sensing studies, plant and canopy health is often assessed by indices that are combinations of the visible and near infrared reflectance (Broge and Leblanc, 2000). These indices react to changes in leaf chlorophyll and canopy structure, corresponding to wavelengths around 670 nm and 800 nm respectively (Haboudane *et al*., 2004). Since small gas leaks affect only the leaf area and not the chlorophyll content (Chapter 2), the best indices for gas detection are those that maximize differences in canopy leaf area or leaf area index (LAI). Since the LAI of the control and gassed canopies at t = 35 was 4.1 and 3.8 respectively (Table 2.4; not taking into account the centre of the gassed plots), the index should be able to distinguish these small differences. Most studies that tried to correlate LAI to reflectance indices acknowledge that at LAI values over 2, distinction between LAI values becomes more difficult due to saturation of the indices (Broge and Leblanc, 2000; Haboudane *et al*., 2004; Thenkabail *et al*., 2000). In this chapter, the LAI values of the maize plants as measured at t = 35 were correlated with reflectance indices to find an index that was linearly related to LAI values over 2. The following indices were calculated:

1. $\frac{BandA}{BandB}$ on all bands between 400 and 2400 nm;
2. $\frac{BandA}{BandB}$ on all bands between 400 and 2400 nm of the first derivative spectra;
3. $\frac{BandA - BandB}{BandA + BandB}$ on all bands between 400 and 2400 nm;

4. $\frac{BandA - BandB}{BandA + BandB}$ on all bands between 400 and 2400 nm of the first derivative spectra.

Prior to analysis the first derivative spectra were smoothed using the Savitsky-Golay polynomial smoothing filter (Savitsky and Golay, 1964).

The correlation coefficient was calculated by taking out one LAI value, subsequently correlating the leftover LAI values with the index values, and repeating this till every LAI value has been taken out once. The indices that led to the lowest root mean square error (RMSE) were then selected for further analysis. A Student's t-test was performed on the selected indices to test whether they could distinguish the control from the gassed plots.

5.2.3 Correlation of reflectance indices with oxygen concentrations

At ten sample points (located at 25 cm, 75 cm and 400 cm from the source) both the oxygen concentration and reflectance were measured. These points were used for two analyses of covariance between reflectance indices and oxygen concentration. The first covariance analysis tested whether there is a reflectance index (continuous predictor) that can predict the soil oxygen concentration (dependent variable) for both species (covariates), while the second covariance analysis examined whether there is a reflectance index that can predict the soil oxygen concentration at several timesteps (covariates). When the predictor had a similar effect for each covariate, a simple linear regression analysis was done to calculate the prediction power at each timestep (t = 16, t = 22, t = 29, t = 35 and t = 42). For this analysis, the assumption was made that the effects by ethane and carbon dioxide are insignificant compared to the effect of oxygen shortage. In Chapter 6 the validity of the assumption is tested. In addition to the indices that have a strong correlation with LAI, 51 hyperspectral indices that are known to react on changes in vegetation vigour were selected for the analysis. Most of the indices are based on reflectance in the visible and near infrared light, while a few are based on the shortwave infrared reflectance (Appendix 1). For prediction accuracy, only those models that had an R^2 of 0.5 or higher (arbitrarily chosen to reduce the number of weakly predicting indices) were selected for modelling oxygen concentrations under the four gassed plots and the two control plots. Based on the measured gas concentrations and the canopy patterns, the expectation was that the predicted oxygen concentration would be lowest close to the gas source, increasing with distance from the source to a value of 20% on the control plots.

5.3 Results

5.3.1 Reflectance

During the whole experiment the canopy reflectance of the centre 50 cm showed a significant decrease in the near infrared region (800 – 1300 nm) and a relative increase in the red region (around 670 nm) in the maize canopy (Figure 5.2).

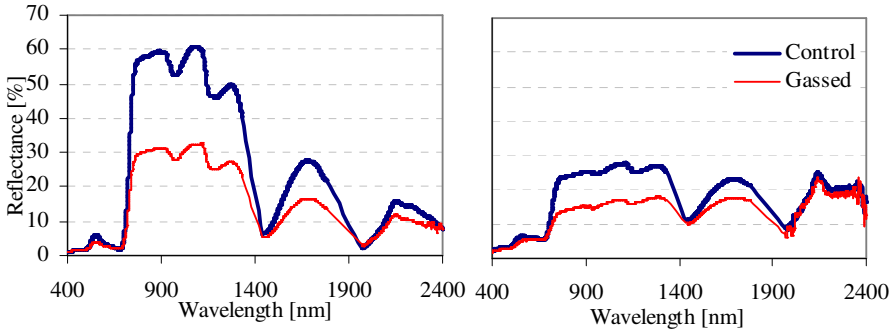

Figure 5.2 Reflectance curves control and gassed maize canopy (left) and wheat canopy (right). The decrease in the near and shortwave infrared (between 800 and 2400 nm) is clearly visible.

Although the overall reflectance in the near infrared is lower in the wheat canopy due to the lower canopy density (Knipling, 1970), the reflectance within the plots shows the same pattern: a strong decrease in NIR in the centre 50 cm.

Commonly used reflectance indices indicated that the plants on the gassed plots were stressed: the NDVI was lower during the whole experiment, while the red edge position was located at shorter wavelengths (Figure 5.3; for equations of NDVI and REP see Appendix 1). This is in accordance with results from several studies (e.g. Smith *et al*., 2004b; Oliveira *et al*., 1997; Table 1.2).

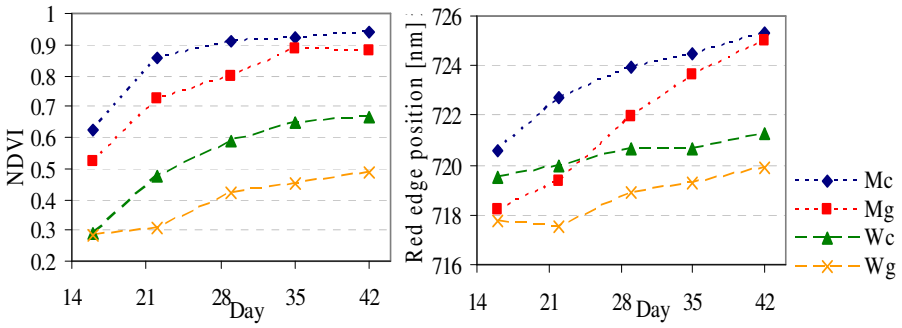

Figure 5.3 NDVI and red edge position with time. Both indices are lower on the gassed plots, suggesting that the gassed canopy is stressed.

5.3.2 Correlation LAI with reflectance indices

The LAI values used for the analysis ranged from 2.0 to 5.3 (n = 34). Correlations between LAI and indices were highest for the first derivative ratios (Table 5.1). Differences between the ratio-type indices and the NDVI-type indices were minimal. The highest correlations were found for indices in the visible light for the first derivative and in the NIR for the normal reflectance.

Table 5.1 Pearson's R for those indices that had the highest correlation with LAI

Ratio	Bands	Pearson's R
A/B (1st derivative)	A: 642; B: 600	-0.78
	A: 599; B: 508	-0.68
(A-B)/(A+B) (1st derivative)	A: 642; B: 600	-0.77
	A: 599; B: 508	-0.66
A/B (reflectance)	A: 1097; B: 928	-0.53
	A: 765; B: 736	0.50
(A-B)/(A+B) (reflectance)	A: 1097; B: 928	-0.53
	A: 765; B: 736	0.50

Figure 5.4 shows the predicted against the measured LAI values. Particularly the first derivative ratios are strongly dependent on the lower LAI values. A Student's t-test showed that the differences between LAI on the control and gassed plots (not taking into account the gassed centre) were not significant at $t = 35$. However, the index using the derivative bands at 642 and 600 nm led to a significant difference ($p \leq 0.05$). Even though the other indices did not lead to significant differences at $t = 35$, they were tested in the following analysis to find out whether they could be used for the detection of low oxygen concentrations over time.

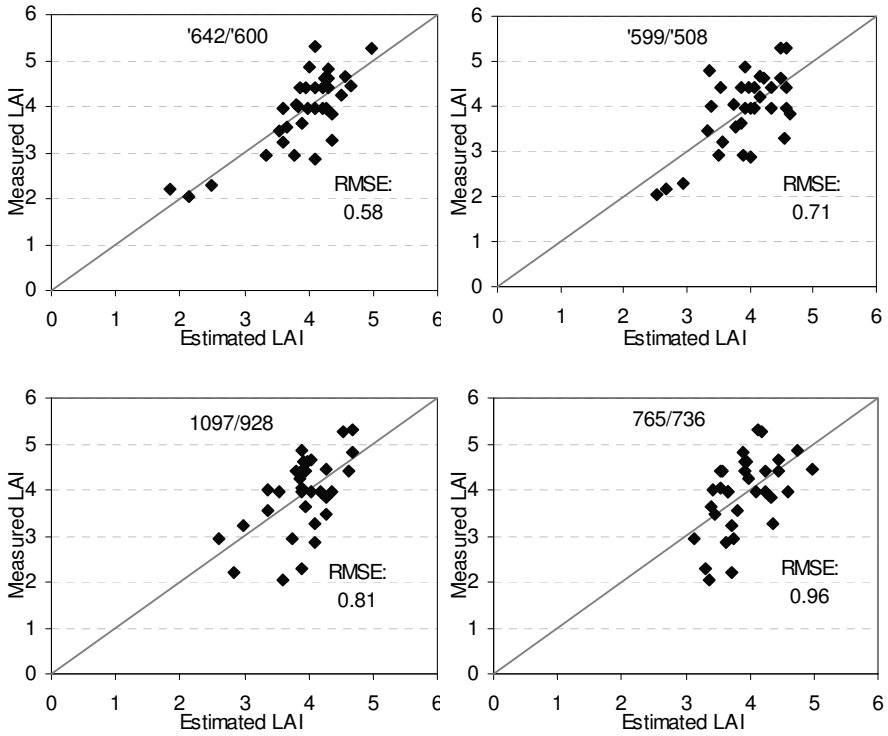

Figure 5.4 Measured versus estimated LAI for the 4 indices with the lowest RMSE.

5.3.3 Covariance analysis between two species

A covariance analysis between each reflectance index and oxygen concentration was performed at t = 16, t = 22, t = 29, t = 35 and t = 42. Those indices that yielded significant correlations ($p \leq 0.05$) were selected to check whether there was a difference between the maize and wheat (covariates). Nine indices resulted in significant models at t = 16, 34 indices at t = 22, 48 indices at t = 29 and 0 indices at t = 35 and t = 42. Of these indices, 2, 18 and 1 indices, respectively at t = 16, t = 22 and t = 29 predicted the oxygen concentration without species effect ("O" in Table 5.2). Scatterplots of the indices against the oxygen concentration indicated that although there is a difference in absolute index values, the slope of the regression equation between oxygen and index was very similar for both species (Figure 5.5).

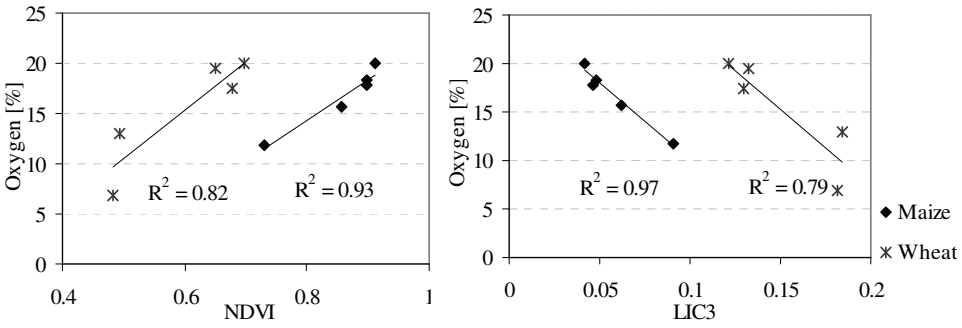

Figure 5.5 Covariance analysis shows that a regression between reflectance indices against oxygen concentration result in almost similar slopes but different intercepts for the two species.

If the difference between the absolute index values could be removed, the models would be expected to be significant without a difference between species. A simple way to remove the difference between species was to subtract the control values of wheat (*Wc*) from the control values of maize (*Mc*), and subsequently add this difference to all wheat values:

Step 1:
Index (*Mc*) – Index (*Wc*) = Index Difference (ID) (5.1)

Step 2:
Index (*Wg*, *Wc*) + ID = Index' (5.2)

Consequently, a new covariance analysis was performed on the transformed data, which resulted in respectively 15, 22 and 23 significant models at t = 16, t = 22, and t = 29 in which the species effect was removed (Table 5.2), while at t = 35 and t = 42 normalization had no effect. Besides the large increase in the number of indices that predict the oxygen concentration, normalization also resulted in a small increase in R^2 for the majority of the indices that were significantly correlated to oxygen before normalization.

Before normalization there were no indices that could predict soil oxygen at each date, yet after normalization there were six indices that could be used to predict soil oxygen at t = 16, t = 22, and t = 29: CTR2, LIC1, LIC3, mNDVI705, OSAVI and NDVI705 (Table 5.2). The highest regression coefficients were found at t = 29.

5.3.4 Covariance analysis between timesteps

Covariance analysis between the five timesteps did not result in significant models for oxygen. Therefore a similar normalization procedure as described in the previous section was performed between the timesteps. Normalization was done by subtracting the control index value of $t(1)$ from the control index value at $t(1+i)$, and adding this difference to each index value at $t(1+i)$. After normalization there were 28 (maize) and 27 (wheat) indices that resulted in significant models for oxygen. Examination of the correlations between the indices and the oxygen concentration at each timestep showed that at $t = 16$ the regression coefficients were lowest and the slope of the regression different from the other dates (Figure 5.6; Table 5.3). Removing $t = 16$ from the analysis increased the number of indices that could predict oxygen concentrations to 33 (maize) and 29 (wheat) and increased the regression coefficient of most indices. Table 5.2 shows the regression coefficients of $t = 22$ till $t = 42$ after normalization. Vog1 ($R740/R720$), ZM ($R750/R710$), GM1 ($R750/R550$) and GM2 ($R750/R700$) had the highest regression coefficients for maize, while LIC3 ($R440/R740$) and REP ($700+40*[((R670+R780/2)-R700)/(R740-R700)]$) had the highest regression coefficients for wheat.

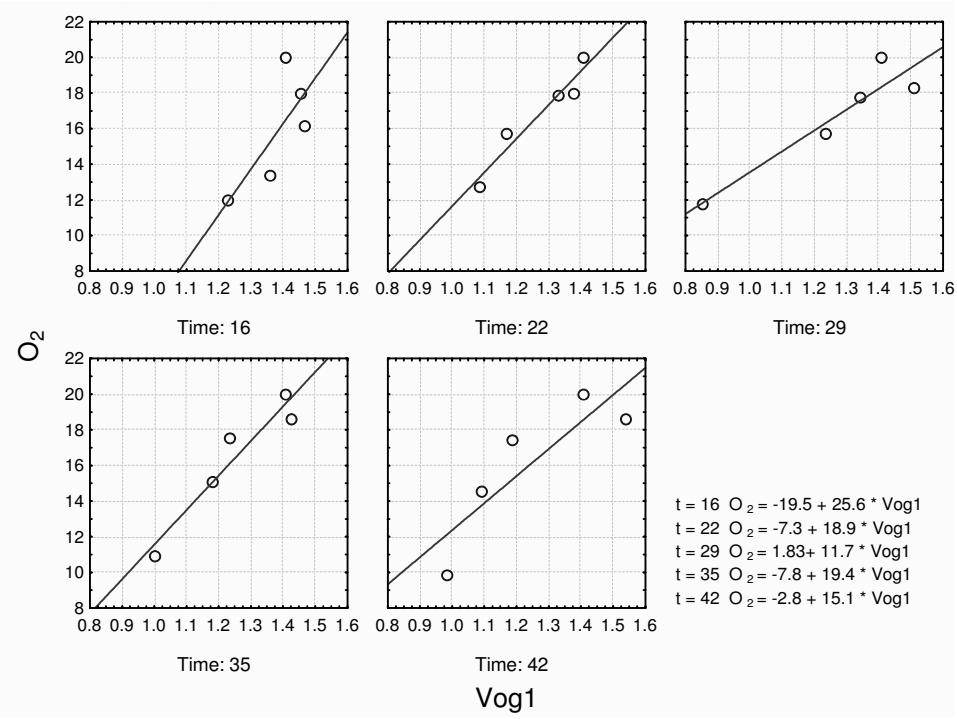

Figure 5.6 Regression lines between Vog1 (Vogelmann et al., 1993) and oxygen concentrations per timestep (maize)

Table 5.3 R^2 at each timestep for Vog1 (maize) and LIC3 (wheat)

Time	Maize	Wheat
t = 16	0.55	0.44
t = 22	0.93	0.67
t = 29	0.88	0.79
t = 35	0.91	0.58
t = 42	0.74	0.62

5.3.5 Predicted oxygen concentrations based on maize and wheat

Overall the regression coefficients of the covariance analysis between species were highest at t = 29 and lowest at t = 16. Since the analysis was based on just 10 points, an additional assessment was made of the variation of the predicted oxygen concentrations on the control plots, where the oxygen concentration should be 20%. The prediction of the control values at t = 29 resulted in values closest to 20% (Table 5.4).

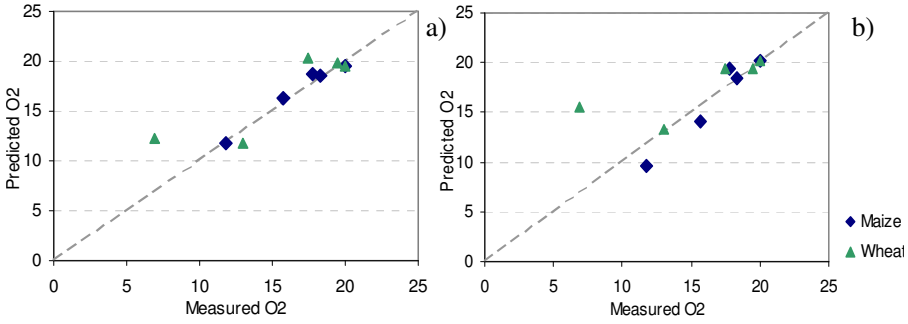

Figure 5.7 Measured versus predicted O_2 values based on LIC3 (a) and OSAVI (b) at t = 29

Graphs of measured against predicted oxygen concentrations show that although the prediction equation was based on both species, in general the indices performed better on the maize plots than on the wheat plots (Figure 5.7).

For the detection of gas leaks, it is important that areas with low oxygen are clearly distinguishable from the unaffected areas. An index that minimizes the differences in the control canopy and enhances the differences between the control and the gassed canopy is therefore preferable. Although LIC3 had the highest regression coefficient, the oxygen prediction under the control wheat plots ranged from 13 to 25%, compared to a range of 16 to 24% based on OSAVI. The pattern of low oxygen close to the gas source, which increases with distance, was most clear on plot Mg1 (Figure 5.8). All indices on this plot showed the same pattern. Mg2, which received less than half the amount of gas

compared to Mg1, showed the same pattern when OSAVI was used, but the other indices showed a less clear pattern. On both wheat plots, OSAVI had the clearest pattern. Since OSAVI maximized the differences between gassed and control canopy while the average predicted oxygen values under the control plots were closest to 20%, this was deemed the best predictor at $t = 29$.

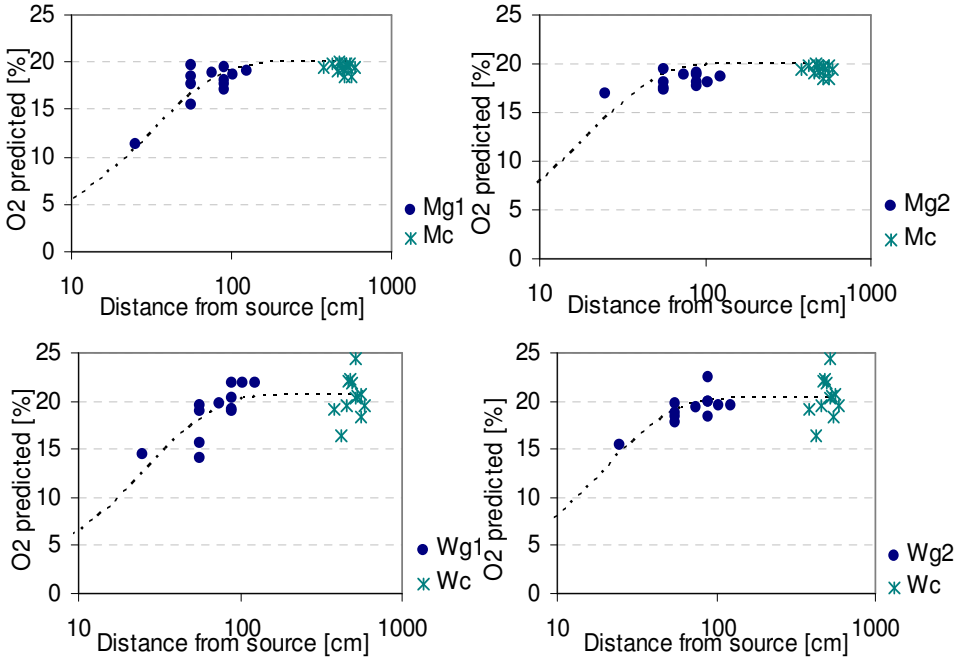

Figure 5.8 Predicted oxygen concentrations of Mg1 and Mc, Mg2 and Mc, Wg1 and Wc, and Wg2 and Wc at $t = 29$, based on OSAVI. An exponential curve that describes the oxygen pattern is fitted through the data.

Table 5.4 Predicted oxygen concentrations ± standard error under the control maize and wheat plots (n = 24) at three timesteps (left) and over time (right). The oxygen concentrations over time are predicted using Vog1 (maize) and LIC3 (wheat).

INDEX	*T = 16*	*T = 22*	*T = 29*	*In time:*	*Maize*	*Wheat*
LIC1	17.61 ± 1.23	19.17 ± 1.75	19.39 ± 2.40	Average:	19.48	16.28
LIC3	18.01 ± 1.78	18.84 ± 1.73	19.52 ± 2.38	*Standard error per timestep:*		
CTR2	18.08 ± 1.42	19.13 ± 2.48	19.32 ± 2.65	$t = 16$	1.33	4.09
mNDVI705	18.50 ± 1.39	20.12 ± 1.70	19.23 ± 2.23	$t = 22$	1.17	4.57
NDVI705	18.46 ± 1.42	20.28 ± 2.13	19.30 ± 2.00	$t = 29$	1.41	4.26
OSAVI	18.02 ± 1.51	17.95 ± 0.66	20.12 ± 1.84	$t = 35$	1.41	4.28
MEAN	*18.11 ± 1.46*	*19.25 ± 1.74*	*19.48 ± 2.25*	$t = 42$	2.33	4.13

At t = 22 all indices had regression coefficients under 0.7, resulting in less reliable predictions of oxygen under the plots than at t = 29. As at t = 29, LIC3 for t = 22 had the highest regression coefficient, but did not predict oxygen reliably on the wheat plots. The best predictor at t = 22 was CTR2 (Figure 5.9), although the patterns for oxygen with distance from the source were less clear than at t = 29.

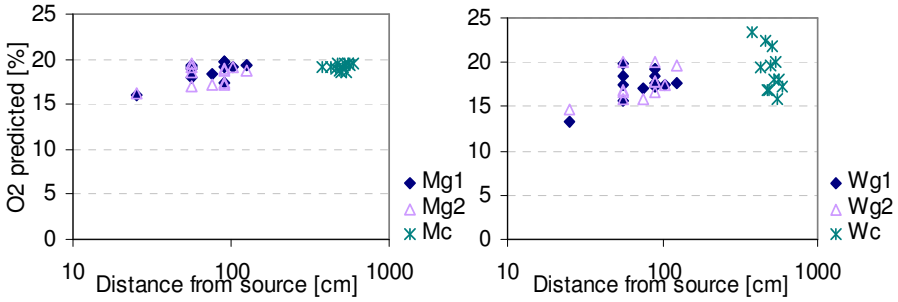

Figure 5.9 Oxygen concentration at t = 22 estimated based on CTR2.

5.3.6 Predicted oxygen concentrations over time

Although six indices have shown to estimate oxygen concentrations based on maize and wheat reflectance, they only have reliable predictions at t = 29. For the detection of gas leakage over time, an index that can predict oxygen at several timesteps is preferable. The covariance analysis in time showed that Vog1 had the highest regression coefficient for maize and LIC3 and REP for wheat. Whereas the average predicted oxygen concentration under the control maize plot was close to 20%, the predicted oxygen under the wheat plots was approximately 4% lower than the expected 20% (Table 5.4). As seen in figure 5.10, the reason for the low average is an underestimation of the highest O_2 concentrations. In contrast, the lowest O_2 concentrations were overestimated with about 5% (Figure 5.10).

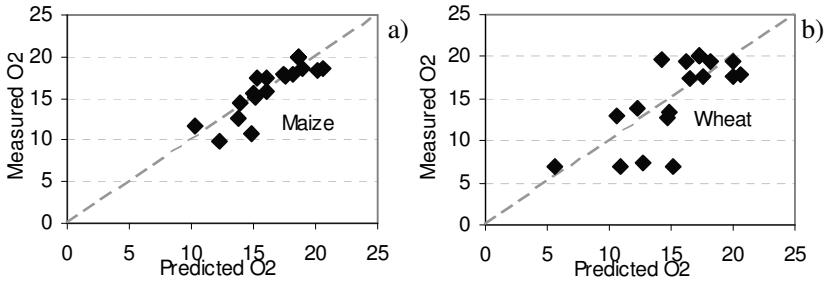

Figure 5.10 Predicted against measured oxygen values based on Vog1 (a) and LIC3 (b)

5.3.7 Maximum range of affected area

To determine the maximum distance between the gas source and the point beyond which there was no oxygen shortage, a curve was fitted through the oxygen values as predicted by OSAVI. This procedure was repeated for the oxygen concentrations in time as predicted by Vog1 on the maize canopy. Since the prediction of O_2 values based on the wheat canopy resulted in less reliable values (Table 5.4), these were not included in the analysis. The assumption was made that the oxygen concentration was 0% in the centre of the gas source, and increased towards 20% at the control areas. The measured oxygen concentrations in the soil followed an exponential relationship with distance:

$$\text{Oxygen concentrations} = 20.0 * (1 - EXP^{(-0.033 * D)}); \quad (5.3)$$

20.0 being the maximum oxygen concentration, -0.033 defining the shape of the fitted curve, and D being the distance to the gas source (R^2 0.94).

The same distribution was found in the predicted oxygen values. An exponential curve was fitted through the predicted values of Mg1 and Mc, Mg2 and Mc, and subsequently the distance was determined beyond which the oxygen concentrations were not distinguishable from those of the control. Since the control concentrations contained minimum values of 16.6% (Table 5.4), only values lower than these are likely to be caused by gas in the soil. Therefore the distance was calculated from the gas source to the point where the oxygen concentration was 16% (Table 5.5). The distances, beyond which the oxygen values were not distinguishable from the control, ranged from 30 to 50 cm, depending on the amount of gas the plot received and on the species.

Table 5.5 Distance from gas source to point where the oxygen concentration is 16% at *t* = 29

	Distance from gas source to 16% O_2 [cm]					
	Based on OSAVI-both species	Based on Vog1 (maize)				
Plot	T = 29	T = 16	T = 22	T = 29	T = 35	T = 42
Mg1	51	23	38	51	33	35
Mg2	31	18	39	27	21	18
Wg1	40					
Wg2	30					

5.4 Discussion

5.4.1 Regression analysis

Although several indices were linearly correlated to oxygen concentrations in the soil, it is not certain that oxygen shortage is also the direct cause of the reflectance changes. Since plant growth is affected by low soil oxygen concentrations (Drew 1991; Huang *et al*., 1994; Huang *et al*., 1997a), it is assumed that the low oxygen concentrations in this study are the cause of the reduced plant growth. Other reasons for the reduced plant growth could be the effect of natural gas itself on plant growth, elevated carbon dioxide concentrations or a shortage of soil moisture due to the drying effect of the gas. Although gas concentrations in the atmosphere were not measured, it is assumed that the effects on plant growth were minimal. Natural gas is lighter than air, so the gas could disperse quickly. Gustafson (1944) showed that aboveground parts of plants were not affected by 2% methane in the atmosphere. Methane is assumed to be harmless to plant roots (Arthur *et al*., 1985), which was supported by the results from Smith *et al*. (2004a) and by the results from Chapter 3. Since the soil oxygen concentrations in this study were very low, it is assumed that any effect of methane would be insignificant compared to the effect of the oxygen shortage. Bacterial methane oxidation may have taken place, resulting in an increase in carbon dioxide concentrations. Chapter 4 has shown that only the effects of 50% CO_2 on leaf reflectance could be detected with certainty. Since CO_2 concentrations in gas leaks rarely reach such high values (Steven *et al.*, 2006), it is expected that the side effect of CO_2 was small. In the next chapter the actual CO_2 concentrations in the gas-plots are calculated. In addition to the direct effects of the gases on plant growth, the high gas flow in the gas-plots could potentially dry out the soil, which could result in reduced water uptake by the plants. To avoid this, the soil was kept moist by watering the plots regularly. Leaf moisture measurements showed that the leaf water content of the gassed plants was similar to the water content of the control

plants (Chapter 2), which suggests that the gas leakage did not lead to water shortage. It is therefore assumed that all measured effects were a result of oxygen shortage in the soil.

The indices used in this study were all based on canopy characteristics such as canopy density, leaf area and chlorophyll content, leading to a clearly visible difference between index values of the control and gassed canopies. Although in this chapter 4 indices were shown to be linearly related with LAI, these indices had a weaker relationship with oxygen concentrations than OSAVI, Vog1 and LIC3. This is probably caused by the fact that the indices only correlated with high LAI values where the soil background is minimal. In the wheat plots and at the centre of the gassed plots, the effect of soil background was significant, affecting the reliability of the indices.

As shown in Figure 5.3, several indices showed a similar pattern in time for both species, but there was a difference in absolute values between the species. In the regression analysis between measured oxygen concentrations and reflectance indices this was visible as a similar slope for both species but a different intercept (Figure 5.5). The most likely reason for the difference in absolute values is the difference in canopy cover. Canopy cover was on average 75% for the maize plots and 40% for the wheat plots. Canopy cover has been shown to be linearly or logarithmically related to reflectance indices based on the visible and near infrared light such as NDVI, the type of relation being dependent on the index (Daughtry *et al*., 2000; Thenkabail *et al*., 2000). Consequently the difference in canopy cover caused the difference in absolute values between the species.

Since the focus of this chapter was on finding a reflectance index that can be used to detect low oxygen concentrations due to gas leakage for different species and at several moments in time, the differences between species and timesteps were normalized based on the indices of the control canopy. In this experiment, there were distinct treatment and control canopies, but in reality it may be difficult to determine which is the unaffected canopy. However, when this method was applied to detect leaks in gas pipelines, the location of the pipeline would generally be known. The control canopy could then be assumed to be more than 5 m away from the pipeline, and an average value of several pixels could serve as control index for a certain species.

After normalization between species, several indices could predict oxygen concentrations, with the highest regression coefficients occurring at $t = 29$. At an earlier stage, the models are less powerful due to the lower canopy cover, while at a later stage the maize plants growing adjacent to the centre 50 cm of the gassed plots grew so large that they partly covered the gassed area, leading to false canopy reflectance indices (Figure 5.11).


Figure 5.11 Maize canopy (left) and wheat canopy (right) at t = 29.

Therefore it is concluded that approximately halfway through the growth cycle of maize and wheat (which was one month after the gas was switched on) the probability of detecting gas leakage was highest. This is in accordance with the findings by Pysek and Pysek (1989), who noticed the first changes in leaf reflectance on plants growing in a simulated gas leak after 15 to 30 days. Smith *et al*. (2004b) found the first visible stress symptoms in grass that was gassed with natural gas 1.5 months after the gassing started, but this experiment took place in autumn, when metabolic activity of the roots is low and plants are less sensitive to oxygen shortage (Smith *et al.*, 2004b).

Normalization between timesteps resulted in differences in regression power between different species. The best indices for predicting O_2 over time were Vog1 and LIC3 for the maize and wheat canopies respectively. Both indices are a ratio of 740 nm (dependent on internal leaf structure and leaf area (Gausman, 1974; Knipling, 1970)) and a chlorophyll absorption feature (440 nm for LIC3 and 720 nm for Vog1). Differences in chlorophyll content however are much better visible in the 720 nm region than in the 440 nm region due to the very strong absorption in the latter (Carter and Miller, 1994). The differences within the wheat canopy are therefore almost fully explained by the changes in the 740 nm feature (or leaf area), whereas the differences within the maize canopy are explained by a combination of leaf area and chlorophyll. Whereas normalization of Vog1 per timestep resulted in reliable predicted O_2 concentrations under the maize canopy, the predicted O_2 concentrations under the wheat canopy had an error of approximately 4%. As visible in Figure 2.8, the wheat canopy cover in the control plots is patchy, which leads to widely varying LIC3 values over the control plot. With patches of low cover occurring on the control plots, the regression between the index (which is sensitive to canopy cover) and oxygen is less accurate. The patches of low cover also explain why the predicted oxygen values under the control plots are too low (Table 5.4).

5.4.2 Predicted oxygen concentrations after normalization for species

Extrapolation of the indices to the control and gassed plots showed that although the regression equation was based on both species, in the field it performed better on the maize than on the wheat canopy. As described in the previous section, the patchy canopy cover on the wheat control plots was the cause of the lower regression coefficient. Whereas at t = 29 LIC3 had the highest regression coefficient, on the control plots it performed worse than OSAVI. OSAVI is based on 670 and 800 nm, wavelengths that are affected by the same plant characteristics as LIC3, but OSAVI is adjusted to remove soil influence (Rondeaux *et al*., 1996). Since the wheat canopy cover was only 40%, the soil had a major influence. Removing the soil influence reduced the standard deviation in oxygen predictions under the control plots by 9%, increasing the reliability of the oxygen predictions.

At t = 22 the predicted oxygen values were overall less accurate, particularly under the wheat canopy. The predicted O_2 control values ranged from 14 to 25% for LIC3, which had the highest regression coefficients but the worst prediction under the wheat canopy. Although at t = 22 the canopy cover was even lower than at t = 29, CTR2 (based on 695 and 760 nm) was a better predictor than OSAVI. Daughtry *et al*. (2000) demonstrated that indices that are insensitive to soil reflectance such as OSAVI are mostly related to canopy characteristics such as LAI and foliage cover, and less to chlorophyll differences. However, Carter's stress index has been shown to be sensitive to changes in chlorophyll (Carter and Miller, 1994; Carter, 1994). At t = 22, the differences in canopy cover between the gassed and control plots were less pronounced than at t = 29 (visible in the slope of the regression equations, Table 5.6).

Table 5.6 Regression equations for the 6 indices that were significant for three timesteps. The equations at t = 16 are not shown as their regression coefficient was lower than 0.5

T_{29}	T_{22}
O_2 = -21.19 + 44.47 * LIC1	O_2 = -1.64 + 24.26 * LIC1
O_2 = 25.99 - 156.0 * LIC3	O_2 = 24.97 - -89.80 * LIC3
O_2 = 23.49 - 48.68 * CTR2	O_2 = 22.25 - -25.27 * CTR2
O_2 = -12.13 + 42.37 * mNDVI705	O_2 = 0.86 + 27.84 * mNDVI705
O_2 = -9.95 + 42.16 * NDVI705	O_2 = 1.40 + 30.36 * NDVI705
O_2 = -6.74 + 32.10 * OSAVI	O_2 = 1.65 + 22.95 * OSAVI

Regression equations after normalization over time:

Maize: O_2 = -2.53 + 15.12 * Vog1

Wheat: O_2 = 43.87 – 106.02 * LIC3

Therefore it is assumed that at t = 29, the differences in canopy cover were so pronounced that differences in leaf chlorophyll were overshadowed, while at t = 22 chlorophyll differences were relatively more pronounced due to the less dense cover. This is seen in the red edge position, which is in general a good predictor of chlorophyll content (Boochs *et al*., 1990; Horler *et al*., 1983): at t = 22 the difference in REP between gassed and control canopy is larger than at t = 29 (Figure 5.3). This resulted in CTR2 being the best predictor at t = 22 and OSAVI being the best predictor at t = 29.

5.4.3 Predicted oxygen concentrations after normalization for time

Although OSAVI could predict the oxygen concentrations based on both species, this was only possible at t = 29. For gas leakage monitoring an index should preferably be able to predict oxygen concentrations at any moment. In contrast to OSAVI, Vog1 and LIC3 had the same regression slopes at each timestep when based on the maize and wheat canopy respectively. The estimated distance from the source to the point where the oxygen concentration was 16% (Table 5.5) was largest at t = 29 (Mg1) and t = 22 (Mg2), which coincides with the results from the normalization between species. The fact that the maximum distance at Mg1 occurred a week later than at Mg2 is related to the differences in gas flow – 102 l/h at Mg1 and 32 l/h at Mg2. The lower gas flow at Mg2 resulted in a smaller affected area and plants growing adjacent to the gassed area could partly cover the gassed area, leading to overestimated O_2 concentrations. For the reason described in section 5.4.1 the indices based on wheat had a low regression with oxygen. Yet, although LIC3 had a regression coefficient of just 0.55, it did detect low oxygen concentrations, which is of crucial importance for gas leak detection. As seen in Figure 5.10, at all points where the predicted oxygen was less than 15%, measured oxygen concentrations were indeed lower than 15%.

5.4.4 Detection of gas leakage

The results of this chapter show that the choice of an index for gas leak monitoring depends on species and time. At t = 22 and t = 29 the relationship between oxygen concentrations and the selected indices was similar for both species. This coincided with a canopy cover between 40 and 80% (Figure 2.6). When canopy cover is under 40%, the difference between the gassed and control areas is so small that leak detection is difficult, whereas at very high cover the plants growing adjacent to a small gas leak can overgrow the gassed plants. Gas leakage detection should therefore optimally take place when canopy cover is 40 - 80%. From a practical point of view, instead of going to the field to check the plant cover, the corresponding NDVI values can be used to determine the cover. Although a slight flattening is visible at the highest

cover, the NDVI was linearly related to canopy cover (Figure 5.12). A canopy of 40% - 80% corresponds to NDVI values between 0.6 and 0.9. The wheat canopy never reached NDVI values over 0.75, whereas the maize canopy had NDVI values over 0.75 apart from the first measurement date (t = 16). Since this chapter has shown that LIC3 and Vog1 could predict O_2 concentrations under the wheat and maize canopies respectively, it is expected that in practice LIC3 will be a better predictor of O_2 under canopies having NDVI values below 0.75, while Vog1 will be a better predictor under canopies of higher NDVI.

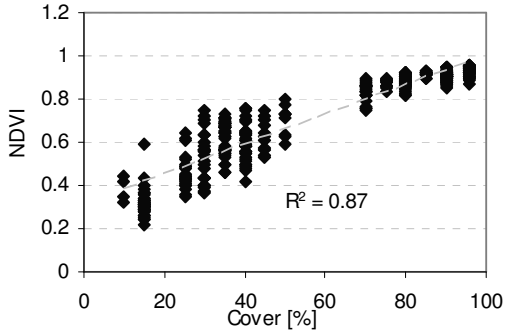

Figure 5.12 The relationship between canopy cover and NDVI.

The maximum distance from the gas source at which the gas leakage could reliably be predicted in this study was 50 cm. The reason for the small extent of the high gas/low oxygen area in this study was the fact that the gas pipe was situated in a clay layer. Gas diffusion is dependent on soil porosity, soil structure (preferential pathways), and moisture content of the soil (Batjes and Bridges, 1992; Moldrup *et al*., 2000). Due to the low porosity of the clay, the gas did not spread far from the exit point of the pipe. In less dense soil, the gas would most likely spread further which would enhance the chance on leakage detection. Since the gas leaked from a point source, low oxygen concentrations could be detected in a circle of 1 m diameter around the source. Thus in order to detect a gas leak of this size by remote sensing, the sensor should have a spatial resolution of at least 1 m. Hyperspectral sensors of this resolution do not exist at present. To increase the possibility of detecting small gas leaks, the pattern of the leak could be incorporated. As seen in Figure 5.8, the lowest oxygen concentrations occurred within 50 cm, but the exponential fit shows a decrease starting approximately 100 cm from the source, increasing the leak to a 2 m round-shaped feature. Incorporation of spatial information significantly improved the detection chance of natural gas seeps in Hungary and California (Van der Werff *et al*., 2006; Van der Werff and Lucieer, 2004). To demonstrate that incorporating the shape of the leak increases the chance of detection, an image was created from the canopy reflectance measurements. The ‘blocks’ as

described in section 5.2.1 were positioned similarly as in the field, while the control plots were positioned around the gassed plots. This was done for each timestep. Subsequently a filter was applied that searches for an exponential shape in all directions. The kernel of the filter was based on a Gaussian shape, as shown in Figure 5.13. Figure 5.14 shows the result for the maize plots till t = 29. It is clearly visible that the leak on the left (Mg1) is best detectable at t = 29 and the leak on the right (Mg2) at t = 22, as was concluded in section 5.4.3.

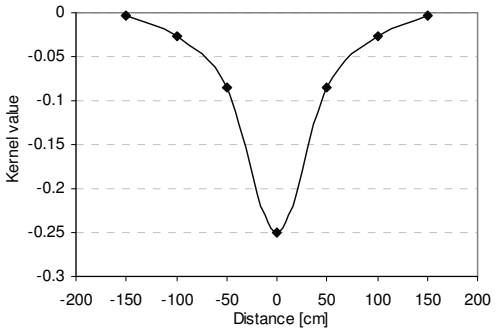

Figure 5.13 Shape of the filter that was used for the detection of the round shaped leak

5.5 Conclusion

The aim of this chapter was to find reflectance indices that are correlated with leaf area and to correlate these indices in addition to 51 indices compiled from literature with soil oxygen concentrations. Since measured LAI in this experiment was high and the differences between gassed and control LAI low, the aim was to find an index that correlated to LAI values over 2. Four indices were selected, of which the first derivative index at 642 and 600 nm was the only index to distinguish the gassed from the control LAIs. All indices were subsequently correlated to the measured oxygen concentrations under the maize (*Zea mays*) and wheat (*Triticum aestivum*) canopies. After normalization between species, six reflectance indices could predict the soil oxygen concentrations under the canopy at three timesteps. However, the performance of each index varied in time, resulting in the best predictions 29 days after gassing started, which was halfway through the growth cycle of the plants. Due to the changing canopy characteristics, it was not possible to find one reflectance index that could be used for both species at any time during the growth cycle. Whereas at t = 29 OSAVI was the best predictor based on the differences in canopy cover, at t = 22 CTR2 was the best predictor due to the less dense canopy and larger differences in leaf chlorophyll content. After normalizing for differences in time, Vog1 could predict oxygen concentrations under the maize canopy, particularly after t = 16. Oxygen concentrations

predicted from LIC3 based on the wheat canopy were less reliable (R^2 of 0.55) due to patchy growth on the control plots.

From a practical point of view, gas leak detection should optimally take place when canopy cover is between 40 and 80%, which translates to an NDVI of 0.6-0.9. LIC3 should be used at NDVI values below 0.75, while Vog1 will be a better predictor under canopies of higher NDVI. The chance of detecting a gas leak is increased when a filter is applied that searches for a round pattern.

Although this chapter has shown that several indices are linearly correlated to oxygen concentrations in the soil, the additional effects of ethane and CO_2 were not considered. It can therefore not be concluded that oxygen shortage is the cause of the reflectance changes. In the following chapter the effects of ethane and carbon dioxide on canopy reflectance are investigated to determine which of the gases (oxygen, carbon dioxide or ethane) affects canopy reflectance most.

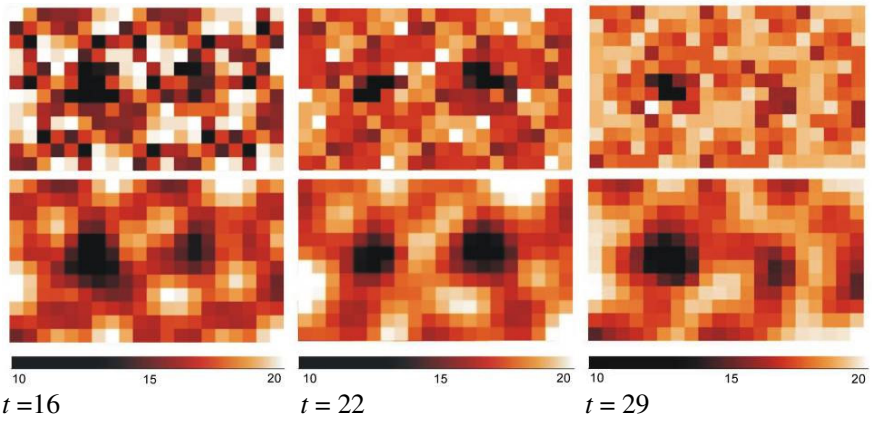

Figure 5.14 Artificial images of the predicted oxygen concentrations under the maize canopy. The upper images are the original images; to the lower images a Gaussian filter has been applied, showing the leaks clearly. Dark to light colours indicate oxygen concentrations between 10 and 20% (see colour bar).

Table 5.2 Significant models ($p \leq 0.05$) and values of R^2 at three timesteps before and after normalization. OS = significant for oxygen and species, or in other words there is a significant difference between maize and wheat; O = significant for oxygen only.

	T = 16		*T = 22*		*T = 29*		*T = 22 to T = 42*	
Index name	Before	After	Before	After	Before	After	Maize	Wheat
ARI1							0.54	
ARI2							0.48	0.24
BGI1			OS	O 0.37	OS		0.32	0.41
BGI2					OS	O 0.40	0.26	0.39
BRI1								
BRI2					OS	O 0.62		
CRI1								0.21
CRI2								
CTR1								
CTR2	O 0.47	O 0.41	OS	O 0.67	OS	O 0.82	0.49	0.40
CUR					OS			
EVI	OS	O 0.46	O 0.44		OS		0.36	0.37
GM1		O 0.43	O 0.59	O 0.57	OS		0.72	0.44
GM2			OS		OS		0.73	0.31
MSAVI	OS	O 0.51			OS		0.33	0.32
LIC1		O 0.33	O 0.54	O 0.62	OS	O 0.84	0.50	0.41
LIC2					O 0.53	O 0.61		
LIC3	O 0.43	O 0.44	OS	O 0.69	OS	O 0.84	0.53	0.55
MCARI	OS							
MCARI1	OS						0.22	0.29
MCARI2	OS	O 0.45	O 0.43		OS		0.40	0.33
mNDVI705		O 0.42	OS	O 0.67	OS	O 0.73	0.50	
mSR705		O 0.39	OS	O 0.60	OS		0.63	
MSR			O 0.47		OS	O 0.40		0.33
MTVI1	OS			O 0.27			0.22	0.29
MTVI2	OS	O 0.45	O 0.37		OS		0.40	0.33
MSI			O 0.43		OS	O 0.82	0.57	0.44
NDII					OS	O 0.76	0.55	0.41
NDNI								0.29
NDVI		OS	O 0.54	O 0.62	OS	O 0.84	0.50	0.41
NDWI					OS	O 0.78		
NPI			O 0.50				0.26	0.36
NPCI					OS	O 0.70		
OSAVI	OS	O 0.43	O 0.55	O 0.53	OS	O 0.64	0.34	0.42
PRI			O 0.47	O 0.54	OS	O 0.58	0.52	
PSRI			O 0.52	O 0.56	OS			0.32
NDVI705		O 0.42	OS	O 0.67	OS	O 0.72	0.60	
REP			O 0.60	O 0.64	OS		0.52	0.51

RGI					OS	O 0.78	0.37	0.20
RDVI	OS	O 0.51	O 0.48		OS		0.28	0.38
SR								0.27
SRPI					OS	O 0.66		
SIPI		OS 0.32	O 0.57	O 0.59	OS	O 0.77	0.23	0.35
SG								
TCARI	OS							
TVI	OS						0.21	0.27
VOG1		O 0.40	O 0.56	O 0.63	OS		0.74	
VOG2			O 0.58	O 0.61	OS		0.71	
VOG3			O 0.57	O 0.60	OS		0.71	
WBI			OS	O 0.53	OS	O 0.75		
ZM		O 0.42	OS	O 0.59	OS		0.73	
642'/600'			OS	O 0.53	OS	O 0.80		0.46
599'/508'								
1097/928					OS	O 0.70		
765/736			OS	O 0.65	OS	O 0.55	0.62	0.46

CHAPTER 6

THE EFFECTS OF ETHANE AND CO_2 ON LEAF AND CANOPY REFLECTANCE IN ADDITION TO OXYGEN SHORTAGE

6.1 Introduction

Three processes can potentially affect plant and canopy growth and reflectance when a large leak develops. Decreased soil oxygen concentrations lead to changes in reflectance commonly associated with plant stress (Chapter 5), ethane may cause increased reflectance in the yellow region (Chapter 3) and oxygen depletion may take place, resulting in anomalous CO_2 concentrations and changes in the reflectance in the chlorophyll and water absorption regions (Chapter 4). In Chapter 5 the relationship between oxygen concentrations in the soil and reflectance indices was explored. It was assumed that the main cause of the reflectance changes was oxygen shortage. In this chapter it is determined whether ethane and CO_2 may have had an additional effect on leaf and canopy reflectance.

6.2 Methods

The same analysis as described in Chapter 3 was used to determine whether ethane affected the reflectance in the field experiment. The effects of carbon dioxide were analysed by calculating the CO_2 concentrations in the soil and comparing them to the concentrations used in Chapter 4. See sections 2.2.2 and 2.2.3 for a description of the experimental set-up and the canopy growth and gas measurements, and section 5.2.1 for a description of the canopy spectral measurements.

6.2.1 Leaf spectral measurements

At t = 16 and t = 35 leaf reflectance measurements were made of 10 leaves per plot, where only leaves within 25 cm of the gas source were selected. The leaves were clipped, cooled in ice and transported to the laboratory within 2 hours after clipping. Leaf spectra were measured in a dark room using an ASD Fieldspec Pro spectroradiometer, which has a sampling interval between 1.4 nm and 12 nm but produces 1 nm interval readings over the full wavelength range (350-2500 nm). An integrating sphere lamp (Macam Photometrics Ltd,

Livingston, Scotland, UK) was used as light source. Per leaf, three spectra were measured and averaged.

6.2.2 Data analysis

6.2.2.1 Ethane

A concentration of 0.75% has shown to affect leaf reflectance in the greenhouse experiment. The natural gas that was used during the field experiment contained approximately 5% ethane. Hence for a concentration of 0.75% ethane in the field, the minimum methane concentration must be 12%. Although over time the average methane concentration in the central 25 cm of the gas-plots was lower than 12% (Table 2.2), at several moments the methane concentrations were well over 15% (Figure 2.4). At 75 cm distance from the gas source, the average methane concentration had reduced to 1%. It is therefore expected that ethane may have had an additional effect on the reflectance within a distance of 25 cm from the gas source only. To test this assumption, a similar analysis as in Chapter 3 was performed on leaf and canopy spectra. The absorption feature depth of the chlorophyll and water absorption regions was calculated on the leaf spectra, in addition to the PRI. The same was repeated for the canopy spectra.

6.2.2.2 CO_2

On those points where the oxygen concentration was measured, the gas concentration was measured too. In a natural situation, the relationship between the gas concentration and oxygen concentration would be as follows (assuming that the oxygen concentration in the soil is 20%):

$$Oxygen\ [\%] = -0.20 * Gas\ [\%] + 20 \qquad (6.1)$$

The measured gas and oxygen concentrations suggest that this relationship does not exist in the field (Figure 2.4). The difference between the expected and the measured oxygen concentration may be the result of bacterial oxygen depletion (Steven *et al*., 2006). Oxygen depletion takes place according to the following formula (Hoeks, 1972a):

$$CH_4 + 2O_2 \Rightarrow CO_2 + 2H_2O \qquad (6.2)$$

The amount of oxygen depletion is therefore directly related to the CO_2 concentration in the soil. To test whether bacterial oxygen depletion took place, the difference between the measured and expected oxygen concentration for each data point was calculated using the method described by Steven *et al*. (2006). To extrapolate the calculation to the whole plot, a similar analysis was performed as in Chapter 5. The results of Chapter 5 showed that Vog1 and Lic3 were linearly related to the oxygen concentration in the soil under the maize and

wheat canopies. Instead of correlating indices with oxygen concentrations, in this chapter they were correlated with methane concentrations. Subsequently the *expected* oxygen was calculated on the extrapolated gas concentrations according to formula 6.1 and the difference between the modelled (Chapter 5) and expected O_2 (this chapter) was calculated. The model described by Steven *et al*. (2006) was used for the calculation of CO_2 concentrations, as this model takes into account the methanotrophic activity and the continuous replenishment of the soil air with gas and air. It first calculates the initial methane concentration by

$$CH_4i = \frac{0.20 * (1 - 2 * CH_4m) - O_2m + 2 * CH_4m}{0.92^{-1} * 0.20 * (1 - 2 * CH_4m) + 2 * (1 - O_2m)} \quad (6.3)$$

where CH_4m is the measured methane concentration, O_2m is the measured oxygen concentration, 0.20 is the assumed control oxygen concentration, and 0.92 is a correction factor for the fact that (in this case) natural gas contains 92% methane. For the extrapolation of CH_4i to the whole plot, the predicted gas and oxygen values calculated earlier were used as input.

Knowing the initial CH_4 concentration, the consumed methane can be calculated as (Steven *et al*., 2006):

$$CH_4c = \frac{0.20 * (1 - 0.92^{-1} * CH_{4i}) - O_2m}{2 * (1 - O_2m)} \quad (6.4)$$

According to formula 6.2 one volume of consumed CH_4 is equal to one volume of produced CO_2, so by calculating consumed methane over the whole plot, the amount of CO_2 is known too.

6.3 Results

Differences in plant growth between the gassed and the control plants were first visible at t = 16, when the plants in the centre of the gassed plots were smaller and had slightly more yellow the leaves than the control plants. Towards the end of the experiment, the wheat leaves turned yellow and the maize leaves turned from yellowish to red (Figure 6.1). In the leaf spectra this is visible as an increase in the yellow and red light (Figure 6.2). In addition, the gassed maize leaves had lower NIR and SWIR than the control leaves, in contrast to the wheat leaves that had similar NIR and SWIR (Figure 6.2).

Figure 6.1 Discolouration of maize leaves (left) and wheat leaves (right) from the centre of the gassed plots at $t = 35$

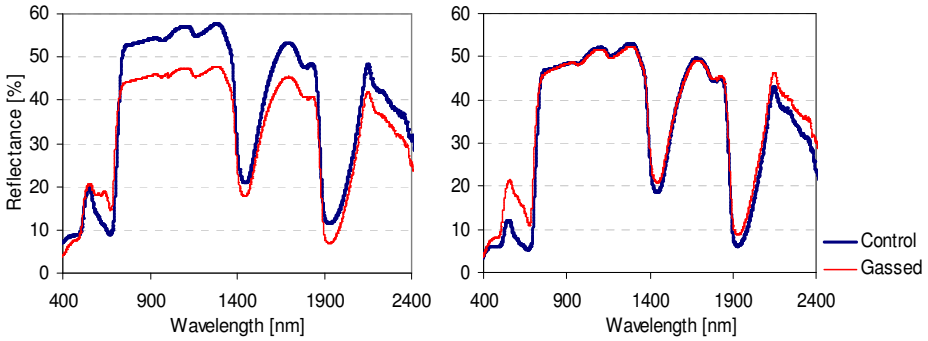

Figure 6.2 Reflectance spectrum of maize leaves (left) and wheat leaves (right) from a control plot and a gassed plot ($t = 35$).

6.3.1 PRI and continuum removed reflectance - leaves

The PRI was significantly higher on the gassed leaves for both species at $t = 16$ (Figure 6.3) and $t = 35$.

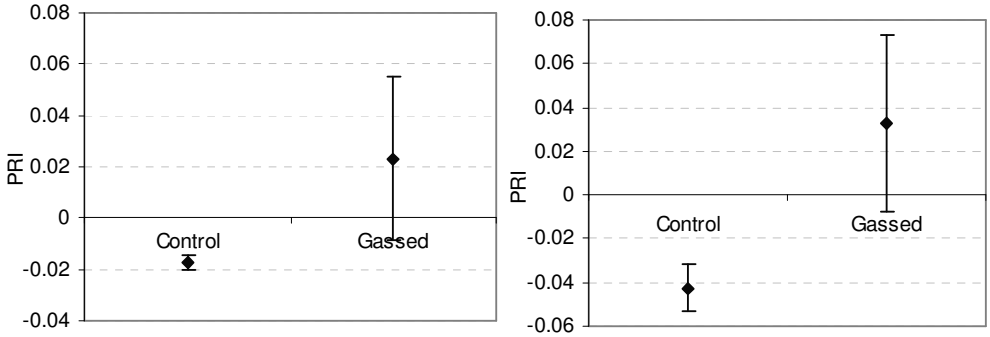

Figure 6.3 PRI of maize (left) and wheat (right) leaves at t = 16

Continuum removal resulted in shallower absorption features for both maize (Figure 6.4) and wheat leaves. The standard deviation of the gassed leaves was much higher than the control leaves. As shown in Figure 6.1 the variety of leaf 'colours' was high in the gassed area, ranging from bright red to green. This variety causes the large standard deviation of the gassed leaf reflectance.
Normalizing the band depths as in Chapter 3 did not result in a shift towards longer wavelengths of the gassed leaf reflectance.

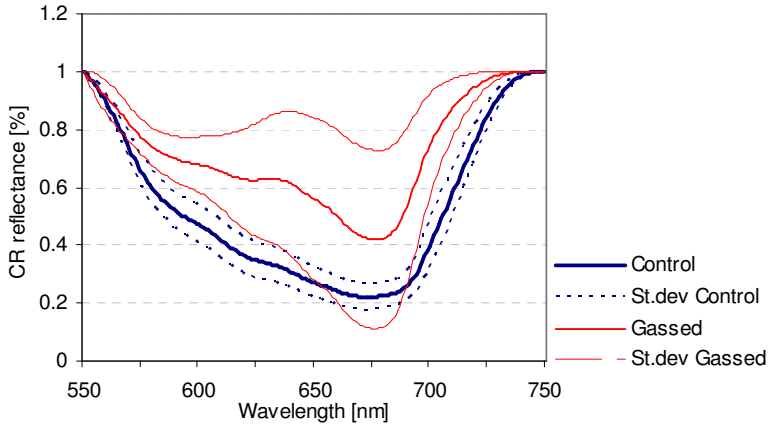

Figure 6.4 Continuum removed (CR) reflectance and its standard deviation of maize leaves from the central 50 cm^2 of the gassed plots

6.3.2 PRI and continuum removed reflectance – canopy

The same procedure was applied to the canopy reflectance. The maize and wheat canopy had a higher continuum removed reflectance in the 560-600 nm

region as well as a higher PRI (Figure 6.5). Similar to the leaf reflectance, normalizing the band depths did not result in a shift towards longer wavelengths of the gassed canopy reflectance.

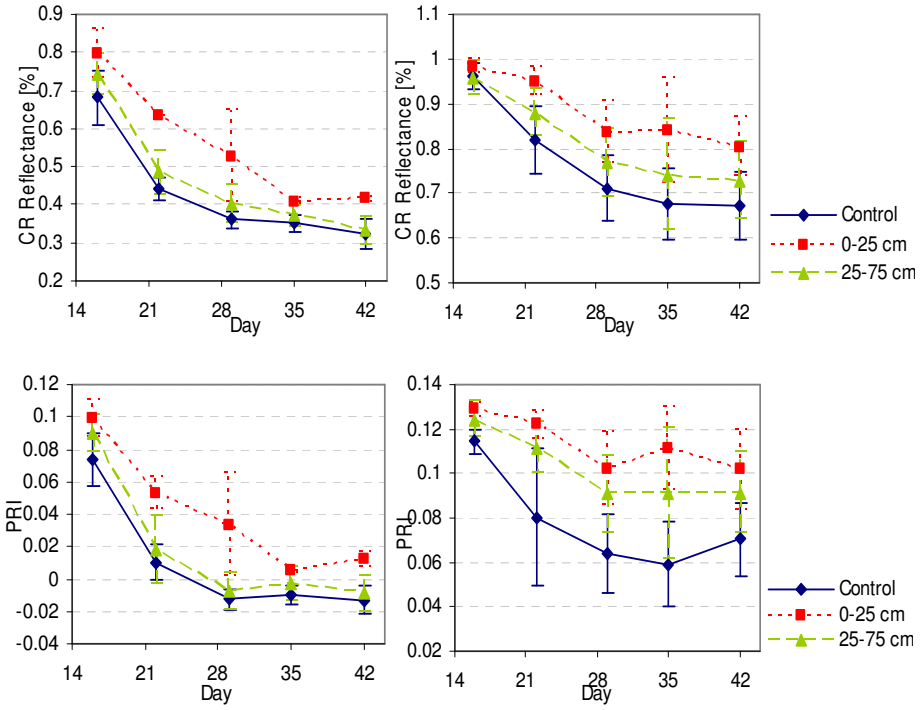

Figure 6.5 Continuum removed (CR) reflectance at 580 nm and the PRI of the maize (left) and wheat (right) canopy over time

6.3.3 CO_2 effect

The average oxygen depletion as calculated for every measurement was 3.91 (standard error 1.9) in the maize plots and 2.78 (standard error 1.6) in the wheat plots. To obtain an indication of the spatial pattern of the oxygen depletion, methane concentrations were estimated over the plots, after which the difference between the expected and predicted oxygen concentrations could be calculated. Although the relationship between gas and oxygen concentrations in the field was weakly linear (Figure 2.4), the same indices as in Chapter 5 were correlated to soil gas concentrations. After normalizing for time (Section 5.3.2) the highest regression coefficients were 0.71 for Vog1 and 0.48 for LIC3 (Table 6.1; Figure 6.6).

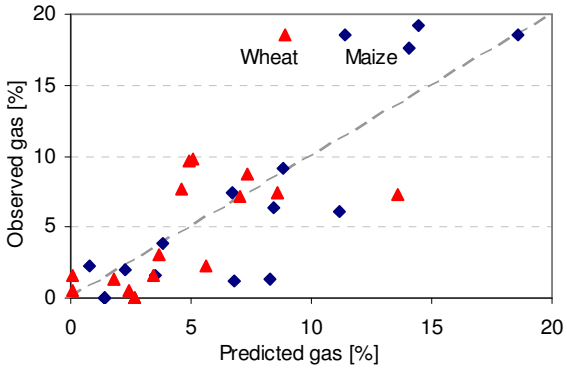

Figure 6.6 Observed against predicted gas concentrations based on Vog1 (maize) and Lic3 (wheat)

Table 6.1 Regression equations between Vog1 (maize) and Lic3 (wheat) and soil gas concentrations

Species	Regression equation	R^2
Maize	CH_4 [%] = 44.99 – 30.94 * Vog1	0.71
Wheat	CH_4 [%] = -20.72 + 100.16 * LIC3	0.48
Expected	O_2 [%] = 20.00 - 0.20 * CH_4 [%]	

Using the regression equations based on these indices, the gas concentrations were calculated on all plots. Based on the predicted gas concentrations, the oxygen concentrations as expected according to equation 6.1 were calculated and compared with the predicted oxygen concentrations as found in Chapter 5. Figure 6.7 shows that only in the gassed centre of the two maize gas-plots the difference is over 2%. The low regression coefficient and the gross underestimation of high gas concentrations under the wheat canopy (Figure 6.6) resulted in unreliable (negative) gas and oxygen estimations.

Initial and consumed methane concentrations calculated on the measured gas concentrations followed a very similar pattern as described by Steven *et al.* (2006), showing the highest methane consumption at initial methane concentrations of about 10% (Figure 6.8).

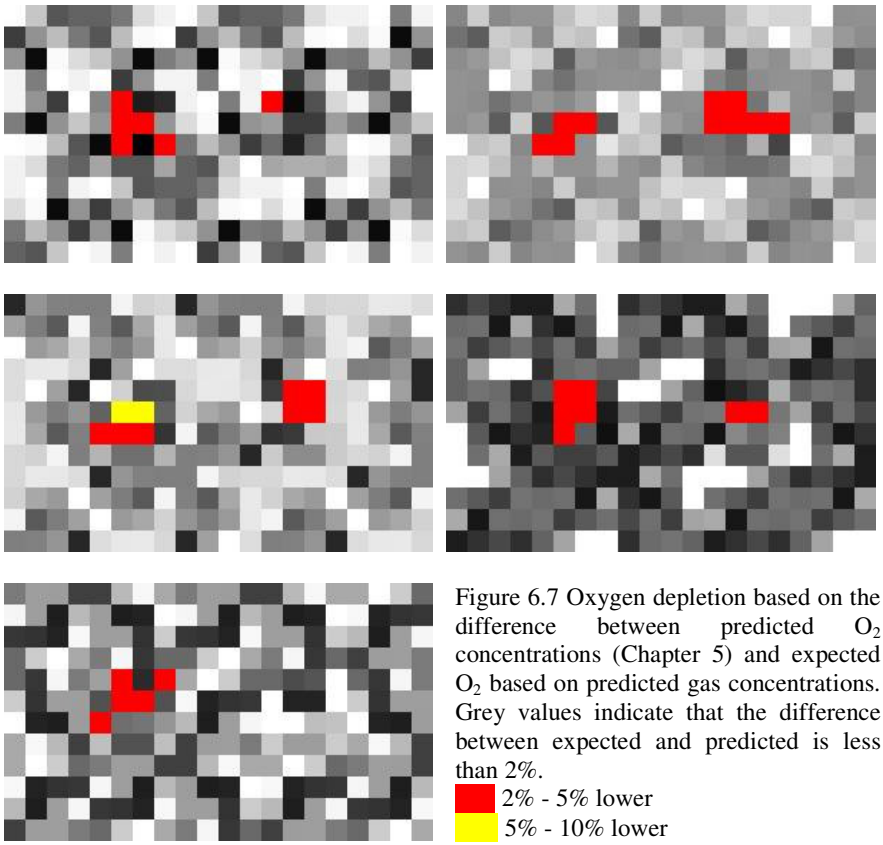

Figure 6.7 Oxygen depletion based on the difference between predicted O_2 concentrations (Chapter 5) and expected O_2 based on predicted gas concentrations. Grey values indicate that the difference between expected and predicted is less than 2%.
2% - 5% lower
5% - 10% lower

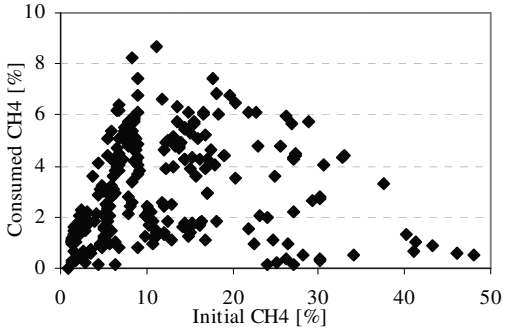

Figure 6.8 Consumed against initial methane

When the same calculations were extrapolated to the maize plots, at only two dates (t = 22 and t = 29) the methane consumption or CO_2 production reached 2%; at all other dates the CO_2 production was under 1.5% (Figure 6.9).

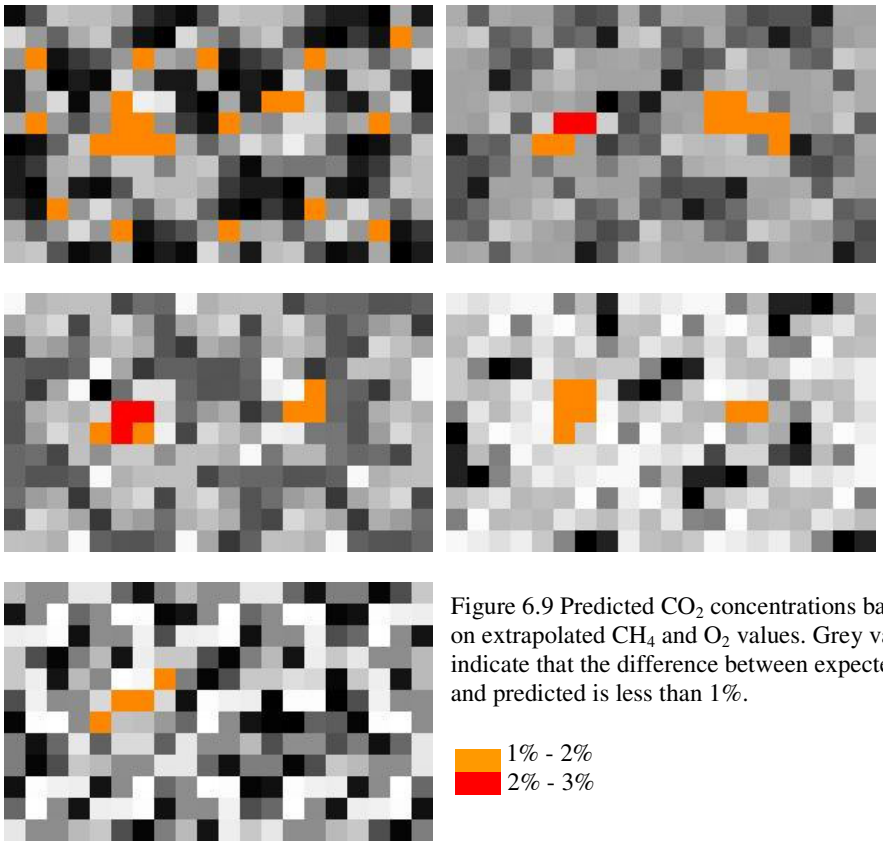

Figure 6.9 Predicted CO_2 concentrations based on extrapolated CH_4 and O_2 values. Grey values indicate that the difference between expected and predicted is less than 1%.

6.4 Discussion

Figure 6.1 shows that the visible difference between the gassed and control maize leaves was much larger than the difference between the gassed and control wheat leaves. Not only did maize leaves have a stronger discolouration than the wheat leaves, they also remained much smaller than the control. The decreased NIR reflectance of the gassed maize leaves suggests that the leaf structure has changed, whereas the gassed and control wheat leaves have a similar NIR reflectance. As was shown in the previous chapters, small gas concentrations did not affect wheat reflectance, while large gas concentrations and the resulting low oxygen concentrations did not have strong correlations

with canopy reflectance. Although wheat reflectance can be used to detect large gas leaks (Chapter 5), maize plants show reactions to soil gas that are easier to detect using leaf and canopy reflectance.

6.4.1 Ethane

The effects of ethane on maize leaves and canopy in a large leak were determined using the PRI and continuum removed reflectance in the red absorption region. The PRI and the CR reflectance of the gassed leaves and canopy were higher than those of the control, which is in accordance with the results of Chapter 3. However, the shape of the curves is very different. When the difference between the control and the gassed leaf reflectance of this study is compared with the greenhouse study (Figure 6.10), it shows that in the greenhouse the largest difference occurred between 560 and 600 nm, while in this chapter the largest difference occurred around 650 and 700 nm. Besides, the magnitude of the difference is up to 6 times larger in this study. The standard deviation indicates that the regions for distinguishing the gassed reflectance from the control are located between 575 and 625 nm and between 700 and 750 nm. The first region overlaps with the 560 – 600 nm region as found in Chapter 3, while the 700 - 750 nm region is the red edge. Both regions are related to leaf chlorophyll (Demetriades-Shah *et al*., 1990; Gitelson and Merzlyak, 1998; Adams *et al*., 1999; Collins, 1978; Boochs *et al*., 1990; Horler *et al*., 1983). The increase in the yellow region in the greenhouse was most likely caused by reduced chlorophyll content early in the experiment (Chapter 3), whereas the large difference in chlorophyll content as found in this study causes an increase in both the yellow and the red edge regions. These results support the conclusion of Chapter 4 that subtle chlorophyll differences are visible in the yellow region, while at higher chlorophyll contents the red edge region can distinguish the differences better. The large chlorophyll differences are the most likely cause for the absence of an apparent shift towards longer wavelengths in the leaf and canopy reflectance, as was caused by ethane.

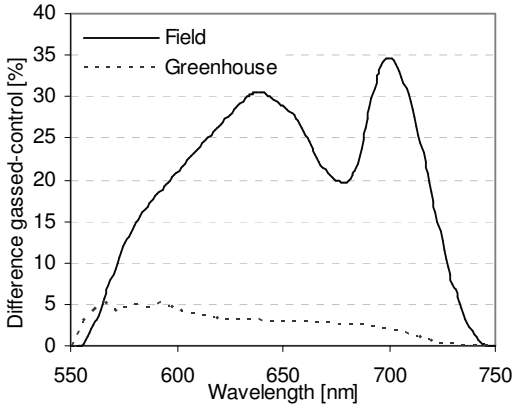

Figure 6.10 Difference in continuum removed reflectance between the control and the gassed leaves.

Since the results have demonstrated that ethane may have affected the reflectance in the central 25 cm of the gas-plots, the regression between oxygen and reflectance indices in Chapter 5 was actually a regression between [oxygen + ethane] and reflectance indices for at least some of the data points. Since ethane and oxygen shortage both caused a decrease in leaf area, the extent of the effects of ethane cannot be quantified. However, since only few data points were affected, it is believed that the overall regression would not lead to significantly different results. To test this assumption, a new regression analysis was performed between Vog1 ($R740/R720$) and oxygen concentrations, taking into account the 'ethane effect'. Vog1 is linearly related to LAI (Figure 6.11a). If ethane would be absent, this would result in a relatively higher LAI and Vog1 value in the centre of the gas-plot (Figure 6.11b). As the exact difference in LAI is not known, an arbitrarily chosen value was added to those data points that were located in the centre of the gas-plots. Yet, since oxygen concentrations were also significantly lower in the centre of the gas-plots, it is reasonable to assume that the Vog1 value at this location was lower than at the other locations. For the centre value to remain lower than the other values, Figure 5.6 shows that a maximum of 0.1 to 0.2 could be added to the lowest Vog1 value. Table 6.2 shows the results when 0.1 respectively 0.2 was added to the lowest Vog1 values. Although the correlation weakens, the regression equation is very similar for each value, resulting in similar predicted O_2 concentrations particularly at higher Vog1 values. It is therefore concluded that the effect of ethane has not affected the results of Chapter 5 significantly.

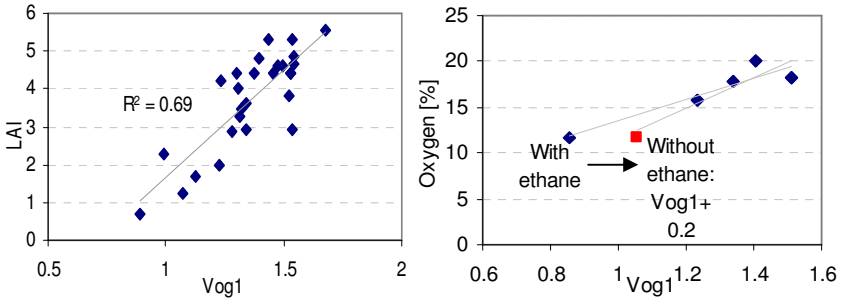

Figure 6.11 a) Correlation between 'Vog1' and leaf area index LAI. b) Increase of Vog1 value if ethane would not be present in the central 25 cm of the gas-plot.

Table 6.2 Regression equations between oxygen concentrations and Vog1, including and (partially) excluding ethane effect (see text for detailed explanation)

Value added to Vog1	Regression equation	R^2
Original	O_2 = -2.5 + 15.1 * Vog1	0.74
Vog1 + 0.1	O_2 = -4.9 + 16.8 * Vog1	0.72
Vog1 + 0.2	O_2 = -5.4 + 16.9 * Vog1	0.54

6.4.2 CO_2

Steven *et al*. (2006) showed that in addition to oxygen displacement by methane, bacterial oxygen depletion may take place, reducing the available oxygen with an additional 1.8 to 4.7 % (as percentage of total soil air). In leaks where bacterial oxygen depletion takes place, the oxygen concentrations may therefore be lower than expected, which may increase the chance of detecting changes in vegetation reflectance. At the same time, methanotrophic bacteria produce CO_2, which has shown to affect leaf reflectance (Chapter 4). In this chapter it was attempted to quantify the oxygen depletion and the related CO_2 concentrations. The average oxygen depletion was 3.91 % in the maize plots and 2.78 % in the wheat plots, which was comparable to the values found by Steven *et al*. (2006) who found an average depletion of 4.2 % under grass, bean and winter wheat plots in the summer. The oxygen depletion as predicted over the whole plot showed that depletion over 2% only occurs in the centre of the gassed plots.

As in this study, Steven *et al*. (2006) found relatively low oxygen depletion (1.8%) in the wheat plots. The rate of bacterial oxygen depletion is dependent on soil moisture, soil temperature and cultivation (Hoeks, 1972a; Hütsch, 2001). Although soil moisture and temperature were not measured, the high vegetation cover on the maize plots may have resulted in lower evaporation from the soil. Since summer 2003 was very dry, a lower evaporation may have caused slightly

higher soil moisture under the maize plots, which may have increased the bacterial activity. Moreover it is expected that due to the high vegetation cover, soil moisture and temperature varied less than under the wheat canopy, creating a more stable environment for bacterial activity. The soil under both species had been cultivated before, leading to a less than optimal oxidation (Hütsch, 2001).

Methane consumption on the measured data had a peak of 8% (Figure 6.8). Although the pattern of the modelled methane consumption over the whole plot was as expected (high values in the centre of the gassed plots), the predicted values were lower than the measured values. The difference can be explained by the regression results: high gas concentrations under the maize plots were underestimated by up to 5%. This led to lower initial methane concentrations and therefore to lower consumed methane concentrations. Assuming that CO_2 concentrations in the gas-plots would reach a maximum of the measured 8%, it is unlikely that CO_2 has an additional effect on the canopy reflectance. Chapter 4 showed that CO_2 concentrations up to 20% could not be distinguished with certainty from the control. Therefore it is concluded that the measured changes in leaf and canopy reflectance are the result of low oxygen concentrations in the soil.

6.5 Conclusion

In the previous chapters it was shown that in a gas leak several gases potentially affect plant reflectance. In Chapter 5 it was shown that a decrease in soil oxygen concentrations is linearly related to several vegetation indices. Chapter 3 and 4 showed that ethane and CO_2 caused changes in leaf reflectance in the visible light. In a large leak ethane, CO_2 and oxygen all occur together and interact with each other, but it was not known which of the three gases had the strongest influence. By repeating the same analysis as in Chapter 3 it could be concluded that ethane may have affected the reflectance, but only in the central 25 cm of the gas-plots. Since only few measurements were affected by ethane, the results of Chapter 5 did not change when the effect of ethane was excluded. The CO_2 concentrations were calculated using a model that incorporates bacterial oxidising activity and continuous replenishment of the soil with methane and air. Although values were underestimated by up to 5%, soil CO_2 did not reach concentrations that have shown to be harmful to plants. It is therefore concluded that in a large leak, a low oxygen concentration is the main cause for changes in reflectance.

CHAPTER 7 *

HYDROCARBON SEEPAGE DETECTION USING VEGETATION REMOTE SENSING

7.1 Introduction

Up to this point, this thesis has dealt with experimental short to medium term gas leakage. The main conclusion from the experiments is that gas leakage – whether through displacement of oxygen or through the effects of ethane – causes a decrease in leaf area. Chapter 5 has shown that several hyperspectral indices correlated with soil oxygen concentrations, where the choice of the best index was dependent on species and moment in time. The chance of detecting a leak was increased when, in addition to the spectral characteristics, the spatial patterns of the leak were taken into account. These results were based on experimental and controlled situations. In this chapter the results obtained so far are tested for their feasibility for gas leak detection using hyperspectral imagery. The test case is a natural hydrocarbon seepage area in the Santa Barbara basin, USA, where long-term gas and oil seepage occurs at several locations. In contrast to the experimental set-up, the vegetation in the area consists of several species. Pysek and Pysek (1989) showed that artificial gas leakage caused a change in vegetation diversity and cover. Therefore, in addition to testing the results of the previous chapters, a vegetation survey was performed to determine whether changes had taken place in the vegetation patterns. Field reflectance measurements were compared to a hyperspectral image to study whether the patterns observed in the field could be recognized in the image.

7.1.1 Site description

The seepage area is located in Upper Ojai Valley, Ventura Basin, USA (Figure 7.1). The area is characterised by large oil fields, which have their source in Miocene to Pleistocene organic rich siliceous shale (Dibblee, 1987). The seep that was sampled in this study is located at Lat. 119°08'24" Lon. 34°25'45" in a meadow with grassland vegetation. Remnants from at least two other seeps were present in the same meadow. Sampling took place between April 20 and April 25, 2003. According to the local villagers, the seepage appeared in the 1980's after an earthquake occurred. The seepage consists of a point source of

* This chapter is based on: Noomen, M.F., Van der Werff, H.M.A and van der Meer, F.D., in preparation. Detecting circular patterns in vegetation canopies caused by underground natural gas seepage. Submission to: Terra Nova.

actively seeping oil, accompanied by light hydrocarbon gases (mainly methane) and CO_2.

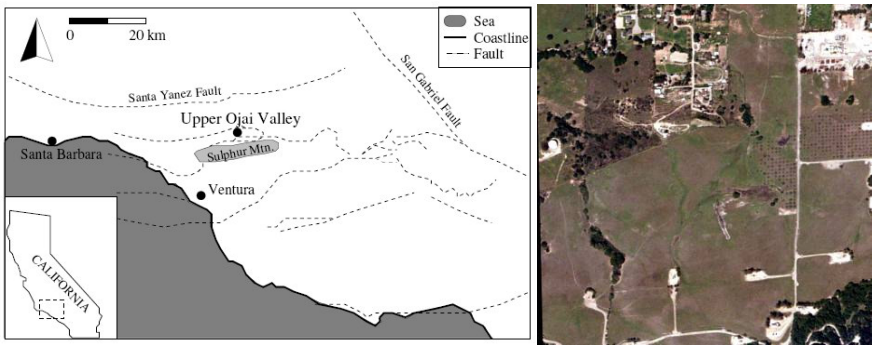

Figure 7.1 Map (left) and aerial photograph (right) of the location of the seepage, Ojai Valley, USA (Source: Van der Werff, 2006). The photograph was acquired mid 90's and covers an area of 950 m (W-E) by 1050 m (N-S).

Van der Werff (2006) has described the soil properties in and around the seep. There were no major differences in mineral composition and pH between the soils in and outside the seep. Soil moisture however was approximately 13% lower in the seep than in the normal soil.

7.2 Methods

7.2.1 Vegetation cover and diversity measurements

The vegetation was sampled along transects to obtain an indication of gradients in species richness. Measurements were performed along a south, east and west transect, with each transect starting at the seep centre. Since oil was leaking towards the north forming an oil 'river' at the surface, no measurements were made along a north transect. The transect length was set on 36 m resulting in a 9 pixel wide west-east transect on the hyperspectral image, with sampling points at every 2 m to include the smaller scale variability. Total vegetation cover was estimated at each sample point using a frame of 1 m^2 as described by Kent and Coker (1992). In a similar manner the cover of each individual species was estimated. Vegetation diversity was measured by counting the number of species within the frame.

7.2.2 Reflectance measurements

Canopy reflectance was measured at each sample point using an ASD Fieldspec Pro spectroradiometer (Analytical Spectral Devices, Inc, Boulder, Colorado,

USA), which has a sampling interval between 1.4 nm and 12 nm but produces 1 nm interval readings over the full wavelength range (350-2500 nm). The sensor was held approximately one meter above ground level viewing an area of 50 by 50 cm. Of each sample point, 10 measurements were taken, which were averaged afterwards to account for the BRDF effect (Nicodemus, 1977) and small-scale irregularities. After each transect, the spectroradiometer was calibrated using a white barium sulphide panel.

7.2.3 Data analysis

The following indices were calculated using the field reflectance (where *R* is the reflectance and *R*' the first derivative reflectance at the specified wavelengths):

1. PRI: $\frac{(R531 - R570)}{(R531 + R570)}$. The PRI is related to subtle changes in plant health, such as caused by ethane (Chapter 3);
2. LIC3: $\frac{(R440)}{(R740)}$. LIC3 was correlated to oxygen concentrations under the wheat canopy (Chapter 5), and is assumed to maximize differences between soil and vegetation at low vegetation cover;
3. Vog1: $\frac{(R740)}{(R720)}$. Vog1 was correlated to oxygen concentrations under the maize canopy (Chapter 5), and is assumed to maximize differences in leaf area at high vegetation cover;
4. OSAVI: $(1 + 0.16)\frac{(R800 - R670)}{(R800 + R670 + 0.16)}$. OSAVI was correlated to oxygen concentrations under maize and wheat canopy (Chapter 5);
5. Ratios: $\frac{(R765)}{(R735)}$ and $\frac{(R'642)}{(R'640)}$. These ratios were able to distinguish high from medium-high LAI of the maize canopy;
6. WBI: $\frac{(R900)}{(R970)}$. This ratio is related to leaf and canopy water content (Penuelas *et al*., 1997). Although this index was not found to be of importance in the experimental gas leaks, in natural situations gas leakage may dry out the soil and cause water shortage. This may be visible as an increase in the water absorption feature at 970 nm.

The patterns that were found in the vegetation cover and diversity were correlated with the indices to identify which index explained the patterns best.

The results were applied to a Probe-1 image (Earth Search Sciences, Inc., Lakeside, USA). The image (spectral range 436-2480 nm, spectral resolution 15 to 20 nm, spatial resolution 8 m) was taken in July 1998. Since the image was acquired five years before the field measurements took place and in a different season, the field reflectance could not be directly correlated to the image. However, Chapter 5 has shown that canopy patterns and their associated reflectance change in a predictable manner over time when exposed to gas, so the aim here was to investigate whether similar changes may have occurred at this natural seep. According to the owner, the meadow in which the seepage was located had not been in use since the seeps appeared. Therefore it was assumed that the main differences between image and field vegetation reflectance were due to the differences in season.

7.3 Results

7.3.1 Vegetation cover and diversity

Total vegetation cover increased with distance from the seep (Figure 7.2a). Within 10 m distance of the seep the cover was under 10% and bare soil dominated. Between 20 and 30 m the cover increased to 100%, but then decreased to values between 80 and 100% outside this area. The east transect is different from the west and south transects, showing an increase in vegetation cover 10 m further from the seepage. It is assumed that this extended distance of bare soil towards the east was caused by anomalous atmospheric gas concentrations carried by the dominant winds from the west.

Vegetation diversity increases after approximately 10 m distance from the seep on both south and west transects, but the east transect shows a less clear pattern (Figure 7.2b). At 30 m distance to the seepage, the diversity appears to stabilize around an average of 8 species. The species that had the highest average occurrence on all sample points outside the centre 10 m are shown in Table 7.1. The largest abundance was found for *Rumex acetosa* and *Tanacetum vulgare*. These and all other species that had an abundance of 1% or more are commonly found species and not specific to the area (Dale, 1986; Niehaus and Ripper, 1976). In both the west and the south transects, *Tanacetum vulgare* appears at 14 to 16 m, followed by a high abundance of *Rumex acetosa* between 20 and 28 m, after which the abundance of the latter decreases and *Tanacetum vulgare* appears again. *Anthemis cotula* and *Vicia benghalensis* accompany both species on both transects.

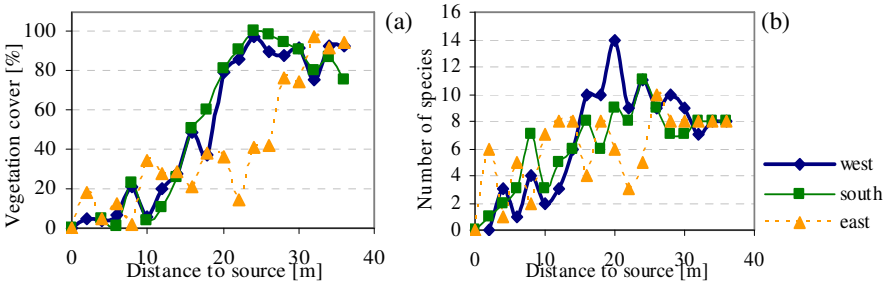

Figure 7.2 Vegetation cover (a) and diversity (b) along a west, south and east transect

Table 7.1 Abundance of the species that had the highest average occurrence on all sample points outside the centre 10 m. The abbreviations are used in following graphs and figures.

Species	Abbrevation	Abundance [%]	Specifics
Rumex acetosa	Ra	34	Common weed
Tanacetum vulgare	Tv	30	Disturbed areas, invasive weed
Anthemis cotula	Ac	17	Fields and waste areas, common
Vicia benghalensis	Vb	16	Road sides, waste areas
Erodium cicutarium	Bc	10	Open waste areas, grassy slopes
Bromus mollis	Bm	7	Common weed in waste areas
Bromus diandrus	Bd	4	Common weed in fields and waste areas
Brassica geniculata	Bg	2	Common
Lolium perenne	Lp	2	Occasionally waste areas, pastures
Hordeum murinum	Hm	2	Weed in waste areas
Convolvulus arvensis	Ca	1	Weed in fields, waste areas
Helianthus spp.	H	1	-

This combination of high cover and a few dominating species occurred in all directions around the seepage source and was visible as a ‘green ring’ around the seepage (Figure 7.3). The vegetation patterns around the sampled seep could thus be described as follows:

- Within 10 m distance to the seepage, bare soil dominates in a halo-like shape;
- Between 20 and 30 m distance a ring of a few dominating species occurs.

To define which samples belong to these three clearly visible classes, a *k*-means clustering algorithm was used. This algorithm divides the sample points in *k* (in this case 3) clusters so that the variability within clusters is minimized and the variability between clusters is maximized (Hartigan and Wong, 1979).

Figure 7.3 A green 'ring' is visible around the seep

Since the patterns on the east transect were less clear, the clustering was based on the vegetation cover and diversity on the south and west transects. Figure 7.4 shows the class means per cluster and the cover translated into three clusters. The average cover and diversity per cluster are shown in Table 7.2. Cluster 1 and 3 clearly represent the bare halo and the ring, whereas Cluster 2 is intermediate in cover, and represented by a high abundance of *Tanacetum vulgare*. A one-way ANOVA showed that only cover and the abundance of *Anthemis cotula* are significantly different for each cluster ($p \leq 0.05$). The abundance of the majority of species is significantly lower in Cluster 1 than in Cluster 3, whereas Cluster 2 sometimes overlaps with either Cluster 1 or Cluster 3.

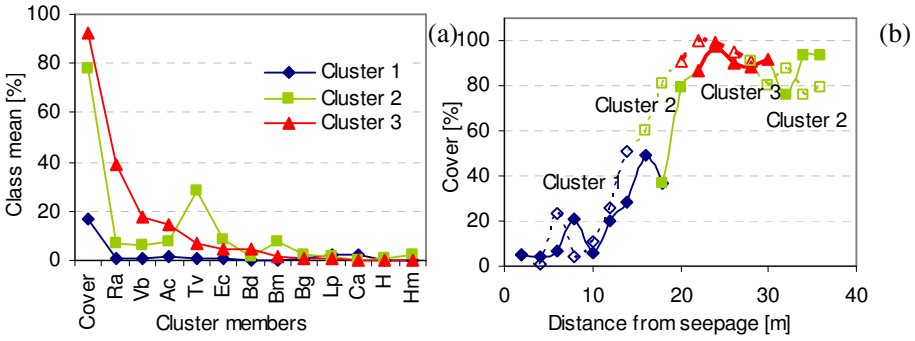

Figure 7.4 Class means per cluster member (a) and the cover on the west and south transects divided into the three clusters (b). The dashed and the continuous lines represent the south and west transect respectively.

Table 7.2 Average cover and number of species per cluster, and the species that has the highest abundance in that cluster.

Cluster	Cover (%)	Number of species	Highest abundance (%)
1	16	4	*Convolvulus arvensis* (2.5%)
2	79	8	*Tanacetum vulgare* (28%)
3	94	9.5	*Rumex acetosa* (39%)

7.3.2 Field reflectance

Based on the vegetation cover and diversity it was concluded that the seepage caused a succession of zones. The specified reflectance indices were calculated for each sample point and averaged for each cluster. To compare the suitability of each index to distinguish the clusters, each index was normalized between 0 and 1 (Figure 7.5). WBI and OSAVI had a very similar pattern, with a very low Cluster 1, a high Cluster 3 and an intermediate Cluster 2. Vog1 and ratio 765/735 are closely related to LAI and they show that –although canopy cover on the west and south transects is similar in Cluster 3 – the LAI of the south transect is higher. LIC3 distinguishes the clusters that contain vegetation (Clusters 2 and 3) from the cluster that hardly contains any vegetation (Cluster 1), but the distinction between the vegetated clusters is not clear. PRI finally is strongly influenced by differences in species type and canopy structure (Filella *et al*., 2004), which makes the PRI less reliable for a health assessment of a multi-species canopy. The first derivative ratio '642/'640 resulted in a very noisy pattern and was not deemed reliable.

In conclusion, with respect to the results from Chapter 5, OSAVI is the most appropriate index for distinguishing differences in vegetation cover; Vog1 and the ratio 765/735 are most accurate in distinguishing differences in LAI at higher cover; and LIC3 distinguishes vegetation from soil at lower cover. PRI is useful to assess photosynthetic activity within one species, but unreliable in a species-rich vegetation. Whereas in the experimental gas leak WBI was of no importance, in the larger long-term leak setting described here, this index shows a decrease in the centre of the leak due to drying of the soil.

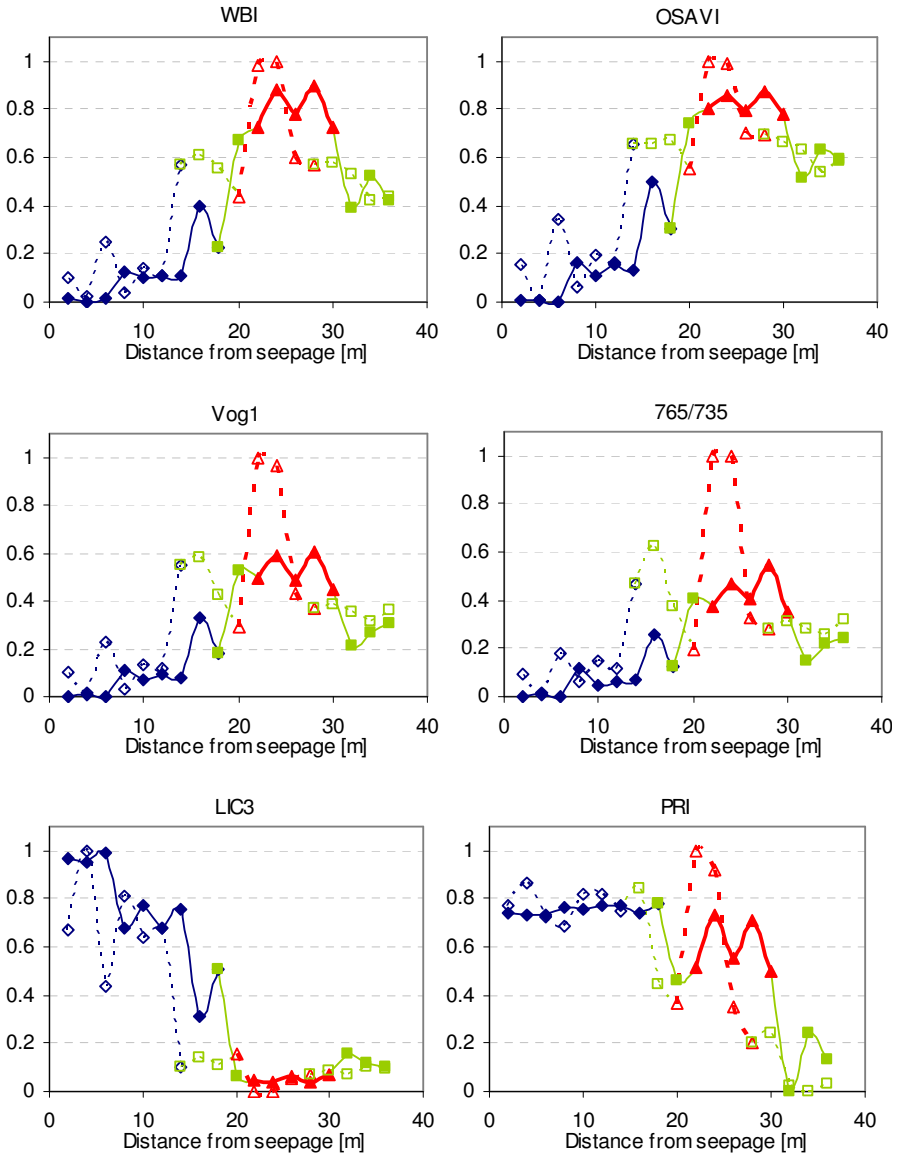

Figure 7.5 Selected indices normalized between 0 and 1, with superimposed clusters in blue (Cluster 1), green (Cluster 2) and red (Cluster 3). Solid line = West transect; Dashed line = South transect.

7.3.3 Image analysis

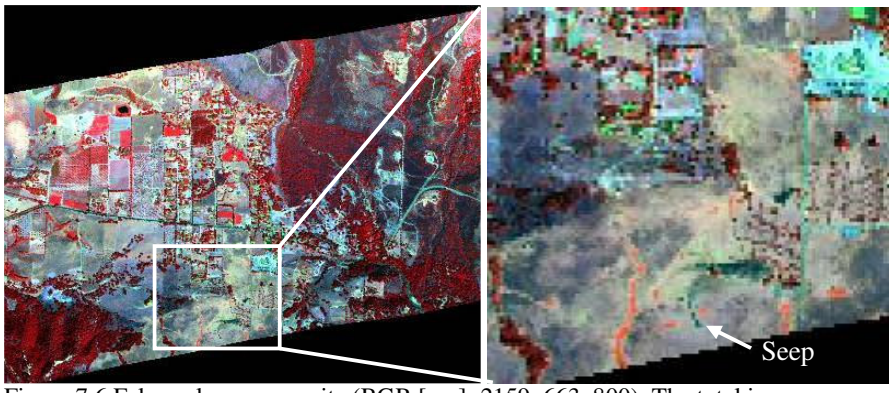

Figure 7.6 False colour composite (BGR [nm]: 2159, 663, 800). The total image measures 3.2 by 1.2 km; the zoomed area is 1050 m by 950 m.

To determine whether these indices can detect the sampled seep on the Probe-1 image (Figure 7.6), the following procedure was followed:

1. NDVI was calculated first; at NDVI values under 0.75 LIC3 was calculated to detect unvegetated areas (Chapter 5), while at NDVI values over 0.75 Vog1 was calculated to detect patterns in LAI.
2. OSAVI and WBI were then calculated to detect patterns in the vegetation cover.

The NDVI values around the seep were on average 0.15 (Figure 7.7). This is a very low value and shows that in July the vegetation is showing signs of senescence. OSAVI showed larger differences in the vegetation whereas WBI had a very speckled pattern. Since the NDVI values were very low, LIC3 was assumed to be the best index. Indeed the difference between the vegetation and unvegetated areas is clearest on the LIC3 image. Vog1 clearly shows the difference between high and low biomass, but the differences within the areas of low biomass are small.

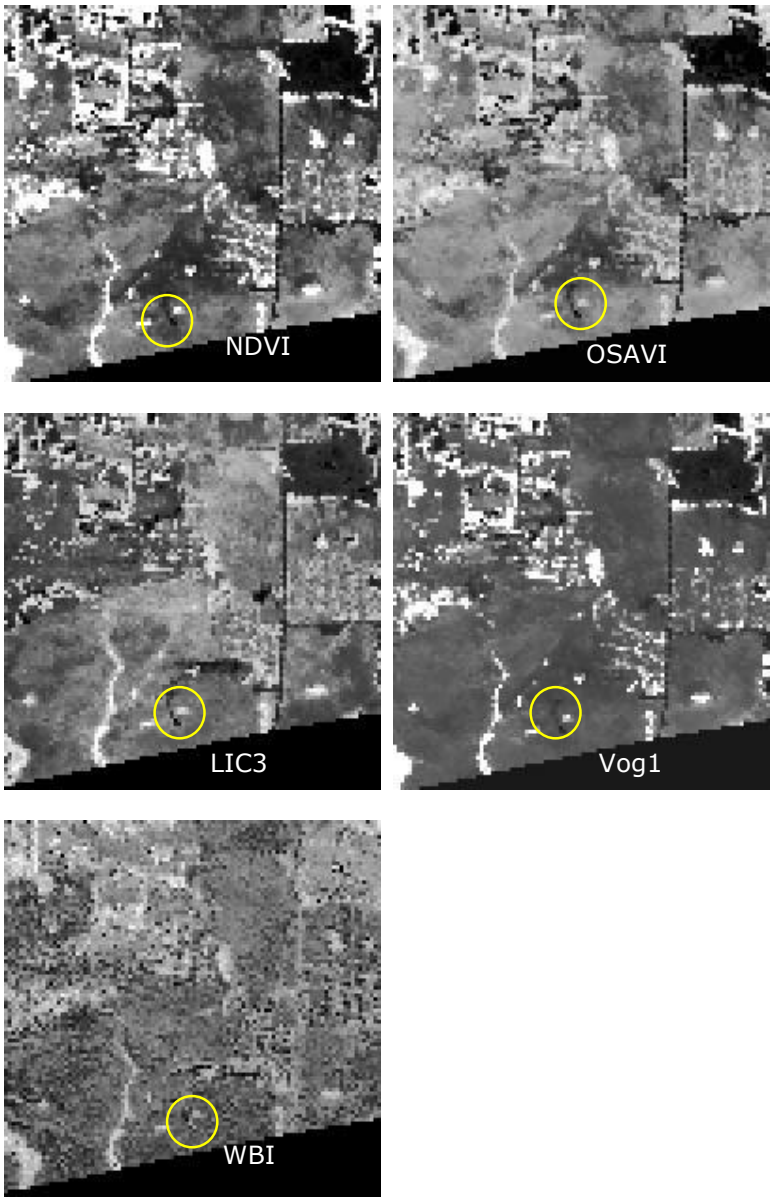

Figure 7.7 Indices calculated on Probe-1 image. The grey tones are stretched to show the best distinction between the seep and the vegetation. Dark tones represent low biomass; light tones represent high biomass. The yellow circle indicates the seep.

As visible in West-East transects over the seep centre, the indices have a slightly increased value directly next to the soil halo in the centre (Figure 7.8). This is possibly the influence of the ring of high biomass around the soil centre (described by Cluster 3).

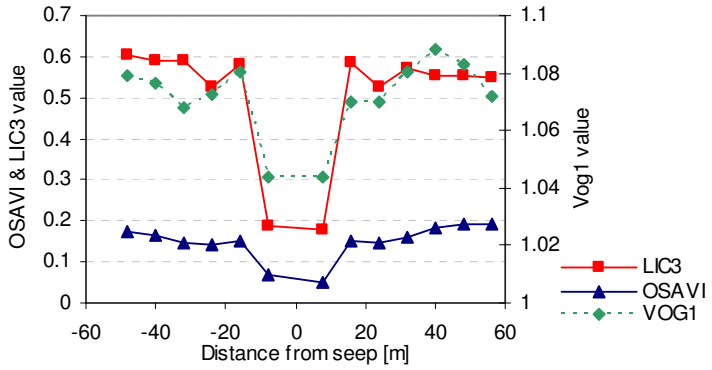

Figure 7.8 W-E transects of OSAVI, Vog1 and LIC3 on the Probe-1 image. The indices show a slightly increased value on the pixel next to the centre halo, which may be the influence of Cluster 3.

7.3.4 Detection of hydrocarbon seepages

The previous section has shown that the seep may be observed using vegetation indices derived from hyperspectral imagery. However, even when the most accurate index is used to map the seeps, many other pixels in the image have the same index values. Figure 7.10a demonstrates that when LIC3 is used to map the seep, other low vegetation areas such as roads and asphalted areas also light up. To reduce the number of false anomalies and to exclude all areas where gas leaks are not expected to take place, metadata such as maps of the geology or gas pipelines could be used to decrease the area of interest. In this study, built-up areas and forests were removed. Although gas leaks and seeps may occur in these areas, the techniques described in this thesis were designed for detecting leaks in grassland and crop vegetation. Further studies should determine which techniques are appropriate to detect gas leaks in built-up and forested areas. The forests were filtered out by thresholding the NDVI, while the built-up areas and roads were removed using topographical maps. In Chapter 5 it was shown that applying a filter that searches for leak-specific spatial patterns assists in identifying leaks. In this chapter it was shown that the seep was surrounded by a ring of vigorous vegetation. Therefore, a filter that looks for a ring of high biomass around a pit of no biomass, or in other words, a filter that resembles the transects in Figure 7.8 may be applied. Since the shape resembles that of a

Gaussian filter, a 6-pixel wide filter was created based on a high-pass Gaussian filter (Figure 7.9) and applied to the OSAVI, LIC3 and Vog1 images. The output images show bright pixels where the filter has a high fit (Figure 7.10b-d). When the 1% brightest pixels are shown (arbitrarily chosen to indicate only those areas that resemble the filter's shape most), OSAVI and Vog1 do not filter out the seep, but LIC3 clearly shows the seep centre in addition to the three remnant seeps. In conclusion, by removing the areas that are not of interest and by applying a filter that searches for the specific spectral and spatial characteristics of the seeps, the number of false anomalies has reduced sharply.

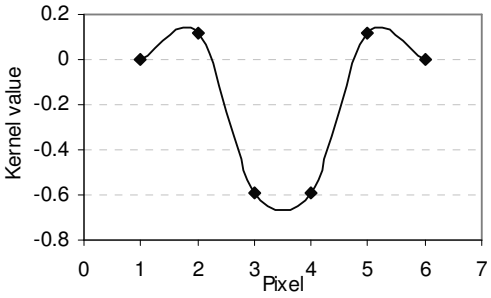

Figure 7.9 Shape of the filter used for the detection of the seeps

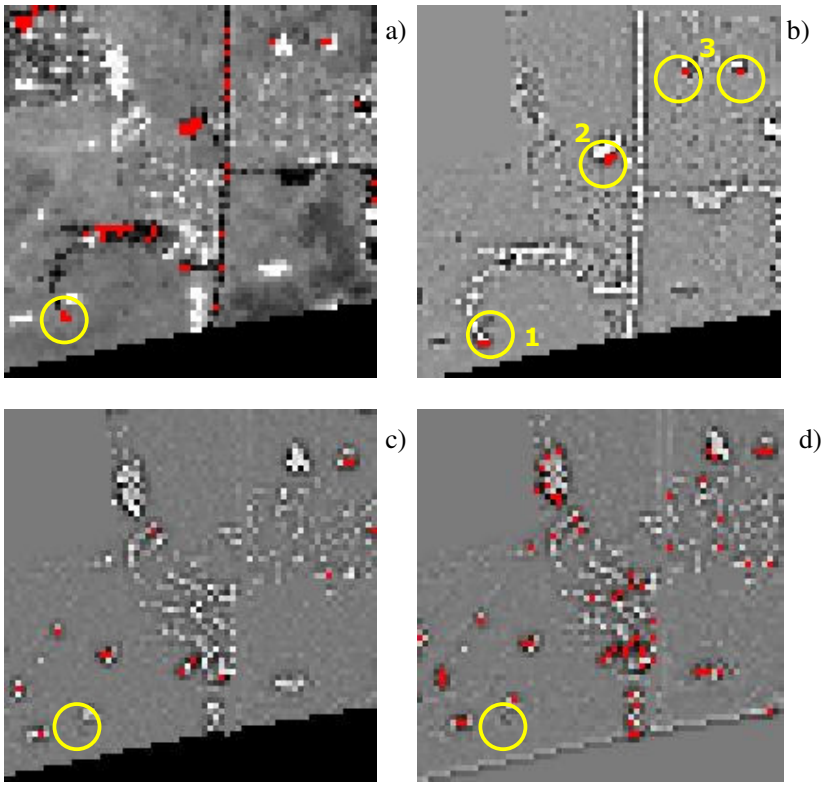

Figure 7.10 a) LIC3 image, showing the seep and several false anomalies that have the same index value as the seep; Filtered and masked images of b) LIC3, c) OSAVI and d) Vog1. The 1% brightest pixels are shown in red.

7.4 Discussion

Vegetation cover and species diversity show that close to the seep, plant life is affected. Within a radius of 10 to 20 meters of the seep, average cover is 16% while the average number of species is 4 (west and south transects), as opposed to a cover and diversity of 94% and 9.5 respectively 10 meters further. Although not measured, it is assumed that a low oxygen concentration in the halo is the reason for the absence of plant growth. As shown in the previous chapters, methane did not affect plant growth, whereas the effects of ethane are difficult to distinguish when oxygen shortage takes place. As was demonstrated in this thesis and by Hoeks (1972a) and Smith *et al*. (2004b), gas concentrations in the soil decrease non-linearly with distance from the seepage. In this thesis it was shown that in a mono-species canopy plant height and leaf area was low in

the centre of the gas leak, but increased with distance to the leak. However, this chapter shows that outside the halo of bare soil, a ring occurs of apparently healthy vegetation (Cluster 3). Vegetation cover in this cluster is 15% higher than in the area surrounding it, and most of the vegetation indices indicate that Cluster 3 contains the highest biomass. Although four species (*Rumex acetosa*, *Tanacetum vulgare*, *Anthemis cotula* and *Vicia benghalensis*) that are commonly found in waste places and roadsides dominate the ring, the average number of species in the ring is higher than outside the ring. A change in species composition next to gas seeps is in accordance with Bizecki Robson *et al*. (2004), who showed that hydrocarbon pollution near oil wells caused a decrease in vegetation cover and species richness, while five species were found to be tolerant. The change in vegetation patterns may have several reasons. Van der Werff (2006) showed that soil moisture was much lower inside than outside the halo. Since long-term gas and oil seepage is known to bring groundwater to the surface (Jones and Drozd, 1983), it is possible that groundwater collected at the edges of the halo, where the gas fluxes are lower than in the central vent. The gas fluxes in the halo were probably so high that the soil dried out completely. This would explain the high values of the water band index (WBI) in the ring. Moreover, the four most common species in Cluster 2 and 3 are known to grow in moist soil. Another possibility is that groundwater seepage did not play a role, but that the decrease in soil moisture in the halo caused a favourable environment for water-use efficient plants compared to plants that are less water-use efficient, thereby causing a shift in species composition. Yet another reason for the shift in species composition may be that just outside the halo small quantities of gas occur in the soil and that oxygen concentrations are sub-optimal. Since species have shown varying sensitivity to root zone oxygen shortage, the species in the ring may have been species that are tolerant to low oxygen concentrations. For the latter two explanations, one would expect a succession of Cluster 1 (halo) to Cluster 3 (ring around halo) to Cluster 2 (probably unaffected). However, since the succession of zones showed that Cluster 2 accompanied Cluster 3 on both sides, the first explanation is the most likely: Cluster 1 being the central vent (dry soil), Cluster 2 the transition zone to Cluster 3 (intermediate soil water content) and Cluster 3 being the groundwater seepage zone (high soil moisture).

The results from this chapter confirm that the selected indices can distinguish the gassed area from the surrounding areas due to the lower vegetation density. Since the scope of this thesis is characterizing the behaviour of vegetation growth and reflectance affected by gas seepage in order to define a general method for gas leak detection, the behaviour of each species and its reflectance in this particular case were not investigated. A detailed investigation of the reflectance of each species would lead to a description of a situation that is only valid in this particular place at this particular time. Although this would give insight in the behaviour of the investigated species in relation to gas seepage,

further research would have to be undertaken to understand the behaviour of these species and their reflectance in time. Instead, the scope of this chapter was to test whether the methods that were defined in the previous chapters could be applied to a field situation. Despite different species, gas fluxes, temperatures, *etcetera*, this chapter shows that the indices defined earlier in this thesis, in combination with spatial information, can observe changes in biomass caused by gas leakage on hyperspectral imagery.

Of course, when using general indices that are related to biomass and chlorophyll, many false anomalies occur. Therefore the classification must be limited to only the areas of interest. In this chapter it was demonstrated that removing all areas that are not of interest and including expert knowledge resulted in a decrease of the number of false anomalies. This is in accordance with the work by Van der Werff and Lucieer (2004) and Van der Werff *et al*. (2006), who demonstrated that the detection of seeps was improved when a contextual algorithm was used that takes into account the spatial patterns. Where they used the round shape of the bare soil as input for the spatial classifier, this study shows that in addition to the bare soil halo, the ring of vigorous vegetation could be included. A complicating factor in the analysis is the variable size of the halo (and so, of the filter), which depends on the gas flux, soil type and season. Filters of variable sizes should therefore be used. The main complication however is not the variability in size, but the small size of the halo compared to the pixel size. Large gas fluxes caused halos of less than a meter wide (simulated gas leaks, 150 l/h for several weeks) up to 20 m wide (natural seeps). Very high spatial resolution images are therefore needed to be able to detect circles of such small size.

7.5 Conclusion

In this chapter the results of the previous chapters were tested in the field. In addition, a vegetation survey was performed to determine whether long-term gas seepage affects vegetation patterns. Close to the seep source plant growth was disturbed. Up to a distance of 20 m from the source, a halo of bare soil prevailed, around which a maximally 10 m wide ring occurred in which a few species grew vigorously. It is hypothesized that a combination of changes in soil oxygen and groundwater caused these patterns. Even though the hyperspectral imagery dated from several years earlier, the patterns observed in the field were also observed in the image when the indices that were suggested in Chapter 5 were used. This supports the conclusion of Chapter 5 that the selected indices are not season dependent and can be used at any moment in time. Moreover, using indices that are related to biomass makes the method generally applicable. The disadvantage is the large number of false anomalies, however, including a

filter that searches for the round patterns in the vegetation reduced the number of false anomalies remarkably and should therefore be an integral part of the detection process.

CHAPTER 8

SYNTHESIS

The aim of this thesis was to characterize the effects of hydrocarbon gases in the soil on vegetation growth and reflectance. Two experiments were conducted to study the effects of anomalous gas concentrations on leaf and canopy reflectance, while the effects of long-term hydrocarbon seepage on vegetation canopy patterns were studied in the field. This chapter discusses the results of each study with regard to their implications for the remote detection of gas seepage.

8.1 Effects of low gas concentrations on plant growth and leaf reflectance

Until now, most studies on the effects of gas leakage on vegetation growth and reflectance were undertaken on large leaks - e.g. 100 l/h (Smith *et al*., 2004b), 250 l/h (Pysek and Pysek, 1989) – and in each of these studies, soil oxygen shortage accompanied the leaks. Since most plants need oxygen in the root zone, any change in growth or reflectance was attributed to the lack of oxygen. It was not known whether natural gas itself affects plant growth and reflectance. If natural gas would affect leaf or canopy reflectance in a different way than oxygen shortage, the exploration for gas leaks could then focus on this feature and differentiate between reflectance changes caused by gas leakage and changes caused by oxygen shortage.

In this thesis the effects of hydrocarbon gases on plant growth and reflectance were tested in an environment where oxygen shortage was avoided. Natural gas, methane and ethane were delivered to the root zone of maize and wheat plants in concentrations ranging from 0.75 to 2.5%. Natural gas and methane did not cause any significant change in maize or wheat growth, but ethane caused a decrease in maize plant height and leaf area. The effect of ethane on the wheat plants was less obvious: although a small increase in the number of leaves and chlorophyll was observed, none of the measured effects was statistically significant. Since there has been no research so far on the effects of ethane on plant growth, interpretation of the results is difficult. Plants can produce ethane when they are wounded, but concentrations are very low (stressed maize plants produced 0.0006 ml ethane per cm^2 of plant material; Kimmerer and Kozlowski, 1982). Concentrations as used in this thesis only occur in hydrocarbon gas seeps and leaks. A possible explanation for the reduced growth

caused by ethane is that bacteria or fungi generated ethylene from ethane, which is a plant hormone that can be inhibitory to plant growth (Leopold and Kriedemann, 1975). The reason for the absence of an effect in the wheat plants may be due to an increased tolerance of wheat plants to ethane or possibly ethylene compared to maize. Since the reactions of plants to ethylene in the soil are dependent on species and even on cultivar (Huang *et al*., 1997a), this is not certain. Another reason for the difference in reaction may be an increased sensitivity by maize plants to external stresses as a result of the relatively low greenhouse temperature.

In contrast to ethane, methane occurs in the (soil) atmosphere as a result of biological activities and plants are known to grow in high methane environments. Moreover, it was recently established that living plants produce methane (Zeeya, 2006). Methane has previously shown to be harmless to plant roots (Arthur *et al*., 1985) and aboveground parts of plants (Gustafson, 1944). This thesis shows that methane did not affect plant growth, which supports the general assumption that methane is harmless to plants.

The difference between the effects of ethane and methane on maize plants was also found in the leaf reflectance. Whereas natural gas and methane caused a minor decrease in band depth in the chlorophyll absorption regions, only ethane caused a significant decrease in band depth in the 550-750 nm absorption feature, in particular in the yellow region (560-600 nm). Since this area is related to leaf chlorophyll, ethane appears to have caused a decrease in leaf chlorophyll early in the experiment. The increased physiological reflectance index PRI confirmed this suggestion. The red edge position (REP) is commonly used to reveal changes in chlorophyll content, particularly in studies related to gas seepage (Table 1.2). However, the very subtle changes in chlorophyll caused by ethane did not result in a shift of the REP. In this thesis it is demonstrated that the yellow reflectance around 580 nm can assess subtle differences in chlorophyll (Chapter 3) and when used in combination with the REP, it increases the correlation with chlorophyll (Chapter 4).

Since the natural gas that was used in the experiment contained 3% ethane, the real concentration of ethane in the natural gas treatments was 0.075% (3% of 2.5%). These small concentrations did not affect maize growth and reflectance significantly.

8.2 Effects of high gas concentrations on plant growth and reflectance

Since concentrations of 0.75% ethane in soil caused an increase in reflectance in the yellow part of the spectrum, it was expected that natural gas concentrations between 4 and 20% (corresponding to approximately 3% to 20% ethane in natural gas) would cause a similar increase in yellow reflectance and the physiological reflectance index (PRI). In Chapter 6, the latter was tested on maize and wheat leaves growing in high concentrations of natural gas. Contrary to the plants in the controlled experiment, these plants experienced oxygen shortage in the root zone and a strong decrease in leaf chlorophyll. Although the expected increase in yellow reflectance and PRI occurred, the changes were much more pronounced than in the controlled experiment and therefore more likely a result of the decreased chlorophyll content. This confirmed that the changes in the yellow reflectance in the controlled experiment had been a result of low leaf chlorophyll content early in the experiment.

High gas concentrations cause a reduction in soil oxygen. Smith *et al*. (2004a) demonstrated that oxygen shortage resulting from different agents had a similar effect on plant reflectance. To test the assumption that oxygen shortage is the main cause of changes in reflectance, several indices that are known to react to changes in canopy cover or leaf area and chlorophyll changes were used to establish a relationship between the soil oxygen and the reflectance. The focus was on finding a reflectance index that is correlated with oxygen levels in the soil during the entire growing season and for both species. It was not possible to find one index that could predict oxygen concentrations under both species over time. However after normalizing for species, the optimized soil adjusted vegetation index (OSAVI) was the best predictor of oxygen concentrations in the soil 29 days after gassing started, whereas after normalizing for time, the Vogelmann (Vog1) and Lichtenthaler (LIC3) indices could predict oxygen concentrations under the maize and wheat canopy respectively. All these indices react on a decrease in biomass and chlorophyll content, which translates as a relative decrease in near infrared (NIR) and increase in red reflectance. In previous studies where oxygen shortage accompanied gas leaks (Smith *et al*., 2004b and Pysek and Pysek, 1989), the same reactions were found. As in this thesis, decreased leaf chlorophyll in combination with decreased biomass in the gassed plots was the cause of the reflectance changes. Since a decrease in chlorophyll and biomass is a generally known sign of stress, it can be concluded that large gas leaks that are accompanied by oxygen shortage can be recognized by any reflectance index that enhances the differences between the red and the NIR.

The confusion that exists about the effects of gas on vegetation reflectance is mainly focused around studies that deal with hydrocarbon microseepage. Microseepage is generally a long-term process, which can result in changes in the soil mineralogy depending on geology and soil type (see Chapter 1 for an overview of the effects of microseepage on soil). The effect these changes have on vegetation reflectance depends again on vegetation type and so a generalization of the effects of microseepage on vegetation reflectance cannot be made. However, the changes in reflectance as found by Reid *et al*. (1988), Bammel and Birnie (1994) and Almeida-Filho *et al*. (1999) have in common that they are similar to those found in vegetation affected by oxygen shortage. As Etiope and Klusman (2002) point out, negative methane fluxes are common in microseepage areas due to methanotrophic oxidation of CH_4. A combination of low seepage rates with oxygen depletion due to methanotrophic oxidation could be the reason for the changes in reflectance. Yang *et al*. (1999) found a shift of the red edge towards longer wavelengths over wheat canopy affected by microseepage. This shift towards longer wavelengths is a result of increased leaf chlorophyll and/or biomass. In this thesis it was demonstrated that small concentrations of methane and ethane did not increase either of these. In contrast to the experimental seepage in this thesis, the microseepage described by Yang *et al*. (1999) is long-term. A possible explanation for the shift of the red edge position (REP) towards longer wavelengths is that methanotrophic oxidation took place, during which water was produced (Steven *et al*., 2006). In dry soils this extra moisture in the soil may have improved the growing conditions of the wheat. Another possibility for the changes in REP could be increased availability of micronutrients, or perhaps the changes in REP were caused by something else than gas seepage, as in this thesis it was demonstrated that wheat leaf and canopy reflectance was not a good predictor of gas seepage.

This thesis has shown that methanotrophic oxygen depletion is an integral part of gas leakage. Oxygen depletion ranged from 2.78% in the wheat plots to 3.91% in the maize plots, which corresponds to average CO_2 concentrations between 1 and 3% (Chapter 6). For the detection of high gas concentrations, the depletion of oxygen is of more importance than the increased CO_2 concentrations. Whereas 10% CH_4 would in theory correspond to 18% O_2 (not harmful to plant growth), methanotrophic oxygen depletion may reduce the oxygen concentrations dramatically to concentrations less than 5%, resulting in adverse growth conditions. An increase in CO_2 concentrations on the other hand has not shown to affect plant growth and reflectance up to concentrations of 10%. 10% and 20% CO_2 even caused an increase in leaf chlorophyll and water content during the first three weeks of CO_2 delivery, suggesting that a moderate CO_2 concentration in the soil may be beneficial to maize growth. This supports the findings by Enoch and Olesen (1993) and Huang *et al*. (1997b). Although leaf chlorophyll, plant height and dry weight decreased with increasing CO_2 concentrations, only concentrations over 20% resulted in significant differences.

The REP-YEP index was the best predictor of CO_2 concentrations, which showed that only 50% CO_2 could be distinguished from the control with certainty. Such concentrations are found in landfills and in CO_2 seeps, but rarely in gas leaks. It is therefore concluded that the CO_2 concentrations that are found in hydrocarbon gas leaks do not significantly contribute to the changes in reflectance.

8.3 Vegetation patterns

A detailed vegetation survey was performed along transects over a hydrocarbon seepage in the Santa Barbara basin, USA, to determine whether vegetation cover and diversity change as a result of long-term gas seepage. It was demonstrated that within 10 m distance to the seep, bare soil dominates in a halo-like shape while between 20 and 30 m distance a ring of a few species occurs. With a filter that searched for this round-shaped pattern, the seep could be detected on hyperspectral imagery, which showed that the indices selected in Chapter 5 were generally applicable and not seasonally dependent.

8.4 General Seepage Model

Based on the results of this thesis and literature, a general overview of the effects of gas leakage on plant growth and reflectance is presented in Figure 8.1.

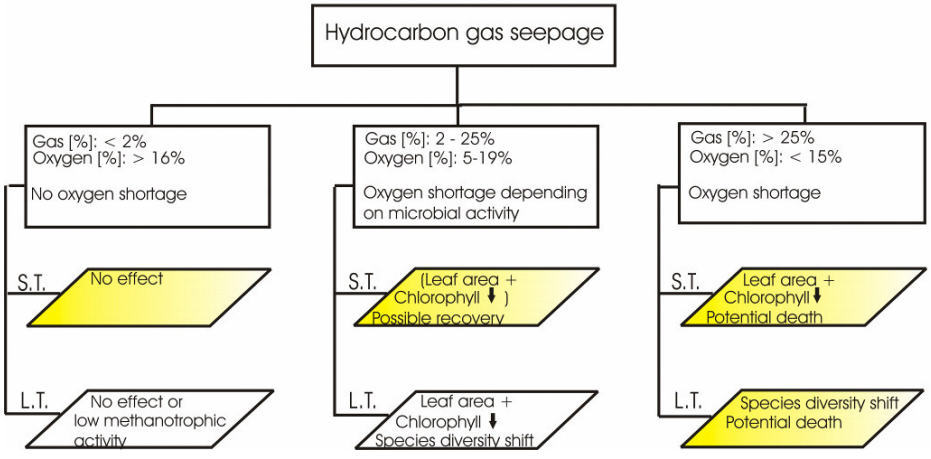

Figure 8.1 Schematic overview of the influence of hydrocarbon gas seepage on vegetation growth. S.T. = short term; L.T. = long term. The information in the coloured rectangles is derived from this thesis.

The effects of gas seepage on vegetation growth were separated into three groups: gas concentrations under 2%, between 2% and 25% and over 25%. The effects of these concentrations on plant growth were subsequently subdivided in short-term gas seepage (S.T. in Figure 8.1) and long-term gas seepage (L.T.). Gas concentrations below 2% as found in microseepage areas correspond to oxygen concentrations between 19% (without oxygen depletion) and 16% (with oxygen depletion). In Chapter 5 it was shown that canopy reflectance of maize and wheat was affected by oxygen concentrations lower than 16%. To illustrate this, the predicted oxygen concentrations under the maize canopy are shown in relation to the measured leaf area (Figure 8.2). This figure shows that maize leaf area reduces significantly when oxygen concentrations are less than 16%. Therefore the concentration under which terrestrial plant growth is affected was set on 16%, even though species differ in their sensitivity to oxygen concentrations. Short-term gas concentrations up to 2% will probably go unnoticed, but long-term low gas concentrations may cause changes in the soil, eventually leading to a shift in vegetation diversity. The oxygen concentrations in the 2%-25% gas concentrations are dependent on bacterial oxygen depletion. In short-term leakage, bacterial oxygen depletion may not take place and effects on plant growth may be unnoticed. However in long-term leaks bacterial oxygen depletion is likely to take place and the effects may be similar to the effects of the highest gas concentrations. Gas concentrations over 25% cause oxygen concentrations that are limiting to plant growth, which can lead to death of the vegetation and in long-term seepage a shift in vegetation diversity.

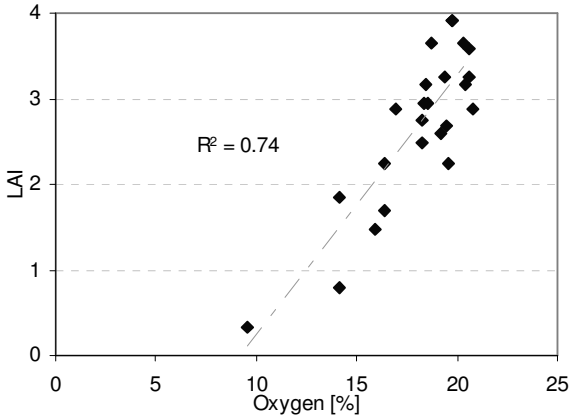

Figure 8.2 Leaf area versus modelled oxygen concentrations in the maize plots (Chapter 5)

All gas concentrations can occur within one gas leak. Methane and ethane concentrations are high close to the gas source, resulting in low oxygen

concentrations. Bacterial depletion cannot take place here due to a limiting oxygen supply, whereas at the far end of the gas distribution the methane supply is limiting and bacterial depletion stops (Steven *et al*., 2006). Between these extremes bacterial activity reduces the oxygen concentration and increases the CO_2 concentration by several percents. A schematic overview of the gas and oxygen patterns in a gas leak is shown in Figure 8.3a, which does not show a scale because the absolute values of methane, ethane oxygen and carbon dioxide vary per seepage. The associated vegetation changes are shown in Figure 8.3b. LAI is shown as an example, as both ethane and oxygen shortage caused changes in LAI. Vegetation cover and leaf chlorophyll showed less clear patterns at low gas concentrations, but at higher gas concentrations they most likely follow the same pattern as LAI. Although the LAI values in Figure 8.3b do not represent measured values, they were estimated based on the changes in LAI as measured in the greenhouse and field experiments. The blue line indicates the decrease in LAI if the leaking gas consisted of pure methane and methanotrophic bacteria would not be present. It is assumed that LAI would decrease at oxygen concentrations lower than 15% (corresponding to a methane concentration of 25%; equation 6.1), until at 5% oxygen (75% methane) the plants would die. However, at methane concentrations over 15%, ethane has an additional –reducing- effect on LAI (yellow line in Figure 8.3b). This effect is assumed to get more evident at higher gas concentrations. Finally, at moderate methane concentrations bacterial oxygen depletion leads to a very fast decrease in oxygen, which in turn leads to a strong reduction in LAI.

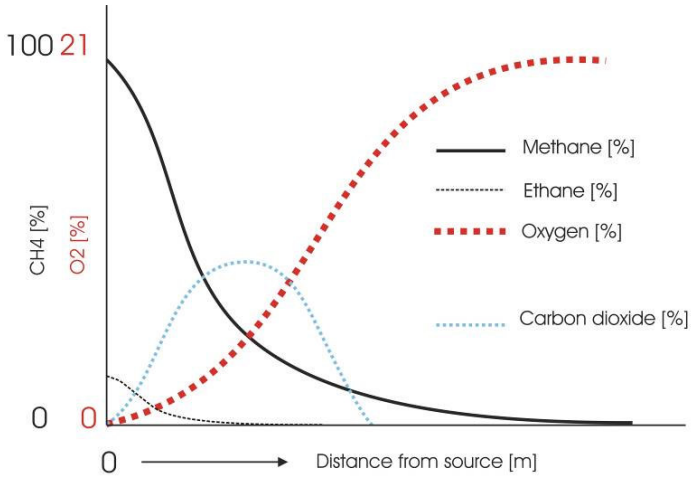

Figure 8.3a Generalized representation of seepage.

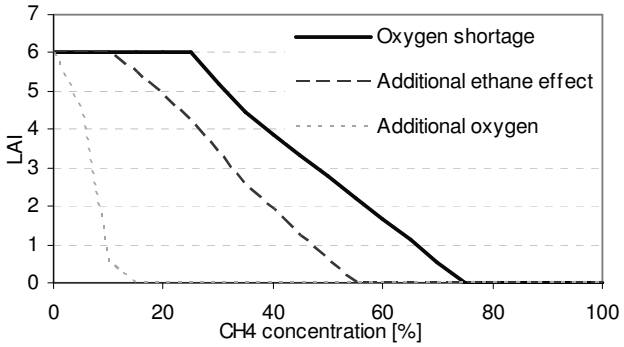

Figure 8.3b Generalized effects of ethane and bacterial oxygen depletion on leaf area in a natural gas leak

8.5 Gas detection using remote sensing

Finally, the implications of the plant growth characteristics described in the previous section for the remote detection of gas seepage can be summarized as follows:

- Methane does not affect maize and wheat reflectance; methane or natural gas concentrations under 2 % are therefore untraceable using vegetation reflectance.
- Ethane caused an increase in maize leaf reflectance in the 580 nm region. This is most likely the result of small changes in chlorophyll content, and not a unique effect of gas leakage; a leaf reflectance feature purely related to gas leakage is therefore not available.
- Since a decrease in leaf area was the most evident result of both small and large soil gas concentrations, reflectance indices that are sensitive to leaf area should be used as indicators of gas leakage. Based on the results of this thesis, it is suggested that LIC3 ($R440/R740$) be used on canopies that have an NDVI under 0.75 and Vog1 ($R740/R720$) on canopies that have higher NDVI values.
- When gas seepage originates from a point source (gas pipeline) or fault and gas concentrations decrease equally to all sides of the source, the changes in reflectance follow a round-shaped pattern. Using an exponential or Gaussian filter increases the chance of detecting the leak.
- Long-term gas seepage causes changes in vegetation diversity in a multi-species canopy. A ring of high biomass surrounds a halo of bare soil. The absence of vegetation in the seepage centre is thought to be the result of low oxygen concentrations in addition to low soil moisture content. Since mains gas is dehydrated during processing (Kennedy 1993), gas pipeline

leakage is also expected to dry out the soil. Although this had been controlled for in the experiments in this thesis, it is expected that a decrease in canopy water content will accompany the changes as found in this thesis.

Finally, the following practical issues should be considered for gas leak monitoring:

- which sensor is suitable?
- what is the best moment for detection?

8.5.1 Sensor

The ideal sensor for the remote detection of gas leakage based on vegetation reflectance should have narrow bands in the visible and NIR, but would not need to be hyperspectral in the whole NIR and SWIR. Instead, the spatial resolution should be as high as possible. In Chapter 5 it was shown that a gas flux of up to 153 l/h in a clayey soil can result in patches of just 1 m wide, whereas the natural hydrocarbon seepage in California affected the vegetation up to a distance of 30 m. Present hyperspectral sensors have a spatial resolution of up to 2 m (Hymap, airborne; Cocks *et al*., 1998) or 15 m (ASTER, spaceborne; URL1). As a result, airborne or spaceborne remote sensing is presently not able to detect leaks that have a spatial extent of less than 2 meters. Larger leaks that cause a patch of bare soil or a larger area of changed vegetation reflectance can be mapped using airborne hyperspectral sensors. It has been shown that including expert knowledge and additional information such as maps of the geology, soil type or vegetation type improves the classification results significantly (Skidmore *et al*., 2001; Schmidt *et al*., 2004, Van der Werff *et al*., 2006). Since the decrease in leaf area and chlorophyll is a-specific of gas leakage, additional information would facilitate the identification of leaks and reduce the number of false anomalies. Since the location of a pipeline is exactly known whereas the locations of microseepage areas or faults are often unknown, it follows that the chance of detecting gas pipeline leaks using vegetation remote sensing is higher than detecting microseepage.

8.5.2 Timing

The best time for gas leak detection is dependent on two factors: I. the species and II. the time of year. As shown in this thesis, different species have different reactions on gas leakage; e.g. wheat was not affected by ethane and the species diversity change described in Chapter 7 showed that some species are more tolerant to low oxygen concentrations than other species. However, species are most sensitive to changes in the root zone (such as oxygen shortage) during early growth, and the effect of stress in the early growth stages is still visible for several weeks after the stress ends (e.g., Chapter 4; Lichtenthaler, 1996). For

annual plants early growth usually corresponds to spring and early summer. In this thesis it was demonstrated that the differences between the gassed and control reflectance were most pronounced when the plants were between 1 and 1.5 months old (Chapter 3 & Chapter 5). At t = 22 and t = 29 the relationship between oxygen concentrations and the selected indices was similar for both species (Chapter 5). This coincided with a canopy cover between 40 and 80% (Figure 2.6). When canopy cover is lower than 40%, the difference between the gassed and control areas is so small that leak detection is difficult, whereas at very high cover the plants growing adjacent to a small gas leak can overgrow the gassed plants. The most optimal situation for detecting gas leakage is therefore early in the growing season on canopies that have a cover of 40 – 80%. As explained in Chapter 5, a canopy of 40% - 80% corresponds to NDVI values between 0.6 and 0.9. The wheat canopy never reached NDVI values over 0.75, whereas the maize canopy had NDVI values over 0.75 apart from the first measurement date (t = 16). Since in Chapter 5 it was shown that LIC3 and Vog1 could predict O_2 concentrations under the wheat and maize canopies respectively, it is expected that in practice LIC3 will be a better predictor of O_2 under canopies having NDVI values below 0.75, while Vog1 will be a better predictor under canopies of higher NDVI.

8.6 Conclusion

The results of this thesis contribute to the understanding of the influence of gas leakage on plant health. Hyperspectral reflectance has shown to be a useful tool to study changes in plant health and canopy patterns as a result of gas leakage. Although no reflectance feature was found that is uniquely related to gas leakage, it was shown that both ethane and oxygen shortage cause a decrease in leaf area and an increase in reflectance in the chlorophyll absorption regions. Most reflectance indices that are sensitive to changes in LAI and chlorophyll can therefore be used as indicators of gas leakage, however two indices are recommended for their insensitivity to changes over time. Since the reflectance changes were a-specific to gas leakage, additional information must be used to verify whether changes are related to gas leakage. Using an exponential or Gaussian filter increases the chance of detecting the leak, while field verification is always needed after a leak is detected.

This thesis has shown that in theory gas leaks can be detected as early as 2 weeks after gas leakage starts. Early detection of gas pipeline leaks will decrease the loss of gas and assist in avoiding a dangerous accumulation of explosive gases in the soil. In undisturbed vegetated areas the detection of anomalous gas concentrations can lead to the discovery of microseepage and related gas or oil reservoirs. It is concluded that if the spectral resolution of the

sensor is high in the visible and NIR and the spatial resolution as high as possible (preferably as high as 1 m), vegetation reflectance can be used as indicator of gas leakage.

Bibliography

Abeles, F.B., Morgan, P.W. and Saltveit, M.E., 1992. Ethylene in plant biology. Academic Press, 414 pp.

Abrams, M.A., 1996. Distribution of subsurface hydrocarbon seepage in near-surface marine sediments. In: D. Schumacher, Abrams, M.A. (Editor), Hydrocarbon migration and its near-surface expression, Tulsa, U.S.A., pp. 1-14.

Adams, M.L., Philpot, W.D. and Norvell, W.A., 1999. Yellowness index: an application of spectral second derivatives to estimate chlorosis of leaves in stressed vegetation. International Journal of Remote Sensing, 20(18): 3663-3675.

Adams, R.S. and Ellis, R., 1960. Some physical and chemical changes in the soil brought about by saturation with natural gas. Soil Science Society of America-Proceedings, 24: 41-44.

Adamse, A.D., Hoeks, J., de Bont, J.A.M. and Van Kessel, J.F., 1972. De microbiologische activiteit in de bodem rondom een aardgaslek. pp. 15.

Aldana, M., Costanzo-Alvarez, V. and Díaz, M., 2003. Magnetic and mineralogical studies to characterize oil reservoirs in Venezuela. The Leading Edge, June 2003: 526-529.

Almeida-Filho, R., Miranda, F.P. and Yamakawa, T., 1999. Remote detection of a tonal anomaly in an area of hydrocarbon microseepage, Tucano basin, north-eastern Brazil. International Journal of Remote Sensing, 20(13): 2683-2688.

Arteca, R.N., Poovaiah, W. and Smith, O.E., 1979. Changes in carbon fixation, tuberization, and growth induced by CO_2 applications to the root zone of potato plants. Science, 205: 1278-1280.

Arthur, J.J., Leone, I.A. and Flower, F.B., 1985. The response of tomato plants to simulated landfill gas mixtures. Journal of Environmental Sciences and Health, A20(8): 913-925.

Bacour, C., Baret, F., Béal, D., Weiss, M. and Pavageau, K., in press. Neural network estimation of LAI, fAPAR, fCover and LAI×C_{ab}, from top of canopy MERIS reflectance data: Principles and validation. Remote Sensing of Environment.

Bammel, B.H. and Birnie, R.W., 1994. Spectral reflectance response of big sagebrush to hydrocarbon-induced stress in the Bighorn Basin, Wyoming. Photogrammetric Engineering & Remote Sensing, 60(1): 87-96.

Banninger, C., 1991. Phenological changes in the red edge shift of Norway spruce needles and their relationship to needle chlorophyll content. Physical Measurements and Signatures in Remote Sensing, 1: 155-158.

Baret, F., Champion, I., Guyot, G. and Podaire, A., 1987. Monitoring wheat canopies with a high spectral resolution radiometer. Remote Sensing of Environment, 22: 367-378.

Barnes, J.D., 1992. A reappraisal of the use of DMSO for the extraction and determination of chlorophylls *a* and *b* in lichens and higher plants. Environmental Experimental Botany, 2: 85– 100.

Batjes, N.H. and Bridges, E.M., 1992. A review of soil factors and processes that control fluxes of heat, moisture and greenhouse gases, ISRIC, Wageningen.

Belay, N. and Daniels, L., 1987. Production of ethane, ethylene, and acetylene from halogenated hydrocarbons by methanogenic bacteria. Applied and Environmental Microbiology, 53(7): 1604-1610.

Benedict, H.M. and Swidler, R., 1961. Nondestructive method for estimating chlorophyll content of leaves. Science, 133: 2015- 2016.

Bergfeld, D., Evans, W.C., Howle, J.F. and Farrar, C.D., 2006. Carbon dioxide emissions from vegetation-kill zones around the resurgent dome of Long Valley caldera, eastern California, USA. Journal of Volcanology and Geothermal Research, 152: 140-156.

Bizecki Robson, D., Knight, J.D., Farrell, R.E. and Germida, J.J., 2004. Natural revegetation of hydrocarbon-contaminated soil in semi-arid grasslands. Canadian Journal of Botany, 82: 22-30.

Bonham-Carter, G.F., 1988. Numerical procedures and computer program for fitting an inverted Gaussian model to vegetation reflectance data. Computers and Geosciences, 14(3): 339-356.

Boochs, F., Kupfer, G., Dockter, K. and Kühbauch, W., 1990. Shape of the red edge as vitality indicator for plants. International Journal of Remote Sensing, 11(10): 1741-1753.

Boru, G., Vantoai, T., Alves, J., Hua, D. and Knee, M., 2003. Responses of soybean to oxygen deficiency and elevated root-zone carbon dioxide concentration. Annals of botany, 91: 447-453.

Bouma, T.J., Nielsen, K.L., Eissenstat, D.M. and Lynch, J.P., 1997. Soil CO_2 concentration does not affect growth or root respiration in bean or citrus. Plant, Cell and Environment, 20: 1495-1505.

Bowman, W.D., 1989. The relationship between leaf water status, gas exchange, and spectral reflectance in cotton leaves. Remote Sensing of Environment, 30: 249-255.

Brady, N.C., 1984. The nature and properties of soils. 9th Edition, McMillan, New York, 750 pp.

Braverman, M.M., Ettinger, I. and Jacobs, M.B., 1962. Determining the cause of death of vegetation by analysis of soil gases. Gas Age, 129: 23-26.

Bray, D.F., 1958. Gas injury to shade trees. Scientific Tree Topics, 2: 19-22.

Broge, N.H. and Leblanc, E., 2000. Comparing prediction power and stability of broadband and hyperspectral vegetation indices for estimation of green leaf area index and canopy chlorophyll density. Remote Sensing of Environment, 76: 156-172.

Bruinsma, J., 1963. The quantitative analysis of chlorophylls *a* and *b* in plant extracts. Photochemistry and Photobiology, 2: 241– 249.

Buschmann, C. and Nagel, E., 1993. In vivo spectroscopy and internal optics of leaves as basis for remote sensing of vegetation. International Journal of Remote Sensing, 14(4): 711-722.

Carter, G.A., 1991. Primary and secondary effects of water content on the spectral reflectance of leaves. American Journal of Botany, 78: 916–924.

Carter, G.A., 1993. Responses of leaf spectral reflectance to plant stress. American Journal of Botany, 80(3): 239-243.

Carter, G.A., 1994. Ratios of leaf reflectances in narrow wavebands as indicators of plant stress. International Journal of Remote Sensing, 15: 697-703.

Carter, G.A. and Miller, R.L., 1994. Early detection of plant stress by digital imaging within narrow stress-sensitive wavebands. Remote Sensing of Environment, 50(3): 295-302.

Ceccato, P., Flasse, S., Tarantola, S., Jacquemoud, S. and Grégoire, J., 2001. Detecting vegetation leaf water content using reflectance in the optical domain. Remote sensing of environment, 77: 22-33.

Chen, J., 1996. Evaluation of vegetation indices and modified simple ratio for boreal applications. Canadian Journal of Remote Sensing, 22: 229– 242.

Cho, M.A. and Skidmore, A.K., 2006. A new technique for extracting the red edge position from hyperspectral data: the linear extrapolation method. Remote Sensing of Environment, 101: 181–193.

Cibula, W.G., Zetka, E.F. and Rickman, D.L., 1992. Response of Thematic Mapper bands to plant water stress. International Journal of Remote Sensing, 13: 1869-1880.

Clark, R.N. and Roush, T.L., 1984. Reflectance spectroscopy: quantitative analysis techniques for remote sensing applications. Journal of Geophysical Research, 89 (B7): 6329-6340.

Cloutis, E.A., 1989. Spectral reflectance properties of hydrocarbons: remote sensing implications. Science, 4914: 165–168.

Cochran, W.C. and Cox, G.M., 1992. Experimental Designs. Wiley & Sons, New York, 611 pp.

Cocks, T., Jenssen, R., Stewart, A., Wilson, I. and Shields, T., 1998. The HyMap(TM) airborne hyperspectral sensor: the system, calibration and performance, 1st EARSEL Workshop on Imaging Spectroscopy, Zurich, Switzerland, pp. 37-42.

Collins, W., 1978. Remote sensing of crop type and maturity. Photogrammetric Engineering & Remote Sensing, 44: 43-55.

Conover, W.J., 1999. Practical Nonparametric Statistics. New York: John Wiley & Sons.

Cramer, M.D. and Lips, S.H., 1995. Enriched rhizosphere CO_2 concentrations can ameliorate the influence of salinity on hydroponically grown tomato plants. Physiologia Plantarum, 94: 425-432.

Curran, P.J., 1989. Remote sensing of foliar chemistry. Remote Sensing of Environment, 30: 271-278.

Curran, P.J., Dungan, J.L. and Peterson, D.L., 2001. Estimating the foliar biochemical concentration of leaves with reflectance spectrometry; Testing the Kokaly and Clark methodologies. Remote Sensing of Environment, 76: 349-359.

Curran, P.J., Windham, W.R. and Gholz, H.L., 1995. Exploring the relationship between reflectance red edge and chlorophyll concentration in slash pine leaves. Tree Physiology, 15: 203-206.

Dale, N., 1986. Flowering plants. The Santa Monica Mountains, coastal & chaparral regions of southern California. Capra Press, Santa Barbara, USA, 239 pp.

Dalziel, M.C. and Donovan, T.J., 1980. Biogeochemical evidence for subsurface hydrocarbon occurrence, recluse oil field, Wyoming: preliminary results. Geological survey circular, 837: 1-11.

Danson, F.M., Steven, M.D., Malthus, T.J. and Clark, J.A., 1992. High-spectral resolution data for determining leaf water content. International Journal of Remote Sensing, 13: 461-470.

Daughtry, C.S.T., 1990. Direct measurements of canopy structure. Remote Sensing Reviews, 5(1): 45-60.

Daughtry, C.S.T., Walthall, C.L., Kim, M.S., Brown de Colstoun, E. and McMurtrey, J.E., 2000. Estimating corn leaf chlorophyll concentration from leaf and canopy reflectance. Remote Sensing of Environment, 74: 229– 239.

Dawson, T.P. and Curran, P.J., 1998. Technical note. A new technique for interpolating the reflectance red edge position. International Journal of Remote Sensing, 19(11): 2133-2139.

De Jong, S., 1998. Imaging spectrometry for monitoring tree damage caused by volcanic activity in the Long Valley caldera, California. ITC Journal, 1: 1-10.

Demetriades-Shah, T.H., Steven, M.D. and Clark, J.A., 1990. High resolution derivative spectra in remote sensing. Remote Sensing of Environment, 33: 55-64.

Dibblee, T., 1987. Geological Map of the Ojai Quadrangle, Ventura County, California.

Drew, M.C., 1983. Plant injury and adaptation to oxygen deficiency in the root environment: A review. Plant and Soil, 75: 179-199.

Drew, M.C., 1990. Sensing soil oxygen. Plant, Cell and Environment, 13: 681-693.

Drew, M.C., 1991. Oxygen deficiency in the root environment and plant mineral nutrition. In: M.B. Jackson, D.D. Davies and H. Lambers (Editors), Plant life under oxygen deprivation. SPB Academic Publishing, The Hague, pp. 303-316.

Drew, M.C., Jackson, M.B. and Giffard, S., 1979. Ethylene-promoted adventitious rooting and development of cortical air spaces (aerenchyma) in roots may be adaptive responses to flooding in *Zea mays L.* Planta, 147: 83-88.

Ehlinger, J.R. and Monson, R.K., 1993. Evolutionary and ecological aspects of photosynthetic pathway variation. Annual Review of Ecology and Systematics, 24: 411-439.

Ellis, J.M., Davis, H.H. and Zamudio, J.A., 2001. Exploring for onshore oil seeps with hyperspectral imaging. Oil and Gas Journal, 99(37): 49-58.

Ellwood, B.B. and Burkart, B., 1996. A test of hydrocarbon-induced magnetic patterns in soils: the sanitary landfill as laboratory. In: D. Schumacher and M.A. Abrams (Editors), Hydrocarbon migration and its near-surface expression, pp. 91-98.

Enoch, H.Z. and Olesen, J.M., 1993. Plant response to irrigation with water enriched with carbon dioxide. New Phytologist, 125: 249-258.

Etiope, G. and Klusman, R.W., 2002. Geologic emissions of methane into the atmosphere. Chemosphere, 49: 779–791.

Evain, S., Flexas, J. and Moya, I., 2004. A new instrument for passive remote sensing: 2. Measurement of leaf and canopy reflectance changes at 531 nm and their relationship with photosynthesis and chlorophyll fluorescence. Remote Sensing of Environment, 91: 175-185.

Filella, I., J. Penuelas, L. Llorens *and* M. Estiarte, 2004. Reflectance assessment of seasonal and annual changes in biomass and CO_2 uptake of a Mediterranean shrubland submitted to experimental warming and drought. Remote Sensing of Environment, 90: 308–318.

Gamon, J.A., Penuelas, J. and Field, C.B., 1992. A narrow-waveband spectral index that tracks diurnal changes in photosynthetic efficiency. Remote Sensing of Environment, 41: 35-44.

Gamon, J.A. and Surfus, J., 1999. Assessing leaf pigment content and activity with a reflectometer. New Phytologist, 143: 105-117.

Gao, B.C., 1995. Normalized Difference Water Index for remote sensing of vegetation liquid water from space. Proceedings of SPIE, 2480: 225-236.

Gates, D.M., Keegan, H.J., Schleter, J.C. and Weidner, V.R., 1965. Spectral properties of plants. Applied Optics, 4: 11- 20.

Gausman, H.W., 1974. Leaf reflectance of near-infrared. Photogrammetric Engineering & Remote Sensing, 40: 183-192.

Gitelson, A.A. and Merzlyak, M.N., 1997. Remote estimation of chlorophyll content in higher plant leaves. International Journal of Remote Sensing, 18: 2691– 2697.

Gitelson, A.A. and Merzlyak, M.N., 1998. Remote sensing of chlorophyll concentration in higher plant leaves. Advances in Space Research, 22(5): 609-692.

Gitelson, A.A., Merzlyak, M.N. and Chivkunova, O.B., 2001. Optical properties and nondestructive estimation of anthocyanin content in plant leaves. Photochemistry and Photobiology, 71: 38-45.

Gitelson, A.A., Zur, Y., Chivkunova, O.B. and Merzlyak, M.N., 2002. Assessing carotenoid content in plant leaves with reflectance spectroscopy. Photochemistry and Photobiology, 75: 272-281.

Godwin, R., Abouguendia, Z. and Thorpe, J., 1990. Lloydminster area operators gas migration team response of soils and plants to natural gas migration from two wells in the lloydminster area. Limited report.

Grubben, G.J.H. and Soetjipto Partohardjono, F., 1996. PROSEA: plant resources of South - East Asia, 10. Backhuys, Leiden, 199 pp.

Gurpinar, A., Serva, L., Celebi, M., 2001. Global blueprints for change. International Workshop on Disaster Reduction. Reston, USA, 10 pp.

Gustafson, F.G., 1944. Is natural gas injurious to flowering plants? Plant Physiology, 19: 551-558.

Guyot, G. and Baret, F., 1988. Utilisation de la haute resolution spectrale pour suivre l'etat des couverts vegetaux, Proceedings 4th International Colloquium on Spectral Signatures of Objects in Remote Sensing, Aussois, France.

Haboudane, D., Miller, J.R., Pattey, E., Zarco-Tejada, P.J. and Strachan, I., 2004. Hyperspectral vegetation indices and novel algorithms for predicting green LAI of crop canopies: Modeling and validation in the context of precision agriculture. Remote Sensing of Environment, 90: 337– 352.

Haboudane, D., Miller, J.R., Tremblay, N., Zarco-Tejada, P.J. and Dextraze, L., 2002. Integrated narrow-band vegetation indices for prediction of crop chlorophyll content for application to precision agriculture. Remote Sensing of Environment, 81: 416-426.

Hanson, R.S. and Hanson, T.E., 1996. Methanotrophic bacteria. Microbiological Review, 60(2): 439-471.

Harbert, W., Jones, V.T., Izzo, J. and Anderson, T.H., 2006. Analysis of light hydrocarbons in soil gases, Lost River region, West Virginia: Relation to stratigraphy and geological structures. AAPG Bulletin, 90(5): 715–734.

Hardisky, M.A., Klemas, V. and Smart, R.M., 1983. The influence of soil salinity, growth form, and leaf moisture on the spectral reflectance of *Spartina Alterniflora* canopies. Photogrammetric Engineering & Remote Sensing, 49: 77-83.

Hartigan, J. A. and Wong, M.A., 1979. Algorithm AS 136: A *K*-Means Clustering Algorithm. Applied Statistics, 28: 100-108.

Henderschot, W.H., Lalande, H. and Duquette, M., 1993. Soil reaction and exchangeable acidity. In: M.R. Carter (Editor), Soil Sampling and Methods of

Analysis. Canadian Society of Soil Science. Lewis Publishers, Boca Raton, pp. 141-145.
Hepple, R.P. and Benson, S.M., 2001. A review of human health and ecological risks due to CO_2 exposure, American Geophysical Union, Spring Meeting, pp. H31C-13.
Hodgson, S., 1980. Onshore oil and gas seeps in California, California Department of Conservation. Division of Oil and Gas.
Hoeks, J., 1972a. Changes in composition of soil air near leaks in natural gas mains. Soil Science, 113(1): 46-54.
Hoeks, J., 1972b. Effect of leaking natural gas on soil and vegetation in urban areas. Wageningen University, Wageningen, 120 pp.
Holloway, S., 2005. Underground sequestration of carbon dioxide - a viable greenhouse gas mitigation option. Energy, 30: 2318-2333.
Hörig, B., Kühn, F., Oschütz, F. and Lehmann, F., 2001. HyMap hyperspectral remote sensing to detect hydrocarbons. International Journal of Remote Sensing, 22(8): 1413-1422.
Horler, D.N.H., Dockray, M. and Barber, J., 1983. The red edge of plant leaf reflectance. International Journal of Remote Sensing, 4: 273-288.
Hornafius, J.S., Quigley, D.C. and Luyendyk, B.P., 1999. The world's most spectacular marine hydrocarbon seeps (Coal Oil Point, Santa Barbara, California): quantification of emissions. Journal of Geophysical Research, 104(C9): 20703–20711.
Horvitz, L., 1972. Vegetation and Geochemical Prospecting for Petroleum. AAPG Bulletin, 56: 925-940.
Huang, B., Johnson, J.W., Box, J.E. and NeSmith, D.S., 1997a. Root characteristics and hormone activity of wheat in response to hypoxia and ethylene. Crop Science, 37: 812-818.
Huang, B., Johnson, J.W. and NeSmith, D.S., 1997b. Responses to root-zone CO_2 enrichment and hypoxia of wheat genotypes differing in waterlogging tolerance. Crop Science, 37: 464-468.
Huang, B., Johnson, J.W., NeSmith, D.S. and Bridges, D.C., 1994. Root and shoot growth of wheat genotypes in response to hypoxia and subsequent resumption of aeration. Crop Science, 34: 1538-1544.
Huete, A.R., Liu, H., Batchily, K. and Van Leeuwen, W., 1997. A comparison of vegetation indices over a global set of TM images for EOS-MODIS. Remote Sensing of Environment, 59: 440-451.
Hunt, E.R. and Rock, B.N., 1989. Detection of changes in leaf water content using near- and middle-infrared reflectances. Remote Sensing of Environment, 30: 43-54.
Hütsch, B.W., 2001. Methane oxidation in non-flooded soils as affected by crop production – invited paper. European Journal of Agronomy, 14: 237–260.
IPCC, 2001. Climate Change 2001: the Scientific Basis. Contribution of Working Group I to the Third Assessment Report of the Intergovernmental Panel on Climate Change, Cambridge University Press, Cambridge.
Jackson, M.B. and Pearce, D.M.E., 1991. Hormones and morphological adaptation to aeration stress in rice. In: M.B. Jackson, D.D. Davies and H. Lambers (Editors), Plant Life under Oxygen Deprivation. SPB Academic Publishing, The Hague, pp. 47-67.

Janssen, D., Grobben, B.G. and Witholt, B., 1987. Toxicity of chlorinated aliphatic hydrocarbons and degradation by methanotrophic consortia. In: O.N. Neijssel, Van der Meer, R. R., Luyben, K.C. (Editors), Proceedings of the 4th European Congress on Biotechnology. Biomedical Press Elsevier, Amsterdam, pp. 515–518.

Jones, V.T. and Burtell, S.G., 1996. Hydrocarbon flux variations in natural and anthropogenic seeps. In: D. Schumacher, Abrams, M.A. (Editors), Hydrocarbon migration and its near-surface expression. AAPG memoir 66, Oklahoma, pp. 203-221.

Jones, V.T. and Drozd, R.J., 1983. Predictions of oil or gas potential by near surface geochemistry. AAPG Bulletin, 67: 932-952.

Jones, V.T., Matthews, M.D. and Richers, D.M., 2000. Light hydrocarbons for petroleum and gas prospecting. In: M. Hale (Editor), Geochemical Remote Sensing of the Subsurface, Handbook of Exploration Geochemistry, 7, pp. 133-212.

Justin, S.H.F.W. and Armstrong, W., 1991. Evidence for the involvement of ethene in aerenchyma formation in adventitious roots of rice (*Oryza sativa L.*). New Phytologist, 117: 49-62.

Kennedy, J. L., 1993. Oil and Gas Pipeline Fundamentals. 2nd Edition, Oklahoma, PennWell Publishing Company, 366 pp.

Kent, M. and Coker, P., 1992. Vegetation description and analysis: a practical approach. CRC Press, London, 363 pp.

Kimmerer, T.W. and Kozlowski, T.T., 1982. Ethylene, ethane, acetaldehyde, and ethanol production by plants under stress. Plant Physiology, 69: 840-847.

Knipling, E.B., 1970. Physical and physiological basis for the reflectance of visible and near-infrared radiation from vegetation. Remote Sensing of Environment, 1: 155-159.

Kokaly, R.F. and Clark, R.N., 1999. Spectroscopic determination of leaf biochemistry using band-depth analysis of absorption features and stepwise multiple linear regression. Remote Sensing of Environment, 67: 267-287.

Kühn, F., Oppermann, K. and Hörig, B., 2004. Hydrocarbon Index – an algorithm for hyperspectral detection of hydrocarbons. International Journal of Remote Sensing, 25(12): 2467–2473.

Kuhn, O., 2000. Odyssey of oil. CSEG Recorder, December 2000: 31-38.

Kumar, L., Schmidt, K.S., Dury, S. and Skidmore, A.K., 2001. Imaging spectrometry and vegetation science. In: F.D. Van der Meer and S.M. De Jong (Editors), Imaging spectrometry : basic principles and prospective applications. Kluwer Academic, Dordrecht, pp. 111-155.

Lamb, D.W., Steyn-Ross, M., Schaare, P., Hanna, M.M., Silvester, W. and Steyn-Ross, A., 2002. Estimating leaf nitrogen concentration in ryegrass (*Lolium spp.*) pasture using the chlorophyll red-edge: theoretical modelling and experimental observations. International Journal of Remote Sensing, 23(18): 3619-3648.

Leifer, I., Roberts, D., Margolis, J. and Kinnaman, F., 2006. In situ sensing of methane emissions from natural marine hydrocarbon seeps: A potential remote sensing technology. Earth and Planetary Science Letters, 245: 509–522.

Leopold, A.C. and Kriedemann, P.E., 1975. Plant growth and development. Tata McGraw-Hill Publishing Company Ltd., Delhi., pp. 545.

Li, Z., Dong, M., Li, S. and Huang, S., 2006. CO_2 sequestration in depleted oil and gas reservoirs - caprock characterization and storage capacity. Energy Conversion and Management, 47: 1372-1382.

Lichtenhaler, H.K., Lang, M., Sowinska, M., Heisel, F. and Mieh, J.A., 1996. Detection of vegetation stress via a new high resolution fluorescence imaging system. Journal of Plant Physiology, 148: 599–612.

Link, W.K., 1952. Significance of oil and gas seeps in world oil exploration. AAPG Bulletin, 6(8): 1505-1540.

Lizaso, J.I., Melendez, L.M. and Ramirez, R., 2001. Early flooding of two cultivars of tropical maize. I. Shoot and root growth. Journal of Plant Nutrition, 24: 979-995.

Luyendyk, B.P., Washburn, L., Banerjee, S., Clark, J.F. and Quigley, D.C., 2003. A methodology for investigation of natural hydrocarbon gas seepage in the northern Santa Barbara channel. MMS OCS Study 2003-054. MMS Cooperative Agreement No. 14-35-0001-30758, Coastal Marine Institute, University of California, Santa Barbara.

Lynch, J., 1995. Root architecture and plant productivity. Plant Physiology, 109: 7-13.

Maas, S.J. and Dunlap, J.R., 1989. Reflectance, transmittance, and absorptance of light by normal, etiolated, and albino corn leaves. Agronomy Journal, 81: 105-110.

MacDonald, I.R., Boland, G.S., Baker, J.S., Brooks, J.M., Kennicutt, M.C. and Bidigare, R.R., 1989. Gulf of Mexico hydrocarbon seep communities. Marine Geology, 101: 235-247.

Macek, I., Pfanz, H., Francetic, V., Batic, F. and Vodnik, D., 2005. Root respiration response to high CO_2 concentrations in plants from natural CO_2 springs. Environmental and Experimental Botany, 54: 90-99.

Maracci, G., Schmuck, G., Hosgood, B. and Andreoli, G., 1991. Interpretation of reflectance spectra by plant physiological parameters, Proceedings of International Geoscience and Remote Sensing Symposium (IGARSS'91). Remote Sensing: Global Monitoring for Earth Management. New York: IEEE, Helsinki University of Technology, Espoo (Finland), pp. 2303– 2306.

Mason, W.K., Pritchard, K.E. and Small, D.R., 1987. Effects of early season waterlogging on maize growth and yield. Australian Journal of Agricultural Research, 38(1): 27 - 35.

Merzlyak, J.R., Gitelson, A.A., Chivkunova, O.B. and Rakitin, V.Y., 1999. Non-destructive optical detection of pigment changes during leaf senescence and fruit ripening. Physiologia Plantarum, 106: 135-141.

Miller, R.G., 1985. Multiple comparisons. In: S. Kotz and N.L. Johnson (Editors), Encyclopedia of Statistical Sciences, New York: Wiley, pp. 679-689.

Moldrup, P., Olesen, T., Schjønning, P., Yamaguchi, T. and Rolston, D.E., 2000. Predicting the gas diffusion coefficient in undisturbed soil from soil water characteristics. Soil Science Society of America Journal, 64: 94-100.

Mutanga, O., Skidmore, A.K., Kumar, L. and Ferwerda, J., 2005. Estimating tropical pasture quality at canopy level using band depth analysis with continuum removal in the visible domain. International Journal of Remote Sensing, 26(6): 1093-1108.

Mutanga, O., Skidmore, A.K. and Prins, H.H.T., 2004. Predicting in situ pasture quality in the Kruger National Park, South Africa, using continuum-removed absorption features. Remote Sensing of Environment, 89: 393-408.

Neue, H., 1993. Methane emission from rice fields: Wetland rice fields may make a major contribution to global warming. BioScience 43: 466-473.
Nicodemus, F.E., 1977. Geometrical considerations and nomenclature for reflectance. National Bureau of Standards monograph, 160: 1-42.
Niehaus, T.F. and Ripper, C.L., 1976. A field guide to Pacific States Wildflowers. A visual approach, arranged by colour, form and detail. The Peterson field guide series. Houghton Hiffin Company, Boston, USA, 432 pp.
N.T.S.B., 2001. National Transportation Safety Board. Natural Gas Explosion and Fire in South Riding, Virginia, July 7, 1998, Washington, DC.
N.T.S.B., 2003. National Transportation Safety Board. Natural Gas Pipeline Rupture and Fire Near Carlsbad, New Mexico, August 19, 2000, Washington, D.C.
Olah, G.A. and Molnar, A., 2003. Hydrocarbon chemistry. Wiley-IEEE, New Jersey, 871 pp.
Oldenburg, C.M., Lewicki, J.L. and Hepple, R.P., 2003. Near-surface monitoring strategies for geologic carbon dioxide storage verification. Lawrence Berkeley National Laboratory: pp. 54.
Oliveira, W.J.d., Crosta, A.P. and Goncalves, J.L.M., 1997. Spectral characteristics of soils and vegetation affected by hydrocarbon gas: a greenhouse simulation of the Remanso do Fogo seepage, Twelfth international conference and workshops on applied geologic remote sensing, Denver, Colorado. Abstract.
Penuelas, J., Filella, I., Lloret, P., Munoz, F. and Vilajeliu, M., 1995. Reflectance assessment of mite effects on apple trees. International Journal of Remote Sensing, 16–14: 2727– 2733.
Penuelas, J., Gamon, J.A., Fredeen, A.L., Merino, J. and Field, C.B., 1994. Reflectance indices associated with physiological changes in nitrogen and water-limited sunflower leaves. Remote Sensing of Environment, 48: 135– 146.
Penuelas, J., Pinol, J., Ogaya, R. and Filella, I., 1997. Estimation of plant water concentration by the reflectance Water Index WI (R900/R970). International Journal of Remote Sensing, 18(13): 2869-2875.
Pirone, P.P., 1960. The response of shade trees to natural gas. The Garden Journal, 10: 25-29.
Pu, R., Gong, P., Biging, G.S. and Larrieu, M.R., 2003. Extraction of red edge optical parameters from Hyperion data for estimation of forest leaf area index. IEEE Transactions on Geoscience and Remote Sensing, 41(4): 916-921.
Pysek, P. and Pysek, A., 1989. Veränderungen der Vegetation durch experimentelle Erdgasbehandlung. Weed Research, 29: 193-204.
Qi, J., Chehbouni, A., Huete, A.R., Keer, Y.H. and Sorooshian, S., 1994. A modified soil vegetation adjusted index. Remote Sensing of Environment, 48: 119– 126.
Reeve, M.J., 1975. Soils I Derbyshire II, Soil survey record, No 27. Adlard and Son, Bartholomew Press.
Reid, N., Iwashita, A., Yamashita, Y. and Thompson, K., 1988. High resolution imaging of geobotanical anomalies associated with subsurface hydrocarbons, Proceedings of the Sixth Thematic Conference on Remote Sensing for Exploration Geology, Houston, Texas, pp. 213-223.
Richers, D.M., Jones, V.T., Matthews, M.D., Maciolek, J., Pirkle, R.J. and Sidle W.C., 1986. The 1983 Landsat soil-gas geochemical survey of Patrick Draw area, Sweetwater County, Wyoming. AAPG Bulletin, 70: 869-887.

Rondeaux, G., Steven, M. and Baret, F., 1996. Optimization of soil-adjusted vegetation indices. Remote Sensing of Environment, 55: 95–107.

Rougean, J.L. and Breon, F.M., 1995. Estimating PAR absorbed by vegetation from bidirectional reflectance measurements. Remote Sensing of Environment, 51: 375–384.

Rouse, J.W., Haas, R.H. and Schell, J.A., 1974. Monitoring the vernal advancement of retrogradiation of natural vegetation, Greenbelt, MD, USA.

Russell, E.W., 1973. Soil conditions and plant growth. Longmans, London.

Sandmeier, S. and Deering, D.W., 1999. Structure analysis and classification of boreal forests using airborne hyperspectral BRDF data from ASAS. Remote Sensing of Environment, 69: 281-295.

Savitzky, A. and Golay, M. J. E., 1964. Smoothing and differentiation of data by simplified least-squares procedures. Analytical Chemistry, 36: 1627–1639.

Schmidt, K.S., Skidmore, A.K., Kloosterman, E.H., Van Oosten H.H., Kumar, L., Janssen, J.A.M., 2004. Mapping coastal vegetation using an expert system and hyperspectral imagery. Photogrammetric Engineering and Remote Sensing, 70, 703-715.

Schollenberger, C.J., 1930. Effect of leaking natural gas upon the soil. Soil Science, 29: 260-266.

Schumacher, D., 1996. Hydrocarbon-induced alteration of soils and sediments. In: D. Schumacher, Abrams, M.A. (Editors), Hydrocarbon Migration and its Near-Surface Expression: AAPG Memoir 66, pp. 71-89.

Schumacher, D., 2000. Surface geochemical exploration for oil and gas: new life for an old technology. The Leading Edge, March 2000: 258-261.

Schumacher, D., 2001. Petroleum exploration in environmentally sensitive areas: opportunities for non-invasive geochemical and remote sensing methods, Rock the foundation convention.

Scott, L.F., McCoy, R.M. and Wullstein, L.H., 1988. A closer look at the Patrick Draw oil field vegetation anomaly, Proceedings of the Sixth Thematic Conference on Remote Sensing for Exploration Geology, pp. 529-535.

Serrano, L., Penuelas, J. and Ustin, S.L., 2002. Remote Sensing of Nitrogen and Lignin in Mediterranean Vegetation from AVIRIS Data: Decomposing Biochemical from Structural Signals. Remote Sensing of Environment, 81: 355-364.

Sims, D.A. and Gamon, J.A., 2002. Relationships Between Leaf Pigment Content and Spectral Reflectance Across a Wide Range of Species, Leaf Structures and Developmental Stages. Remote Sensing of Environment, 81: 337-354.

Sims, D.A. and Gamon, J.A., 2003. Estimation of vegetation water content and photosynthetic tissue area from spectral reflectance: a comparison of indices based on liquid water and chlorophyll absorption features. Remote Sensing of Environment, 84: 526-537.

Skidmore, A.K., Schmidt, K.S., Kloosterman, H., Kumar, L., Van Oosten H.H., 2001. Hyperspectral imagery for coastal wetland vegetation mapping. Beleidscommissie Remote Sensing (BCRS), 01-31, pp. 63.

Smith, K.L., Steven, M.D. and Colls, J.J., 2004a. Spectral responses of pot-grown plants to displacement of soil oxygen. International Journal of Remote Sensing, 25(20): 4395-4410.

Smith, K.L., Steven, M.D. and Colls, J.J., 2004b. Use of hyperspectral derivative ratios in the red-edge region to identify plant stress responses to gas leaks. Remote Sensing of Environment, 92: 207-217.

Smith, R. and Rowe, J., 1997. A new regional exploration method for detecting hydrocarbon alteration plumes: the ALTREX(TM) method. Exploration Geophysics, 28: 286-291.

Sokolov, V.A., 1933. The gas survey as a method of prospecting for oil and gas formations. Technika, NGRI no. 1.

Steven, M.D., Smith, K.L., Beardsley, M.D. and Colls, J.J., 2006. Oxygen and methane depletion in soil affected by leakage of natural gas. European Journal of Soil Science (*In press*).

Stewart, D. W., Costa, C., Dwyer, L. M., Smith, D. L., Hamilton, R. I. and Ma, B. L., 2003. Canopy structure, light interception, and photosynthesis in maize. Agronomy Journal 95: 1465-1474.

Strachan, I.B., Pattey, E. and Boisvert, J.B., 2002. Impact of nitrogen and environmental conditions on corn as detected by hyperspectral reflectance. Remote Sensing of Environment, 80(2): 213-224.

Tedesco, S.A., 1995. Surface geochemistry in petroleum exploration. Chapman & Hall, NY, 206 pp.

Thenkabail, P.S., Smith, R.B. and De Pauw, E., 2000. Hyperspectral vegetation indices and their relationships with agricultural crop characteristics. Remote Sensing of Environment, 71(2): 158-182.

Thenot, F., Methy, M. and Winkel, T., 2002. The photochemical reflectance index (PRI) as water-stress index. International Journal of Remote Sensing, 23(23): 5135-5139.

Tóth, E., Boros, D., Samuelsson, L., Deák, F., Marx, G. and Sükösd, C., 1994. High radon activity in Northeast Hungary. Physica Scripta, 50: 726-730.

Tucker, C.J., 1980. Remote sensing of leaf water content in the near infrared. Remote Sensing of Environment, 10: 23-32.

URL1: http://asterweb.jpl.nasa.gov/instrument.asp, 2006.

Van der Meer, F.D., Yang, H., Kroonenberg, S.B., 2000. Imaging spectrometry and petroleum geology: hydrocarbon microseepage as a source of global methane production. Proceedings of the 28th International Symposium on Remote Sensing of the Environment: information for sustainable development, March 27-31, 2000. Cape Town, South Africa. Cat. 5. pp. 36-39.

Van der Werff, H.M.A., 2006. Knowledge-based remote sensing of complex objects: recognition of spectral and spatial patterns resulting from natural hydrocarbon seepages. Ph.D. thesis, ITC dissertation nr. 131

Van der Werff, H.M.A., Bakker, W.H., Van der Meer, F.D. and Siderius, W., 2006. Combining spectral signals and spatial patterns using multiple Hough transforms: An application for detection of natural gas seepages. Computers & Geosciences, In Press.

Van der Werff, H.M.A. and Lucieer, A., 2004. A contextual algorithm for detection of mineral alteration halos with hyperspectral remote sensing. In: S.M. de Jong and F.D. van der Meer (Editors), Remote sensing image analysis: including the spatial domain. Kluwer Academic Publishers, Dordrecht, the Netherlands, pp. 201-210.

Van Persie, M., Van der Kamp, A. and Algra, T., 2004. Simulation and optimisation of a high resolution optical remote sensing system for monitoring of the European gas pipeline network, XXth ISPRS Congress, Istanbul, Turkey.

Vogelmann, J.E., Rock, B.N. and Moss, D.M., 1993. Red edge spectral measurements from sugar maple leaves. International Journal of Remote Sensing, 14: 1563–1575.

Wagner, M., Wagner, M., Piske, J. and Smit, R., 2002. Case histories of microbial prospection for oil and gas, onshore and offshore in northwest Europe. In: D. Schumacher and L.A. LeSchack (Editors), Surface exploration case histories: Applications of geochemistry, magnetics, and remote sensing. AAPG Studies in Geology, pp. 453–479.

Webster, R. and Oliver, M.A., 1990. Statistical methods in soil and land resource survey. Oxford University Press, New York, 316 pp.

Wellburn, A.R., 1994. The spectral determination of chlorophylls *a* and *b*, as well as total carotenoids, using various solvents with spectrophotometers of different resolution. Journal of Plant Physiology, 144(3): 307-313.

White, R.E., 1997. Principles and practice of soil science: the soil as a natural resource. Blackwell Science, Oxford, 348 pp.

Wu, S.H., 1994. Effect of manganese excess on the soybean plant cultivated under various growth conditions. Journal of Plant Nutrition, 17: 991-1003.

Yang, H., Zhang, J., Van der Meer, F. and Kroonenberg, S.B., 1999. Spectral characteristics of wheat associated with hydrocarbon microseepages. International Journal of Remote Sensing, 20(4): 807-813.

Yang, H., Zhang, J., Van der Meer, F.D., Kroonenberg, S.B., 2000. Imaging spectrometry data correlated to hydrocarbon microseepage. International Journal of Remote Sensing, 21: 197-202.

Zaidi, P.H., Rafique, S. and Singh, N.N., 2003. Response of maize (*Zea mays L.*) genotypes to excess soil moisture stress: morpho-physiological effects and basis of tolerance. European Journal of Agronomy, 19: 283-399.

Zarco-Tejada, P.J., Berjon, A., Lopez-Lozano, R., Miller, J.R., Martin, P., Cachorro, V, Gonzalez, M.R. and de Frutos, A., 2005. Assessing vineyard condition with hyperspectral indices: Leaf and canopy reflectance simulation in a row-structured discontinuous canopy. Remote Sensing of Environment, 99: 271-287.

Zarco-Tejada, P.J., Miller, J.R., Mohammed, G.H. and Noland, T.L., 2000. Chlorophyll fluorescence effects on vegetation apparent reflectance: I. Leaflevel measurements and simulation of reflectance and transmittance spectra. Remote Sensing of Environment, 74: 582– 595.

Zarco-Tejada, P.J., Miller, J.R., Mohammed, G.H., Noland, T.L. and Sampson, P.H., 2001. Scaling-up and model inversion methods with narrow-band optical indices for chlorophyll content estimation in closed forest canopies with hyperspectral data. IEEE Transactions on Geoscience and Remote Sensing, 39: 1491– 1507.

Zeeya, M., 12 January 2006. The lungs of the Planet are belching methane. New Scientist (2534): 13.

Zirnig, W., Hausamann, D. and Schreier, G., 2002. High-resolution remote sensing used to monitor natural gas pipelines. Earth Observation Magazine, 3: 1-8.

Appendix 1 Reflectance indices tested in Chapter 5.

Index name	Equation	Reference
Anthocyanin Reflectance Index 1 (ARI1)	$(1/R550) - (1/R700)$*	(Gitelson *et al*., 2001)
Anthocyanin Reflectance Index 2 (ARI2)	$R800$ *$[(1/R550) - (1/R700)]$	(Gitelson *et al*., 2001)
Blue/Green Index (BGI1)	$(R400/R550)$	(Zarco-Tejada *et al*., 2005)
Blue/Green Index (BGI2)	$R450/R550$	(Zarco-Tejada *et al*., 2005)
Blue/Red Index (BRI1)	$R400/R690$	(Zarco-Tejada *et al*., 2005)
Blue/Red Index (BRI2)	$R450/R690$	(Zarco-Tejada *et al*., 2005)
Carotenoid Reflectance Index 1 (CRI1)	$(1/R510) - (1/R550)$	(Gitelson *et al*., 2002)
Carotenoid Reflectance Index 2 (CRI2)	$(1/R510) - (1/R700)$	(Gitelson *et al*., 2002)
Carter Indices (CTR)	CTR1 = $R695/R420$	(Carter, 1994)
	CTR2 = $R695/R760$	(Carter, 1994)
Curvature Index (CUR)	$(R675*R690)/R^2683$	(Zarco-Tejada *et al*., 2000)
Enhanced Vegetation Index (EVI)	$2.5*(R\text{NIR}-R\text{Red})/(R\text{NIR}+6*R\text{Red}-7.5*R\text{Blue}+1)$	(Huete *et al*., 1997)
Gitelson and Merzlyak (GM)	GM1 = $R750/R550$	(Gitelson and Merzlyak, 1997)
	GM2 = $R750/R700$	(Gitelson and Merzlyak, 1997)
Improved SAVI with self-adjustment factor L (MSAVI)	$0.5*[2*R800+1-((2*R800+1)^2 - 8*(R800-R670))^{0.5}]$	(Qi *et al*., 1994)
Lichtenthaler Indices (LIC)	LIC1 = $(R800-R680)/(R800+R680)$	(Lichtenhaler *et al*., 1996)
	LIC2 = $R440/R690$	(Lichtenhaler *et al*., 1996)
	LIC3 = $R440/R740$	(Lichtenhaler *et al*., 1996)
Modified C_{ab} Absorption in Reflectance Index (MCARI)	$[(R700-R670)-0.2*(R700-R550)]*(R700/R670)$	(Daughtry *et al*., 2000)
Modified Chlorophyll Absorption in Reflectance Index (MCARI1)	$1.2*[2.5*(R800-R670)-1.3*(R800-R550)$	(Haboudane *et al*., 2004)
Modified Chlorophyll Absorption in Reflectance Index (MCARI2)	$\frac{1.5*[2.5*(R800-R670)-1.3*(R800-R550)}{\sqrt{((2*R800+1)^2 - (6*R800-5*\sqrt{R670}))-0.5}}$	(Haboudane *et al*., 2004)
Modified Red Edge Normalized Difference Vegetation Index (mNDVI705)	$(R750-R705)/(R750+R705-2*R445)$	(Sims and Gamon, 2002)
Modified Red Edge Simple Ratio Index (mSR705)	$(R750-R445)/(R705-R445)$	(Sims and Gamon, 2002)
Modified Simple Ratio (MSR)	$\frac{(R\text{NIR}/R\text{Red} -1)}{((R\text{NIR}/R\text{Red})^{0.5}+1)}$	(Chen, 1996)
Modified Triangular Vegetation Index (MTVI1)	$1.2*[1.2*(R800-R550)-2.5*(R670-R550)$	(Haboudane *et al*., 2004)
Modified Triangular Vegetation Index (MTVI2)	$\frac{1.5*[1.2*(R800-R550)-2.5*(R670-R550)}{\sqrt{((2*R800+1)^2 - (6*R800-5*\sqrt{R670}))-0.5}}$	(Haboudane *et al*., 2004)
Moisture Stress Index (MSI)	$R1599/R819$	(Hunt and Rock, 1989)
Normalized Difference Infrared Index (NDII)	$(R819 - R1649)/(R819 + R1649)$	(Hardisky *et al*., 1983)
Normalized Difference Nitrogen Index (NDNI)	$\frac{\log(1/R1510) - \log(1/R1680)}{\log(1/R1510) + \log(1/R1680)}$	(Serrano *et al*., 2002)
Normalized Difference Vegetation Index (NDVI)	$(R\text{NIR}- R\text{Red})/(R\text{NIR} + R\text{Red})$	(Rouse *et al*., 1974)

Normalized Difference Water Index (NDWI)	($R857$- $R1241$)/($R857$ + $R1241$)	(Gao, 1995)
Normalized Phaeophytinization Index (NPI)	($R415$- $R435$)/($R415$ + $R435$)	(Barnes, 1992)
Normalized Pigment Chlorophyll Index (NPCI)	($R680$- $R430$)/($R680$ + $R430$)	(Penuelas *et al*., 1994)
Optimized Soil-Adjusted Vegetation Index (OSAVI)	(1+0.16)*($R800$-$R670$)/($R800$+$R670$+0.16)	(Rondeaux *et al*., 1996)
Photochemical Reflectance Index (PRI)	($R531$- $R570$)/($R531$ + $R570$)	(Gamon *et al*., 1992)
Plant Senescence Reflectance Index (PSRI)	($R680$-$R500$)/$R750$	(Merzlyak *et al*., 1999)
Red Edge Normalized Difference Vegetation Index (NDVI705)	($R750$ - $R705$)/($R750$ + $R705$)	(Sims and Gamon, 2002)
Red Edge Position Index (REP)	700+40*[(($R670$+$R780$/2)-$R700$)/($R740$-$R700$)]	(Guyot & Baret, 1988)
Red/Green Index (RGI)	$R690$/$R550$	(Zarco-Tejada *et al*., 2005)
Renormalized Difference Vegetation Index (RDVI)	($R800$- $R670$)/√($R800$- $R670$)	(Rougean and Breon, 1995)
Simple Ratio Index (SR)	*R*NIR/*R*Red	(Rouse *et al*., 1974)
Simple Ratio Pigment Index (SRPI)	$R430$/$R680$	(Penuelas *et al*., 1995)
Structure Insensitive Pigment Index (SIPI)	($R800$ – $R450$)/($R800$ + $R650$)	(Penuelas *et al*., 1995)
Sum Green Index (SG)	Average of $R500$ till $R600$	(Gamon and Surfus, 1999)
Transformed CARI (TCARI)	3*[($R700$-$R670$)-0.2*($R700$-$R550$)*($R700$/$R670$)]	(Haboudane *et al*., 2002)
Triangular Vegetation Index (TVI)	0.5*[120*($R750$-$R550$) - 200*($R670$-$R550$)]	(Broge and Leblanc, 2000)
Vogelmann Indices (VOG)	VOG1 = $R740$/$R720$	(Vogelmann *et al*., 1993)
	VOG2 = ($R734$ - $R747$)/($R715$ + $R726$)	(Vogelmann *et al*., 1993)
	VOG3 = ($R734$ - $R747$)/($R715$ + $R720$)	(Vogelmann *et al*., 1993)
Water Band Index (WBI)	$R900$/$R970$	(Penuelas *et al*., 1997)
Zarco and Miller (ZM)	$R750$/$R710$	(Zarco-Tejada *et al*., 2001)

* *R* is reflectance at the specified wavelength

Biography

Marleen Noomen was born on the 9th of November 1976 in Hoenderloo, The Netherlands. After finishing pre-university education in 1995, she went to India to become a volunteer in a Tibetan refugee village in the Indian Himalaya. Here she helped in a solid waste project that was initiated to teach the local inhabitants about reducing and recycling garbage. From 1996 to 2001 she studied Physical Geography at the University of Utrecht, the Netherlands, with a specialisation in land degradation. During her study she modelled the impact of skiing on vegetation patterns on ski runs in Sölden, Austria, while her internship at the Indian Institute of Remote Sensing (Dehra Dun, India) dealt with land cover mapping of the mountainous regions in Himachal Pradesh (India). From 2002 to 2006 she worked on her Ph.D. research at the International Institute for Geo-information Science and Earth Observation (ITC). Her research dealt with the influence of underground natural gas leakage on vegetation reflectance, which resulted in this thesis.

Publications

1 **Noomen, M.F.**, Smith, K.L., Colls, J.J., Steven, M.D., Skidmore, A.K., Van der Meer, F.D., *accepted for publishing.* Predicting soil oxygen concentrations using indices based on hyperspectral reflectance of maize and wheat canopies. *International Journal of Remote Sensing*.

2 **Noomen, M.F.,** Skidmore, A.K., van der Meer, F.D., Prins, H.H.T., 2006. Continuum removed band depth analysis for detecting the effects of natural gas, methane and ethane on maize reflectance. *Remote Sensing of Environment*, 105: 262-270.

3 **Noomen, M.F.,** Skidmore, A.K., *In review after revision.* The effects of high soil CO_2 concentrations on the first derivative of maize leaf reflectance. *International Journal of Remote Sensing.*

4 Van der Werff, H.M.A., **Noomen, M.F.**, Van der Meijde, M., Kooistra, J.F., Van der Meer, F.D., 2007. Use of hyperspectral remote sensing to detect hazardous gas leakage from pipelines. In: *New Developments and Challenges in Remote Sensing*, Z. Bochenek (ed.), Millpress, Rotterdam. pp. 707-715

5 Van der Werff, H.M.A., **Noomen, M.F.**, Van der Meijde, M., Van der Meer, F.D., *in press*. Remote sensing of onshore hydrocarbon seepage: Problems and solutions. Geological Society of London, *Special Issue on Engineering Geology*

6 Van der Meer, F.D., Van der Meijde, M., Kooistra, J.F., Van der Werff, H.M.A., **Noomen, M.F.**, 2006. Detection of hazardous gas leakage from pipelines using anomalous spectral reflectance features of vegetation. In: Proceedings of the 25th EARSeL Symposium: Global Developments in Environmental Earth Observation from Space, Porto, Portugal. pp. 191-198

7 **Noomen, M.F.**, Ekpenyong, F.U., van der Meer, F.D., 2005. Hydrocarbon leakage detection using vegetation remote sensing. In: Proceedings of the 2nd Asian Space Conference, Hanoi Vietnam. 8 p.

8 **Noomen, M.F.,** van der Meer, F.D., Skidmore, A.K., 2005. Hyperspectral remote sensing for detecting the effects of three hydrocarbon gases on maize reflectance. In: Proceedings of the 31st International Symposium on Remote Sensing of Environment: global monitoring for sustainability and security, St. Petersburg, Russia. 4 p.

9 **Noomen, M.F.,** Skidmore, A.K., van der Meer, F.D., 2005. The effect of natural gas leakage on plant and canopy reflectance (Abstract). In: Proceedings of the 4th EARSeL Workshop on Imaging Spectroscopy: New Quality in Environmental Studies, Warsaw, Poland. pp. 62.

10 **Noomen, M.F.**, Skidmore, A.K., van der Meer, F.D., Smith, K.L., Steven, M.D., Colls, J.J., 2004. The influence of gas pipeline leakage on plant development and reflectance. In: Proceedings of the 25th Asian Conference on Remote Sensing, ACRS 2004 Silver jubilee, Chiang Mai, Thailand. pp. 637-642

11 **Noomen, M.F.,** Van der Werff, H.M.A., Van der Meer, F.D., *to be submitted to Terra Nova.* Detecting circular patterns in vegetation canopies caused by underground natural gas seepage.

ITC DISSERTATION LIST

1. **Akinyede** (1990), Highway cost modelling and route selection using a geotechnical information system
2. **Pan He Ping** (1990), 90-9003-757-8, Spatial structure theory in machine vision and applications to structural and textural analysis of remotely sensed images
3. **Bocco Verdinelli, G.** (1990), Gully erosion analysis using remote sensing and geographic information systems: a case study in Central Mexico
4. **Sharif, M**. (1991), Composite sampling optimization for DTM in the context of GIS
5. **Drummond, J.** (1991), Determining and processing quality parameters in geographic information systems
6. **Groten, S.** (1991), Satellite monitoring of agro-ecosystems in the Sahel
7. **Sharifi, A.** (1991), 90-6164-074-1, Development of an appropriate resource information system to support agricultural management at farm enterprise level
8. **Zee, D. van der** (1991), 90-6164-075-X, Recreation studied from above: Air photo interpretation as input into land evaluation for recreation
9. **Mannaerts, C.** (1991), 90-6164-085-7, Assessment of the transferability of laboratory rainfall-runoff and rainfall - soil loss relationships to field and catchment scales: a study in the Cape Verde Islands
10. **Ze Shen Wang** (1991), 90-393-0333-9, An expert system for cartographic symbol design
11. **Zhou Yunxian** (1991), 90-6164-081-4, Application of Radon transforms to the processing of airborne geophysical data
12. **Zuviria, M. de** (1992), 90-6164-077-6, Mapping agro-topoclimates by integrating topographic, meteorological and land ecological data in a geographic information system: a case study of the Lom Sak area, North Central Thailand
13. **Westen, C. van** (1993), 90-6164-078-4, Application of Geographic Information Systems to landslide hazard zonation
14. **Shi Wenzhong** (1994), 90-6164-099-7, Modelling positional and thematic uncertainties in integration of remote sensing and geographic information systems
15. **Javelosa, R.** (1994), 90-6164-086-5, Active Quaternary environments in the Philippine mobile belt
16. **Lo King-Chang** (1994), 90-9006526-1, High Quality Automatic DEM, Digital Elevation Model Generation from Multiple Imagery
17. **Wokabi, S.** (1994), 90-6164-102-0, Quantified land evaluation for maize yield gap analysis at three sites on the eastern slope of Mt. Kenya
18. **Rodriguez, O.** (1995), Land Use conflicts and planning strategies in urban fringes: a case study of Western Caracas, Venezuela
19. **Meer, F. van der** (1995), 90-5485-385-9, Imaging spectrometry & the Ronda peridotites
20. **Kufoniyi, O.** (1995), 90-6164-105-5, Spatial coincidence: automated database updating and data consistency in vector GIS
21. **Zambezi, P.** (1995), Geochemistry of the Nkombwa Hill carbonatite complex of Isoka District, north-east Zambia, with special emphasis on economic minerals
22. **Woldai, T.** (1995), The application of remote sensing to the study of the geology and structure of the Carboniferous in the Calañas area, pyrite belt, SW Spain

23. **Verweij, P.** (1995), 90-6164-109-8, Spatial and temporal modelling of vegetation patterns: burning and grazing in the Paramo of Los Nevados National Park, Colombia
24. **Pohl, C.** (1996), 90-6164-121-7, Geometric Aspects of Multisensor Image Fusion for Topographic Map Updating in the Humid Tropics
25. **Jiang Bin** (1996), 90-6266-128-9, Fuzzy overlay analysis and visualization in GIS
26. **Metternicht, G.** (1996), 90-6164-118-7, Detecting and monitoring land degradation features and processes in the Cochabamba Valleys, Bolivia. A synergistic approach
27. **Hoanh Chu Thai** (1996), 90-6164-120-9, Development of a Computerized Aid to Integrated Land Use Planning (CAILUP) at regional level in irrigated areas: a case study for the Quan Lo Phung Hiep region in the Mekong Delta, Vietnam
28. **Roshannejad, A.** (1996), 90-9009-284-6, The management of spatio-temporal data in a national geographic information system
29. **Terlien, M.** (1996), 90-6164-115-2, Modelling Spatial and Temporal Variations in Rainfall-Triggered Landslides: the integration of hydrologic models, slope stability models and GIS for the hazard zonation of rainfall-triggered landslides with examples from Manizales, Colombia
30. **Mahavir, J.** (1996), 90-6164-117-9, Modelling settlement patterns for metropolitan regions: inputs from remote sensing
31. **Al-Amir, S.** (1996), 90-6164-116-0, Modern spatial planning practice as supported by the multi-applicable tools of remote sensing and GIS: the Syrian case
32. **Pilouk, M.** (1996), 90-6164-122-5, Integrated modelling for 3D GIS
33. **Duan Zengshan** (1996), 90-6164-123-3, Optimization modelling of a river-aquifer system with technical interventions: a case study for the Huangshui river and the coastal aquifer, Shandong, China
34. **Man, W.H. de** (1996), 90-9009-775-9, Surveys: informatie als norm: een verkenning van de institutionalisering van dorp - surveys in Thailand en op de Filippijnen
35. **Vekerdy, Z.** (1996), 90-6164-119-5, GIS-based hydrological modelling of alluvial regions: using the example of the Kisaföld, Hungary
36. **Pereira, Luisa** (1996), 90-407-1385-5, A Robust and Adaptive Matching Procedure for Automatic Modelling of Terrain Relief
37. **Fandino Lozano, M.** (1996), 90-6164-129-2, A Framework of Ecological Evaluation oriented at the Establishment and Management of Protected Areas: a case study of the Santuario de Iguaque, Colombia
38. **Toxopeus, B.** (1996), 90-6164-126-8, ISM: an Interactive Spatial and temporal Modelling system as a tool in ecosystem management: with two case studies: Cibodas biosphere reserve, West Java Indonesia: Amboseli biosphere reserve, Kajiado district, Central Southern Kenya
39. **Wang Yiman** (1997), 90-6164-131-4, Satellite SAR imagery for topographic mapping of tidal flat areas in the Dutch Wadden Sea
40. **Saldana-Lopez, Asunción** (1997), 90-6164-133-0, Complexity of soils and Soilscape patterns on the southern slopes of the Ayllon Range, central Spain: a GIS assisted modelling approach

41. **Ceccarelli, T.** (1997), 90-6164-135-7, Towards a planning support system for communal areas in the Zambezi valley, Zimbabwe; a multi-criteria evaluation linking farm household analysis, land evaluation and geographic information systems
42. **Peng Wanning** (1997), 90-6164-134-9, Automated generalization in GIS
43. **Lawas, C.** (1997), 90-6164-137-3, The Resource Users' Knowledge, the neglected input in Land resource management: the case of the Kankanaey farmers in Benguet, Philippines
44. **Bijker, W.** (1997), 90-6164-139-X, Radar for rain forest: A monitoring system for land cover Change in the Colombian Amazon
45. **Farshad, A.** (1997), 90-6164-142-X, Analysis of integrated land and water management practices within different agricultural systems under semi-arid conditions of Iran and evaluation of their sustainability
46. **Orlic, B.** (1997), 90-6164-140-3, Predicting subsurface conditions for geotechnical modelling
47. **Bishr, Y.** (1997), 90-6164-141-1, Semantic Aspects of Interoperable GIS
48. **Zhang Xiangmin** (1998), 90-6164-144-6, Coal fires in Northwest China: detection, monitoring and prediction using remote sensing data
49. **Gens, R.** (1998), 90-6164-155-1, Quality assessment of SAR interferometric data
50. **Turkstra, J.** (1998), 90-6164-147-0, Urban development and geographical information: spatial and temporal patterns of urban development and land values using integrated geo-data, Villaviciencia, Colombia
51. **Cassells, C.** (1998), 90-6164-234-5, Thermal modelling of underground coal fires in northern China
52. **Naseri, M.** (1998), 90-6164-195-0, Characterization of Salt-affected Soils for Modelling Sustainable Land Management in Semi-arid Environment: a case study in the Gorgan Region, Northeast, Iran
53. **Gorte B.G.H.** (1998), 90-6164-157-8, Probabilistic Segmentation of Remotely Sensed Images
54. **Tegaye, Tenalem Ayenew** (1998), 90-6164-158-6, The hydrological system of the lake district basin, central main Ethiopian rift
55. **Wang Donggen** (1998), 90-6864-551-7, Conjoint approaches to developing activity-based models
56. **Bastidas de Calderon, M.** (1998), 90-6164-193-4, Environmental fragility and vulnerability of Amazonian landscapes and ecosystems in the middle Orinoco river basin, Venezuela
57. **Moameni, A.** (1999), Soil quality changes under long-term wheat cultivation in the Marvdasht plain, South-Central Iran
58. **Groenigen, J.W. van** (1999), 90-6164-156-X, Constrained optimisation of spatial sampling: a geostatistical approach
59. **Cheng Tao** (1999), 90-6164-164-0, A process-oriented data model for fuzzy spatial objects
60. **Wolski, Piotr** (1999), 90-6164-165-9, Application of reservoir modelling to hydrotopes identified by remote sensing
61. **Acharya, B.** (1999), 90-6164-168-3, Forest biodiversity assessment: A spatial analysis of tree species diversity in Nepal

62. **Akbar Abkar, Ali** (1999), 90-6164-169-1, Likelihood-based segmentation and classification of remotely sensed images
63. **Yanuariadi, T.** (1999), 90-5808-082-X, Sustainable Land Allocation: GIS-based decision support for industrial forest plantation development in Indonesia
64. **Abu Bakr**, **Mohamed** (1999), 90-6164-170-5, An Integrated Agro-Economic and Agro-Ecological Framework for Land Use Planning and Policy Analysis
65. **Eleveld, M.** (1999), 90-6461-166-7, Exploring coastal morphodynamics of Ameland (The Netherlands) with remote sensing monitoring techniques and dynamic modelling in GIS
66. **Yang Hong** (1999), 90-6164-172-1, Imaging Spectrometry for Hydrocarbon Microseepage
67. **Mainam, Félix** (1999), 90-6164-179-9, Modelling soil erodibility in the semiarid zone of Cameroon
68. **Bakr, Mahmoud** (2000), 90-6164-176-4, A Stochastic Inverse-Management Approach to Groundwater Quality
69. **Zlatanova, Z.** (2000), 90-6164-178-0, 3D GIS for Urban Development
70. **Ottichilo, Wilber K.** (2000), 90-5808-197-4, Wildlife Dynamics: An Analysis of Change in the Masai Mara Ecosystem
71. **Kaymakci, Nuri** (2000), 90-6164-181-0, Tectono-stratigraphical Evolution of the Cankori Basin (Central Anatolia, Turkey)
72. **Gonzalez, Rhodora** (2000), 90-5808-246-6, Platforms and Terraces: Bridging participation and GIS in joint-learning for watershed management with the Ifugaos of the Philippines
73. **Schetselaar, Ernst** (2000), 90-6164-180-2, Integrated analyses of granite-gneiss terrain from field and multisource remotely sensed data. A case study from the Canadian Shield
74. **Mesgari, Saadi** (2000), 90-3651-511-4, Topological Cell-Tuple Structure for Three-Dimensional Spatial Data
75. **Bie, Cees A.J.M. de** (2000), 90-5808-253-9, Comparative Performance Analysis of Agro-Ecosystems
76. **Khaemba, Wilson M**. (2000), 90-5808-280-6, Spatial Statistics for Natural Resource Management
77. **Shrestha, Dhruba** (2000), 90-6164-189-6, Aspects of erosion and sedimentation in the Nepalese Himalaya: highland-lowland relations
78. **Asadi Haroni, Hooshang** (2000), 90-6164-185-3, The Zarshuran Gold Deposit Model Applied in a Mineral Exploration GIS in Iran
79. **Raza, Ale** (2001), 90-3651-540-8, Object-oriented Temporal GIS for Urban Applications
80. **Farah, Hussein** (2001), 90-5808-331-4, Estimation of regional evaporation under different weather conditions from satellite and meteorological data. A case study in the Naivasha Basin, Kenya
81. **Zheng**, **Ding** (2001), 90-6164-190-X, A Neural - Fuzzy Approach to Linguistic Knowledge Acquisition and Assessment in Spatial Decision Making
82. **Sahu, B.K.** (2001), Aeromagnetics of continental areas flanking the Indian Ocean; with implications for geological correlation and reassembly of Central Gondwana

83. **Alfestawi, Y.** (2001), 90-6164-198-5, The structural, paleogeographical and hydrocarbon systems analysis of the Ghadamis and Murzuq Basins, West Libya, with emphasis on their relation to the intervening Al Qarqaf Arch
84. **Liu, Xuehua** (2001), 90-5808-496-5, Mapping and Modelling the Habitat of Giant Pandas in Foping Nature Reserve, China
85. **Oindo, Boniface Oluoch** (2001), 90-5808-495-7, Spatial Patterns of Species Diversity in Kenya
86. **Carranza, Emmanuel John** (2002), 90-6164-203-5, Geologically-constrained Mineral Potential Mapping
87. **Rugege, Denis** (2002), 90-5808-584-8, Regional Analysis of Maize-Based Land Use Systems for Early Warning Applications
88. **Liu, Yaolin** (2002), 90-5808-648-8, Categorical Database Generalization in GIS
89. **Ogao, Patrick** (2002), 90-6164-206-X, Exploratory Visualization of Temporal Geospatial Data using Animation
90. **Abadi, Abdulbaset M.** (2002), 90-6164-205-1, Tectonics of the Sirt Basin – Inferences from tectonic subsidence analysis, stress inversion and gravity modelling
91. **Geneletti, Davide** (2002), 90-5383-831-7, Ecological Evaluation for Environmental Impact Assessment
92. **Sedogo, Laurent G.** (2002), 90-5808-751-4, Integration of Participatory Local and Regional Planning for Resources Management using Remote Sensing and GIS
93. **Montoya, Lorena** (2002), 90-6164-208-6, Urban Disaster Management: a case study of earthquake risk assessment in Carthago, Costa Rica
94. **Ahmad, Mobin-ud-Din** (2002), 90-5808-761-1, Estimation of Net Groundwater Use in Irrigated River Basins using Geo-information Techniques: A case study in Rechna Doab, Pakistan
95. **Said, Mohammed Yahya** (2003), 90-5808-794-8, Multiscale perspectives of species richness in East Africa
96. **Schmidt, Karin** (2003), 90-5808-830-8, Hyperspectral Remote Sensing of Vegetation Species Distribution in a Saltmarsh
97. **Lopez Binnquist, Citlalli** (2003), 90-3651-900-4, The Endurance of Mexican Amate Paper: Exploring Additional Dimensions to the Sustainable Development Concept
98. **Huang, Zhengdong** (2003), 90-6164-211-6, Data Integration for Urban Transport Planning
99. **Cheng, Jianquan** (2003), 90-6164-212-4, Modelling Spatial and Temporal Urban Growth
100. **Campos dos Santos, Jose Laurindo** (2003), 90-6164-214-0, A Biodiversity Information System in an Open Data/Metadatabase Architecture
101. **Hengl, Tomislav** (2003), 90-5808-896-0, PEDOMETRIC MAPPING, Bridging the gaps between conventional and pedometric approaches
102. **Barrera Bassols, Narciso (**2003), 90-6164-217-5, Symbolism, Knowledge and management of Soil and Land Resources in Indigenous Communities: Ethnopedology at Global, Regional and Local Scales
103. **Zhan, Qingming** (2003), 90-5808-917-7, A Hierarchical Object-Based Approach for Urban Land-Use Classification from Remote Sensing Data

104. **Daag, Arturo S.** (2003), 90-6164-218-3, Modelling the Erosion of Pyroclastic Flow Deposits and the Occurrences of Lahars at Mt. Pinatubo, Philippines
105. **Bacic, Ivan** (2003), 90-5808-902-9, Demand-driven Land Evaluation with case studies in Santa Catarina, Brazil
106. **Murwira, Amon** (2003), 90-5808-951-7, Scale matters! A new approach to quantify spatial heterogeneity for predicting the distribution of wildlife
107. **Mazvimavi, Dominic** (2003), 90-5808-950-9, Estimation of Flow Characteristics of Ungauged Catchments. A case study in Zimbabwe
108. **Tang, Xinming** (2004), 90-6164-220-5, Spatial Object Modelling in Fuzzy Topological Spaces with Applications to Land Cover Change
109. **Kariuki, Patrick** (2004), 90-6164-221-3, Spectroscopy and Swelling Soils; an integrated approach
110. **Morales, Javier** (2004), 90-6164-222-1, Model Driven Methodology for the Design of Geo-information Services
111. **Mutanga, Onisimo** (2004), 90-5808-981-9, Hyperspectral Remote Sensing of Tropical Grass Quality and Quantity
112. **Šliužas, Ričardas V.** (2004), 90-6164-223-X, Managing Informal Settlements: a study using geo-information in Dar es Salaam, Tanzania
113. **Lucieer, Arko** (2004), 90-6164-225-6, Uncertainties in Segmentation and their Visualisation
114. **Corsi, Fabio** (2004), 90-8504-090-6, Applications of existing biodiversity information: Capacity to support decision-making
115. **Tuladhar, Arbind** (2004), 90-6164-224-8, Parcel-based Geo-information System: Concepts and Guidelines
116. **Elzakker, Corné van** (2004), 90-6809-365-7, The use of maps in the exploration of geographic data
117. **Nidumolu, Uday Bhaskar** (2004), 90-8504-138-4, Integrating Geo-information models with participatory approaches: applications in land use analysis
118. **Koua, Etien L.** (2005), 90-6164-229-9, Computational and Visual Support for Exploratory Geovisualization and Knowledge Construction
119. **Blok, Connie A.** (2005), Dynamic visualization variables in animation to support monitoring of spatial phenomena
120. **Meratnia, Nirvana** (2005), 90-365-2152-1, Towards Database Support for Moving Object Data
121. **Yemefack, Martin** (2005), 90-6164-233-7, Modelling and monitoring Soil and Land Use Dynamics within Shifting Agricultural Landscape Mosaic Systems
122. **Kheirkhah, Masoud** (2005), 90-8504-256-9, Decision support system for floodwater spreading site selection in Iran
123. **Nangendo, Grace** (2005), 90-8504-200-3, Changing forest-woodland-savanna mosaics in Uganda: with implications for conservation
124. **Mohamed, Yasir Abbas** (2005), 04-15-38483-4, The Nile Hydroclimatology: impact of the Sudd wetland (Distinction)
125. **Duker, Alfred, A.** (2005), 90-8504-243-7, Spatial analysis of factors implicated in *mycobacterium ulcerans* infection in Ghana
126. **Ferwerda, Jelle, G.,** (2005), 90-8504-209-7, Charting the Quality of Forage: Measuring and mapping the variation of chemical components in foliage with hyperspectral remote sensing

127. **Martinez, Javier** (2005), 90-6164-235-3, Monitoring intra-urban inequalities with GIS-based indicators. With a case study in Rosario, Argentina
128. **Saavedra, Carlos** (2005), 90-8504-289-5, Estimating spatial patterns of soil erosion and deposition in the Andean region using Geo-information techniques. A case study in Cochabamba, Bolivia
129. **Vaiphasa, Chaichoke** (2006), 90-8504-353-0, Remote Sensing Techniques for Mangrove Mapping
130. **Porwal, Alok** (2006), 90-6164-240-X, Mineral Potential Mapping with Mathematical Geological Models
131. **Werff, Harald van der** (2006), 90-6164-238-8, Knowledge-based remote sensing of complex objects: recognition of spectral and spatial patterns resulting from natural hydrocarbon seepages
132. **Vlag, Daniël van de** (2006), 90-8504-384-0, Modeling and visualizing dynamic landscape objects and their qualities
133. **Joshi, Chudamani** (2006), 90-8504-470-7, Mapping cryptic invaders and invisibility of tropical forest ecosystems: *Chromolaena odorata* in Nepal
134. **Bandara, K.M.P.S.** (2006), 90-8504-406-5, Assessing irrigation performance by using remote sensing
135. **Dilo, Areti** (2006), 90-8504-461-8, Representation of and Reasoning with Vagueness in Spatial Information. A system for handling vague objects
136. **Debba, Pravesh** (2006), 90-8504-462-6, Sampling scheme optimization from hyperspectral data
137. **Huisman, Marco** (2006), 90-6164-246-9, Assessment of rock mass decay in artificial slopes
138. **Lemmens, Rob** (2006), 90-6164-250-7, Semantic interoperability of distributed geo-services
139. **Chacón Moreno, Eulogio** (2007), 90-8504-559-2, Ecological and spatial modeling: Mapping ecosystems, landscape changes, and plant species distribution in Llanos del Orinoco, Venezuela
140. **Amer, Sherif** (2007), 90-6164-253-1, Towards Spatial Justice in Urban Health Services Planning
141. **Obakeng, Obolokile Thothi** (2007), 90-6164-254-X, Soil moisture dynamics and evapotranspiration at the fringe of the Botswana Kalahari, with emphasis on deep rooting vegetation
142. **Cho, Moses Azong** (2007), 978-90-8504-622-6, Hyperspectral remote sensing of biochemical and biophysical parameters
143. **Farifteh, Jamshid** (2007), 978-90-6164-259-6, Imaging Spectroscopy of salt-affected soils: Model-based integrated method
144. **Minang, Peter Akong**, (2007), 978-90-6164-260-2, Implementing global environmental policy at local level: community carbon forestry perspectives in Cameroon

PE&RC PhD Education Certificate

With the educational activities listed below the PhD candidate has complied with the educational requirements set by the C.T. de Wit Graduate School for Production Ecology and Resource Conservation (PE&RC) which comprises of a minimum total of 32 ECTS (= 22 weeks of activities)

Review of Literature (5.6 credits)
Detecting the influence of hydrocarbon seepage on vegetation using hyperspectral remote sensing (2002)

Writing of Project Proposal (7 credits)
Research proposal: Detecting the influence of hydrocarbon seepage on vegetation, using hyperspectral remote sensing (2002)

Laboratory Training and Working Visits (5 credits)
Field training spectrometry; ITC (2002)
Working visit Nottingham-preparation; Nottingham University (2002)
Working visit Nottingham; Nottingham University (2003)

Post-Graduate Courses (4 credits)
ArcGIS basics; ITC (2003)
IDL Programming course; ITC (2004)

Competence Strengthening / Skills Courses (2 credits)
Scientific writing course; ITC (2002)
Presentation course; ITC (2002)

Discussion Groups / Local Seminars and other Scientific Meetings (7.9 credits)
NRS tutorial (2002-2006)
PhD day ITC (2004)
NRS + ESA science days (2002-2006)

PE&RC Annual Meetings, Seminars and the PE&RC Weekend (1.2 credits)
PE&RC introduction weekend (2002)
PE&RC symposium spatial ecology (2003)

International Symposia, Workshops and Conferences (9 credits)
ACRS-Thailand (2004)
ISRSE-Russia (2005)
ASC-Vietnam (2005)